

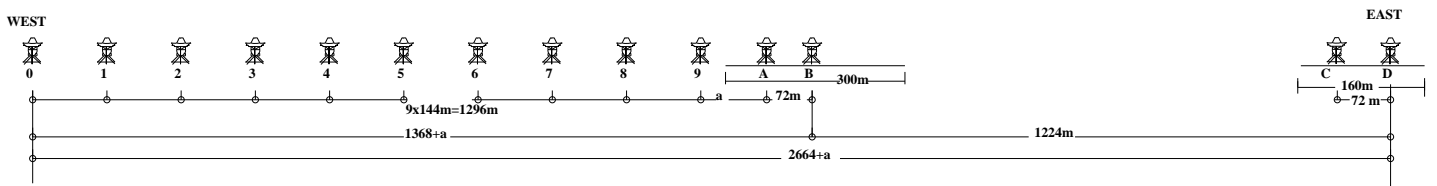
WSRT USER DOCUMENTATION

PART III

SPECIFIC ASPECTS OF THE WSRT

July 16, 1993

Version: 1.0.0





CONTENTS OF PART III

This is part III of the WSRT User Documentation.

The WSRT User Documentation consists of 7 Parts; we may refer to other parts of the User Documentation. To get more information about how to obtain a copy and/or updates of parts of the User Documentation please send an e-mail request to wsrt@nfra.nl

The roman number in the pagenumber indicates the part.

1	Technical Specifications of the WSRT	III-1-1
1.1	Geometry of the Array	III-1-1
1.2	Observing Modes	III-1-1
1.3	Receivers and backends	III-1-2
1.3.1	The spectral line backend (DXB)	III-1-2
1.3.2	The continuum backend (DCB)	III-1-4
1.3.3	Very Long Baseline Interferometry (VLBI)	III-1-4
1.4	Future developments	III-1-5
1.4.1	Pulsar Filterbank	III-1-5
1.4.2	The DZB backend	III-1-5
1.4.3	The multifrequency front ends	III-1-5
2	The calculation of the sensitivity	III-2-1
2.1	Sensitivity Calculations	III-2-1
2.1.1	Calculating the sensitivity for a standard setup	III-2-1
2.1.2	Calculating the sensitivity for a non-standard setup	III-2-2
3	Specifying the backend setup	III-3-1
3.1	Choosing the instrumental setup	III-3-1
3.2	The setup for line observations	III-3-1
3.2.1	Examples	III-3-4
3.3	The setup for continuum observations	III-3-5
3.4	The setup for other modes of operation	III-3-6
3.4.1	Autocorrelation	III-3-6
3.4.2	Pulsar observations with the DCB.	III-3-7
3.5	References	III-3-7
4	Polarization measurements with the WSRT	III-4-1
4.1	Description	III-4-1
4.2	Definitions	III-4-2
4.3	Examples	III-4-4
4.4	Errors	III-4-7
4.5	References	III-4-7

5	On the use of redundant baselines	III-5-1
5.1	A sketch of the technique	III-5-1
5.2	Redundancy and the WSRT	III-5-2
5.3	References	III-5-3
6	Mosaicing	III-6-1
6.1	Introduction	III-6-1
6.2	Theoretical Background	III-6-1
6.3	Mosaic Implementations	III-6-2
6.4	Spatial frequency coverage optimization	III-6-2
6.5	Information for users interested in the use of mosaicing observations	III-6-4
6.6	References	III-6-4
7	The WSRT Correlators	III-7-1
7.1	Digital Correlators - a synopsis of theory	III-7-1
7.2	The DLB/DXB	III-7-2
7.2.1	The WSRT receiver system	III-7-4
7.2.2	The Frontends	III-7-4
7.2.3	The IF to video conversion	III-7-4
7.2.4	The A/D conversion	III-7-5
7.2.5	The Digital Delay	III-7-5
7.2.6	Correlator Modes	III-7-6
7.3	The DCB	III-7-6
7.4	References	III-7-6
8	WSRT Beams	III-8-1
8.1	WSRT primary beam properties	III-8-1
8.1.1	Introduction	III-8-1
8.1.2	Some theory	III-8-1
8.1.3	Beam properties	III-8-3
8.1.4	Pointing effects	III-8-4
8.1.5	Beam determination	III-8-4
8.1.6	Main beam total power and polarization patterns	III-8-5
8.1.7	Sidelobe patterns	III-8-7
8.1.8	Suggestions for further work	III-8-8
8.1.9	References	III-8-8
8.2	WSRT Baselines	III-8-9
8.3	Synthesized Beam cross-cuts and integrals	III-8-9
8.3.1	Calculation of synthesized beams	III-8-11
9	Shadowing	III-9-1
9.1	Introduction	III-9-1
9.2	Geometrical Shadowing calculation	III-9-1
9.3	Antenna Shadowing and Observing Limits	III-9-4
9.4	Remarks	III-9-5
9.5	References	III-9-5
10	Baselines, delays and fringes	III-10-1
10.1	Delay Path lengths	III-10-1
10.2	Fringe frequency	III-10-2
10.3	Position angle of the projected baseline on the sky	III-10-3

WSRT PART III

USER DOCUMENTATION CHAPTER 1

TECHNICAL SPECIFICATIONS OF THE WSRT

1.1 GEOMETRY OF THE ARRAY

The WSRT consists of an East-West array of fourteen equatorially mounted parabolic 25-m dishes. Ten (labeled 0-9) are on fixed mountings, 144 meters apart; the four (2×2) remaining dishes (labeled A, B, C and D) are movable along two rail tracks, one, 300 m long, adjacent to the fixed array and another, 180 m long, $9 \times 144\text{m}$ towards the East (see figure). The movable dishes can be used at any position on the rail tracks. The pointing accuracy of the dishes is 15 to 20 arcseconds, the surface accuracy is of the order of 1-2 mm. In the focal plane ($f/D = 0.35$) of the dishes, exactly on the 'optical axis', the frontend feeds are mounted. These feeds consist of two perpendicular probes for the detection of linearly polarized radiation (dipole cross) designated X and Y. The dipole crosses can be rotated. In the most common case the X and Y dipoles on all telescopes have the same orientation (indicated by ++) but it is possible to rotate dipoles such that interferometers are formed for which the dipole crosses differ in orientation by 45° (indicated by $+\times$). In the backend correlation system for Westerbork all 4 possible combinations can be produced for each interferometer.— *i.e.* XX,XY,YX and YY. The geographical coordinates are: altitude 16 m, longitude -6.60417, and latitude 52.91692.

1.2 OBSERVING MODES

In its 'normal', *local mode* of operation the WSRT is used as an aperture synthesis array with a total length of 2.8 km. It then consists of a basic set of 40 interferometers, each interferometer comprising one fixed and one movable dish, and a variable number of 'redundant' interferometers (fixed-fixed and/or movable-movable).

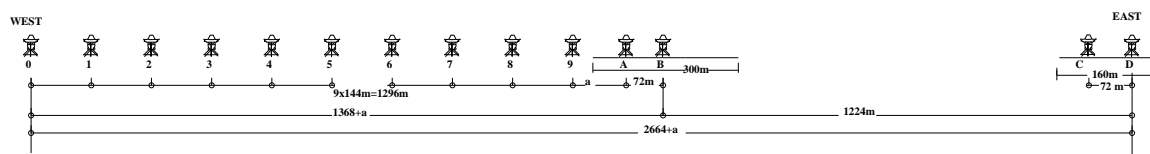


Figure 1.1: Geometry of the Westerbork East West array of 10 fixed 25 meter dishes, spaced by 144m and 4 movable dishes on rail tracks. Standard available baselines are 36 to 2772m in 18m increments (4×12^h) but spacing increments of 12m (6×12^h) or 9m (8×12^h) are also possible

standard mode of operation for line and continuum observations	e.g. PART III Chapter 2 and Chapter 3
standard mode for polarization measurements	Part III Chapter 4
standard mode using redundant baselines	Part III Chapter 5
mosaicing mode	Part III Chapter 6
autocorrelation mode	Part III section 3.4.1
pulsar mode	Part III section 3.4.2

Table 1.1: The various observing modes of the WSRT. For more information read the indicated chapters elsewhere in the user documentation

The redundant interferometers are generally used when high dynamic range is important, to calibrate the short term phase and amplitude variations caused by instabilities in the atmosphere and drifts in the receivers. This method, in combination with self-calibration techniques allow very high dynamic ranges to be obtained in continuum observations in particular. The redundant interferometers can, of course, also be used to contribute to aperture synthesis maps at the expense of a less clean sidelobe pattern.

A new method of using the WSRT in mosaic mode was developed in 1990. This mosaic method allows mapping of large areas of the sky in a relatively short time. During one twelve hour period the telescopes, along with the fringe-stopping and delay centers, cycle through a grid of positions a number of times. The grid may contain as many as 120 positions specified by the user; it can be arranged in a flexible way. If done sensibly no more than 10 seconds are required to change positions within the grid. The method allows large surveys of continuum or line radiation in those cases where sky coverage is more important than sensitivity. Part of the time the WSRT is used for *Very Long Baseline Interferometry (VLBI)* along with other telescopes in Europe and elsewhere (mainly the USA). The fourteen WSRT dishes are then used as a ‘tied array’, together yielding the equivalent of one 93-meter single dish in the VLBI network. The tied array mode will also be used sometimes for pulsar observations.

The WSRT can also been used as 14 independent 25 m dishes. This mode has been used for a Deuterium search at $\lambda = 92$ cm.

1.3 RECEIVERS AND BACKENDS

Table 1.2 summarizes the characteristics of the WSRT at each of the five wavelengths for which receivers are currently available. At 18 cm there are only five (cryogenically cooled) receivers which can be mounted in telescopes 0, A, B, C, D. In the near future also telescope 9 will be equipped for a cryogenic frontend. At this wavelength the WSRT is generally used in the VLBI tied-array mode. For the other four wavelengths a complete set of 14 receivers can be used. All receivers have two linear polarization channels.

Two digital correlators and two VLBI recording systems can be used to combine the signals from the array for different types of observations. A summary of their characteristics is given in the table 1.3

1.3.1 THE SPECTRAL LINE BACKEND (DXB)

The basic number of independent 1-bit complex correlation products which the DXB¹ can produce simultaneously is 2560. In 2-bit mode the correlator produces half the number of products (1280) with a sensitivity improved by approximately 1.25. When the observed spectrum can be covered adequately with an overall bandwidth (B) narrower than its maximum value (10 MHz), the clockrate of the correlator (20 MHz) allows the number of correlation products to be increased by a factor $10/B$ to a maximum of 40960 ($10/B$ is a power of 2). The number of complex channels, obtained after Fourier transformation of the correlation functions,

¹The correlator actually consists of a DLB and a DXB unit. For 10 MHz bandwidth the DLB is used. For $B < 10$ MHz the DXB is used to obtain more channels by recirculation of the interferometer channels over the DLB input channels. For clarity we do not make a distinction between the DLB and DXB in this documentation. And we will refer to the DLB/DXB spectral line backend as DXB.

wavelength(cm)	6	18	21	49	92
frequency range at RF (MHz)	4770-5020	1590-1730	1365-1425	607-610	305-385
field size HPBW(degr)	0.17	0.5	0.6	1.4	2.6
max. bandwidth at IF (MHz)	80	80	80	2.5	80
T _{sys} of frontend (K)					
cooled	55	60	35	–	–
uncooled	150	–	90	110	140 [†]
synthesized beam in RA for 2.8 km maximum baseline (arcsec)	3.7	11	13	30	55
for a standard 12 h measurement with 40 baselines and a standard taper:					
distance to grating ring in RA (arcmin)	2.9	8.5	10	24	44
theoretical continuum sensitivity (r.m.s. in 12 ^h obs) (mJy/beam)	0.07	–	0.05	0.6*	0.5* [‡]

[†]: In the coldest regions of the sky

*: At these wavelengths a 12^h observation is confusion limited and will not reach the theoretical sensitivity.

[‡]: This value is based on 5 MHz bandwidth while a wider bandwidth may be unuseable in practice.

Table 1.2: Characteristics of the WSRT and its receivers

DXB spectral line backend								
bandwidth options(MHz):	10	5	2.5	1.25	.625	.313	.156	.078
# of complex channels (2-bit):	1280	2560	5120	10240	20480	40960	40960	40960
# of complex channels (1-bit):	2560	5120	10240	20480	40960	40960	40960	40960
channel separation (kHz):								
91 interferom. 4 polariz.2-bit [†]	-	-	-	-	19.5	9.77	4.88	2.44
10 interferom. 1 polariz.1-bit	39.06	19.53	9.77	4.88	2.44	1.22	0.61	0.31
40 interferom. 2 polariz.1-bit	312.5	78.1	19.53	4.88	2.44	1.22	0.61	0.31
DCB continuum backend								
total bandwidth (MHz):	8 × 10 = 80	40						
bandwidth options (MHz):	10	5						
# of complex channels:	2048	2048						
MK2 VLBI backend								
max. total bandwidth (MHz)	2							
bandwidth options (MHz)	2	1	.5	.25	.125	.0625		
MK3 VLBI backend								
max. total bandwidth (MHz)	14 × 4 = 56							
bandwidth options (MHz)	4	2	1	.25	.125	.0625		

[†]: See part III, table 5.2 for the DXB settings used for this configuration.

Table 1.3: Characteristics of the WSRT backends

may be distributed over interferometers and polarization channels of the array. How one chooses to do this depends not only on the spectral resolution required but also on the sensitivity needed per frequency point (= complex channel) on each interferometer. Sensitivity may be increased by observing in 2-bit mode and with two independent polarization channels.

The number of independent frequency channels N_F in each observed spectrum depends on the overall bandwidth B (MHz), the correlator bit-mode N_B (1 or 2), the number of interferometers N_I and the number of polarization channels N_P by the relation:

$$N_F \cdot N_B \cdot N_I \cdot N_P = 2560 \times \frac{10}{B(\text{MHz})} \quad (1.1)$$

The maximum number of frequency channels, set by the capacity of the on-line computer and software, is 256. As an example the channel separation is given in table 1.3 for each of the eight possible overall bandwidths available and for two rather extreme choices: (i) use of 91 interferometers in 4 polarization channels and 2-bit correlation mode for maximum sensitivity (e.g. for HI absorption and polarization studies), and (ii) use of all possible correlation products on, for instance, 10 interferometers in one polarization channel in 1-bit correlation mode for high spectral resolution. We also show a more common case of 40 interferometers in a 1-bit mode observing at 2 polarizations.

1.3.2 THE CONTINUUM BACKEND (DCB)

The digital continuum backend, DCB, is a broadband backend with a maximum total bandwidth of 80 MHz. This 80 MHz is divided in 8 bands of 10 MHz maximum width to avoid bandwidth smearing at the edges of the maps.

The 8 frequency bands are independent in the sense that each of them can be set to either 5 or 10 MHz width and that they can be tuned independently over the whole frequency range available (table 1.2) with the restriction that the IF bandwidth is limited to a maximum of about 110 MHz at all frequencies. For 49 cm only 2.5 and for 92 cm only 5 MHz **total** bandwidth are available. In most practical cases there is no need to use the DCB at 49 and 92 cm and so the DXB is used for continuum observations at these wavelengths.²

The DCB has a total of 4096 interferometer channels, or 512 channels per band. For each band these 512 channels are divided over the telescopes in the same, fixed, way. This is different from the DXB for which the division of channels over the telescopes can be chosen by the user.

The 512 channels are 256 complex channels (256 pairs of cos and sin correlations). These are divided in 160 standard and 96 non-standard complex channels. The standard channels comprise all the fixed-movable telescope (*i.e.* the standard baselines) and all polarization combinations.

The non-standard channels are used to determine telescope errors using the baseline redundancy in the non-standard baselines. Therefore enough correlated power must be available in the non-standard baselines; for this reason the cross-channels (XY and YX) are not used. The 96 available non-standard channels are divided over 47 XX and 47 YY combinations. For the WSRT there are 51 independent non-standard baseline combinations possible for each polarization. Interferometers 0-5, 0-6, 1-6 and 1-7 are not measured in this case.

1.3.3 VERY LONG BASELINE INTERFEROMETRY (VLBI)

Any combination of the WSRT dishes can be used as a 'tied array' to serve as one station in the VLBI network. Two types of VLBI backends are available: The narrow-band Mark2 system and the wide band Mark3 system. Input to the recording terminals is from one of the normal WSRT backends: the DXB in combination with the MK2 and the DCB in combination with the MK3. It is possible to observe with two polarization channels simultaneously with the MK3 system. With the MK2 system one can switch between polarizations but one cannot observe them simultaneously.

²In the near future a DCB configuration for 92 cm will become available. It is then possible to cover 40 MHz total bandwidth in 8 bands each with a width of 5 MHz

1.4 FUTURE DEVELOPMENTS

1.4.1 PULSAR FILTERBANK

In the autumn of 1993 a new backend will become available. This backend is especially designed for work on pulsars. In the near future specifications will be published in this documentation.

1.4.2 THE DZB BACKEND

In the future the DZB correlator will replace the DCB and DLB/DXB backend. The most important improvement over the previous backends is that:

- it will provide adequate $< 1\%$ spectral resolution for spectral line observations with bandwidths ranging from 160 MHz down to 156 kHz.
- it will measure all redundant baselines to enhance dynamic range and sensitivity.
- it will extend the continuum bandwidth by a factor 2 to 160 MHz.
- it supports a tied array mode for VLBI and pulsar observations.
- it will support gating facilities for pulsar observations and interference suppression.

More details of the DZB can be found in the NFRA internal technical report by Bos (1993).

1.4.3 THE MULTIFREQUENCY FRONT ENDS

In 1996 the multi frequency front ends (MFFE's),(ready in 1996/97), will replace the current 6, 21, 49, and 92 cm frontend boxes in all 14 telescopes. The frequencies at which these frontend will be able to operate are shown below. More information about the MFFE's can be found in the note by Tan (1990)

wavelength (cm)	frequency (MHz)	System Temp. (K)	Bandwidth (MHz)
92	305-386	<120	>10
49	608 ± 2	<100	>10
21	1200 - 1450	27	160
18	1590 - 1750	26	160
13	2215 - 2375	52	160
6	4770 - 5020	53	160
3.6	8150 - 8650	84	160
UHF low	250 - 460	<150	>10
UHF high	700 - 1200	<100	>10

THE CALCULATION OF THE SENSITIVITY

2.1 SENSITIVITY CALCULATIONS

In this section we will give all parameters necessary to calculate the thermal (*i.e* receiver) noise expressed in flux density.

2.1.1 CALCULATING THE SENSITIVITY FOR A STANDARD SETUP

To facilitate noise estimates we reduced equation 7.20 of part II by including the properties of the WSRT and giving only a wavelength dependent constant which relates the noise per channel for a 12 h observation, ΔS_{rms} , to the number of polarizations, N_P , and noise equivalent bandwidth, $\Delta\nu_{kHz}$. We assume a standard 12 hour synthesis observation using the 38 different movable-fixed telescope combinations:

$$\Delta S_{rms} = \frac{K_\lambda}{\sqrt{\Delta\nu_{kHz} N_P}} \text{mJy} \quad (2.1)$$

The factor $K(\lambda)$ is tabulated below.

λ	6	21	49	90
K_λ	28	17	42	50

$K(\lambda)$ is valid for 49 and 92 cm if the correlation is done in 1-bit mode, and, for 6 and 21 cm if correlation is done in 2-bit mode. For 21 cm we calculated the sensitivity per channel in table 2.4. Note that the noise equivalent bandwidth for a uniform taper equals the channel separation ($b = B/N_F$, where B is bandwidth and N_F is the number of frequency channels.), for a Hanning taper the noise equivalent bandwidth equals $8b/3$. For 92 observations the actual noise in a single 12 h continuum observation is not determined by the thermal noise, but by confusion from sources in the field and sidelobes.

A standard way to increase the sensitivity for low surface brightness structures is to convolve the images to lower frequency or spatial resolution. In the former case the noise decreases as $\sqrt{\frac{\Delta\nu_{convolved}}{\Delta\nu_{original}}}$

The case of spatial smoothing is somewhat more complicated. We must now consider the r.m.s. error in the brightness temperature, δ_T , and the noise in the observed flux, ΔS .

Lowering the resolution implies increasing the beam area, but at the same time effectively decreasing the number of interferometers which contribute to the image.

Hence the noise in the measured flux will increase with a factor proportional $\sqrt{\frac{N_{old}}{N_{new}}}$. Increasing the beam area will decrease the noise in the temperature brightness, determined from a given flux per beam, by a factor proportional to $\sqrt{\frac{\Omega_{A_{new}}}{\Omega_{A_{old}}}}$, where Ω_A is the beam area.

Hence the error in the brightness temperature does not simply decrease as $\sqrt{\frac{\Omega_{A\text{new}}}{\Omega_{A\text{old}}}}$, but as $\sqrt{\frac{\Omega_{A\text{new}}}{\Omega_{A\text{old}}}} \cdot \sqrt{\frac{N_{\text{old}}}{N_{\text{new}}}}$.
If N the number of (non-redundant) baselines going into the map then

$$\Delta S(\text{mJy}) \propto \frac{1}{\sqrt{N}} \quad (2.2)$$

$$\delta T(\text{K}) \propto N^{3/2} \quad (2.3)$$

2.1.2 CALCULATING THE SENSITIVITY FOR A NON-STANDARD SETUP

The r.m.s. noise in the measured flux, ΔS , can be written according to equation 7.21 (part II) as :

$$\Delta S = M P_s \sigma = \frac{M}{\sqrt{N_P}} \frac{D}{\eta_g \sqrt{N_I}} \frac{k}{2\eta_a A_T} \frac{T_S \sqrt{2}}{\sqrt{\Delta\nu t}} \quad (\text{Watts m}^{-2}\text{Hz}^{-1} = 10^{26}\text{Jansky(Jy)}) \quad (2.4)$$

where:

k =Boltzmann's constant ($1.38 \times 10^{-23} \text{Joule K}^{-1}$)

T_s =Interferometer system temperature (K), equal to $T_s = \sqrt{(T_F + T_A)(T_M + T_A)}$ where T_F and T_M are the noise of the fixed and the movable receiver respectively and T_A is the antenna temperature due to the noises in the field. T_A is closely similar for all fixed and movable receivers.

η_a =aperture efficiency

A_T =geometrical surface area of an individual antenna (m^2)

N_P =Number of polarization channels

P_s =Polarizations summation factor ($=\frac{1}{\sqrt{N_P}}$).

M =dipole position angle factor

D =degradation factor with respect to analogue correlation, due to analogue to digital conversion.

N_I =Number of interferometers.

$\Delta\nu$ =the noise equivalent bandwidth of the observation (Hz)

η_g =grading efficiency factor

t =total observing time (seconds)

REMARKS ON EQUATION 2.4

– **System temperature** T_s and η_a are given in the table 2.1. The system temperature of the interferometer is the effective temperature for an interferometer consisting of one cooled and one uncooled receiver. At 6 and 21 cm this is the way how the interferometers are formed (fixed/uncooled with movable/cooled receiver). At 49 and 92 cm the system temperature of the fixed receiver equals that of the movable receiver $T_M = T_F$.

– **Degradation factor** The degradation factor is given in table 2.2

– **Noise equivalent bandwidth, $\Delta\nu$**

The noise equivalent bandwidth, $\Delta\nu$ for continuum observations is equal to 0.93 times the bandwidth of the observation (at 20 dB points). This is a good estimate of the bandwidth between the 3db points of the filter.

For line observations we have the possibility of using different frequency tapers. (more properties of frequency tapers can be found in chapter 8 of part II).

1. The uniform taper

In this case the noise equivalent bandwidth, $\Delta\nu = B/N_F$ and the grading factor, $\eta_g = 0.9$ The effective frequency resolution for a uniform taper is $1.2B/N_F$.

2. **The Hanning taper** In this case the noise equivalent bandwidth, $\Delta\nu = 2.67B/N_F$ and $\eta_g = 1.47$. The effective frequency resolution for a Hanning taper is $2B/N_F$.

Wavelength (<i>cm</i>)	6	18	21	49	92
Frequency range (<i>MHz</i>)	4770-5020	1590-1730	1365-1425	607-610	305-385
System Temperature (<i>K</i>)					
cooled frontend	55	60	35	-	-
uncooled frontend	150	-	90	110 [†]	140 [†]
interferometer	91	60	56	-	-
η_a	0.48	0.53	0.53	0.59	0.59

[†]: only on the coolest regions of the sky.

Table 2.1: System temperature and antenna efficiency, for the different WSRT observing wavelengths.

Number of bits correlated	Degradation factor with respect to analog system	Number of correlator channels per correlator output (N_B)	Remarks
1×1	1.57	1	–
1×1.5	1.44	1	for $B=10$ MHz
1×2	1.32	1	for $B \leq 5$ MHz
2×1.5	1.21	2	for $B=10$ MHz
2×2	1.12	2	for $B \leq 5$ MHz

Table 2.2: The correlator modes. The degradation factor corresponds to the increase in effective temperature as compared to an analog correlator

3. The Hamming taper

In this case the noise equivalent bandwidth, $\Delta\nu = 2.52B/N_F$ and $\eta_g = ???$. The effective frequency resolution for a Hanning taper is $1.82B/N_F$.

where N_F is the number of frequency channels. Note that while the noise per frequency channel decreases, the number of independent frequency points rises. Also note that the first channel and the last 7% of the frequency channels lie on the edge of the bandpass and the S/N there is worse than calculated with the formulæ above. B/N_F is tabulated in table 2.3.

The properties of the tapers are described in section 8 of part II.

- The r.m.s. error in the observed flux ΔS in a single 12 hour continuum observations at 92 cm is higher than calculated from equation 7.21. At this wavelength sidelobe confusion noise becomes the limiting factor for sensitivity in **total intensity** (Stokes I). The theoretical sensitivity can be reached in Stokes Q , U and V in a single 12 hour observation and also Stokes I if sidelobe confusion is suppressed by observing for 4×12 hours with different 9A spacing.
- By using redundant spacings in an image (often available for 49 and 92 cm observations but also possible for 6 and 21 cm observations) it is possible to obtain better sensitivity than calculated with the formula above at the expense of a non-uniform u, v coverage, *i.e.* a dirty beam.

Exact sensitivity calculations can be performed but one has to take in to account that for 6 and 21 cm the system temperatures differ for different sets of interferometers. There is one set (standard telescope combinations) with cooled-uncooled interferometers and one set (non standard combinations) with only uncooled-uncooled interferometers.

noise equivalent bandwidth, $\Delta\nu$ (KHz), for uniform frequency taper								
N_F	Bandwidth, B , (kHz)							
	10	5	2.5	1.25	0.625	0.313	0.156	0.078
8	1250	625	313	156	78	39	20	10
16	625	313	156	78	39	20	10	5
32	313	156	78	39	20	10	5	2.4
64	156	78	39	20	10	5	2.4	1.2
128	78	39	20	10	5	2.4	1.2	0.6
256	39	20	10	5	2.4	1.2	0.6	0.3

noise equivalent bandwidth, $\Delta\nu$ (KHz), for Hanning frequency taper								
N_F	Bandwidth, B , (kHz)							
	10	5	2.5	1.25	0.625	0.313	0.156	0.078
8	3338	1669	834	417	209	104	52	26
16	1669	834	417	209	104	52	26	13
32	834	417	209	104	52	26	13	6.5
64	417	209	104	52	26	13	6.5	3.3
128	209	104	52	26	13	6.5	3.3	1.6
256	104	52	26	13	6.5	3.3	1.6	0.8

Table 2.3: Noise equivalent, $\Delta\nu$ bandwidth with uniform taper (top) and with Hanning taper (bottom).

channel separation $b = \frac{B}{N_F}$ (kHz)								
N_F	Bandwidth, B , (MHz)							
	10	5	2.5	1.25	0.625	0.313	0.156	0.078
8	1250	625	313	156	78	39	20	10
16	625	313	156	78	39	20	10	5
32	313	156	78	39	20	10	5	2.4
64	156	78	39	20	10	5	2.4	1.2
128	78	39	20	10	5	2.4	1.2	0.6
256	39	20	10	5	2.4	1.2	0.6	0.3

channel separation $b = \frac{B}{N_F}$ (kHz)	velocity per channel (km/s)	velocity resolution FWHM (km/s)		r.m.s. noise per channel 12 h obs. (mJy)	
		Uniform	Hanning	Uniform	Hanning
1250	264	317	528	0.48	0.29
625	132	158	264	0.68	0.42
313	66	79	132	0.96	0.59
156	33	40	66	1.36	0.83
78	17	20	33	1.9	1.2
39	8	10	17	2.7	1.7
20	4	5	8	3.8	2.4
10	2.1	2	4	5.4	3.3
5	1.0	1.2	2.1	7.7	4.7
2.4	0.5	0.6	1.0	11	6.7
1.2	0.26	0.31	0.5	15	9.4
0.6	0.13	0.15	0.26	22	13
0.3	0.06	0.08	0.13	31	19

Table 2.4: Noise per channel for 21 cm observations with Uniform or Hanning taper. b is the channel width and can be found in the upper panel as a function of total bandwidth B and number of used frequency channels, N_F . Calculations were done for 2 bit mode ($N_B = 2$) and one polarization ($N_P = 1$) and assuming a 12^h synthesis observation with 38 interferometers.

SPECIFYING THE BACKEND SETUP

3.1 CHOOSING THE INSTRUMENTAL SETUP

The instrument can be used in so many different ways that it is important to consider which setup best serves the scientific needs of the observing program. For continuum observations one would usually observe in the standard setup, providing 4 polarizations, standard and non-standard baselines and the widest possible bandwidth. For line observations one has to tailor the frequency resolution, total bandwidth, number of polarizations and number of interferometers to the particular needs of the observing program.

The following sections are meant to provide an overview of the different possibilities and serve as a guide for choosing the setup of your observation.

3.2 THE SETUP FOR LINE OBSERVATIONS

For line observations the DXB spectral line backend is used. The basic number of independent complex 1-bit correlations the DXB can produce simultaneously is 2560. In 2-bit mode the correlator produces half the number of products (1280) with a sensitivity improved by approximately 1.4. (This number comes from digital correlator theory, in practice increasing the bitmode will not improve the sensitivity by 1.4 but by a factor of about 1.3) When the observed spectrum can be covered adequately in an overall bandwidth, B , narrower than its maximum value (10 MHz), the clockrate of the correlator (20MHz) allows the number of correlation products obtained in one integration time to be increased by a factor $10/B$ to a maximum of 40960 (B decreased from 10MHz in steps of 2). The number of complex channels, obtained after Fourier transformation of the correlation function, may be distributed over interferometers and polarization and frequency channels. How one chooses to do this depends not only on the spectral resolution required but also on the sensitivity required per frequency point (= complex channel). Sensitivity may be increased by changing the correlator's bit-mode, but also by observing the same spectrum simultaneously in two independent polarization channels.

The number of independent frequency channels, N_F , in each observed spectrum depends on the overall bandwidth B (MHz), the correlator bit-mode, N_B (1 or 2), the number of interferometers, N_I , and the number of polarization channels, N_P , are related as:

$$N_F \cdot N_B \cdot N_I \cdot N_P = 2560 \cdot \frac{10}{B(\text{MHz})}$$

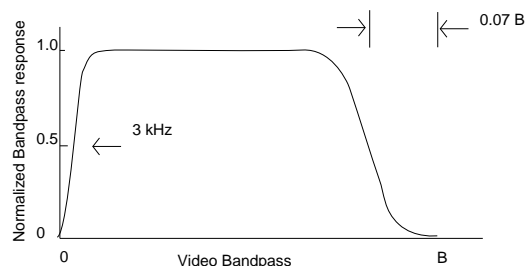
Below we give a general procedure for selecting the appropriate setup for a line observations. Remember that the product of N_I , N_F , N_B and N_P should be equal or less than $25600/B$.

Step I

Choose the a total bandwidth, B , which covers the entire velocity range of interest. When doing this one should remember that a certain number of the N_F frequency channels distributed over B are not

usable because of the tapering by the IF unit bandpass filter and because of the time to frequency Fourier transform (see section 8).

First note that frequency channel 0, the first frequency point, samples the frequency at a video frequency of 0Hz and thus never contains any phase information. Because this data is useless, the on-line computer at Westerbork deletes the data and replaces it by an average of the values found in the remaining $N_F - 1$ channels. Thus the data in frequency channel 0 is called the continuum emission over the bandwidth B (with tapered edge). Some of the remaining $N_F - 1$ frequency points are also not usable.



Due to the shape of the IF bandpass filter the first frequency channel cannot be used if a Hanning taper is used. The last frequency points ($\approx 7\%$ of the N_F channels) drop below the 3dB point of the band and thus have a greatly increased noise.

Note: radio frequency scales different with frequency channel for different wavelengths. At 6 and 21 cm increasing frequency channel number corresponds to decreasing radio frequency. At 49 and 92 cm increasing frequency channels correspond to increasing radio frequencies.

Also note that the central velocity (or corresponding frequency) specified by the astronomer is assigned by the Westerbork on-line computer to the central frequency channel of the $N_F - 1$ frequency channels with phase information. (e.g. for an observation with $N_F = 32$, channel 16 would be at the specified frequency). However, because the limitations above, this channel does not correspond to the center of the usable part of the frequency band. The astronomer should take this fact into consideration when specifying the velocity of the observation.

Remember that the maximum number of frequency channels, N_F , is 256.

Step II

Choose the number of frequency channels, N_F such that the effective resolution in frequency, $\Delta\nu$, is enough to see the line in a few noise independent channels ($\leq 3-5 \sigma$). The effective resolution in frequency is related to the type of taper chosen for the time-frequency transform. At present three different types of taper may be specified by the astronomer.

1. **Uniform taper** (or no taper) yields a synthesized bandpass per frequency channel which has a frequency resolution, $(\Delta\nu)_{RES}$, full width half maximum (FWHM) of $1.2 \frac{B}{N_F}$, where $\frac{B}{N_F}$ is the increment in frequency channel. The synthesized bandpass has a negative side lobe of 23% of the main beam response, so the noise power bandwidth per frequency channel, $\Delta\nu$, which is the parameter needed for calculations of the r.m.s. sensitivity in a line channel (section 2 of part III), is equal to B/N_F . Each frequency channel of a uniformly tapered observation has a noise distribution which is essentially uncorrelated with the noise distribution in any other frequency channel. However, use of uniform taper can lead to a substantial amplitude and phase ripple (up to $\sim 18\%$ between adjacent channels) in the frequency spectrum. This ripple is a sidelobe effect caused by the existence, in the data, of phases different from zero which make the sampling of the time correlation function asymmetrical. The non-zero phases can be due to both the use of improper on-line phase zero correction values and *emission from sources away from the field center*. Thus the observations made with uniform taper should be approached with caution.
2. **Hanning taper** yields a synthesized bandpass per frequency channel which has a frequency resolution $(\Delta\nu)_{RES}$ (FWHM) of $2 \frac{B}{N_F}$ but the first negative sidelobe is now reduced to 2.5% of the main beam response. Because of the smaller negative sidelobes, the noise power bandwidth, $\Delta\nu$, per frequency channel is increased to $2.67 \frac{B}{N_F}$. However adjacent frequency channels of Hanning tapered observation have correlated noise distributions and one does not obtain a \sqrt{N} reduction in the noise by averaging N adjacent channels together. In fact, if one wished to reduce the noise by averaging every second channel together, one obtains a noise reduction of 1.2 instead of the $\sqrt{2}$ reduction that should occur if the channels would be completely independent; however for purposes of detecting a line we can consider every second frequency point to be an (almost)

independent point. Hanning taper does have the advantage that the amplitude and phase ripple is reduced to $< 0.5\%$.

3. **Hamming taper** yields a synthesized bandpass per frequency channel which has a frequency resolution $(\Delta\nu)_{RES}$ (FWHM) of $1.81 \frac{B}{N_F}$ and the first negative sidelobe is now reduced to 0.7% of the main beam response. For this taper the noise in adjacent channels is also correlated.

Tapers are also discussed in chapter 8 “Effects in Fourier Transformed spectra” in part II and by Harris (1978)

Step III

You should always start choosing the number of standard interferometers as large as possible ($N_I = 40$). If the source is strong then detection of small spatial structures will be possible with a low bit-mode and only one polarization. If complex channels are still available you may choose to increase the number of polarizations or to increase the bit-mode. For increasing the sensitivity, adding the cross polarizations, XY and/or YX, is in most cases not useful unless polarization is to be measured in the line.

Only if the source is weak and extended you should invest the complex channels to increase the sensitivity rather than to use the maximum spatial resolution. In this case you should first use a thinned array (say $N_I = 10$) and then try to increase the number of polarizations to be measured to 2 (XX and YY) and try to increase the bitmode.

If complex channels are still available you can increase the number of interferometers to increase both sensitivity and spatial resolution.

Other considerations

When choosing the baseline, bitmode or polarization you should consider the following:

- For most line observations the 1×2 correlator-mode (bit-mode, degradation factor=1.338) can usually be used. Changing the bit mode to 2 (2×2) only gives an increase in sensitivity of 1.2 as the degradation factor drops to 1.116. The maximum increase in sensitivity is 1.4 (when going from 1×1 to 2×2 correlation mode the corresponding degradation factors change from 1.57 to 1.12). However, the values above are theoretical ones and in practice the increase in sensitivity is lower.
- The increase in the number of polarization channels from 1 to 2 gives an increase in sensitivity of $\sqrt{2}$. (If $N_P = 1$ XX or YY are used, if $N_P = 2$ XX and YY is used.) Increasing the number of polarizations to 4 does not increase the sensitivity any further. $N_P = 4$ should only be chosen for polarization measurements.
- If 2 polarizations are used, one does not loose an entire baseline if one channel in a particular receiver fails for some reason.
- Adding a movable telescope increases the number of interferometers by a factor 2. (e.g. table 3.1
- Try to choose baseline combinations which minimize the possibility that one telescope will look into the back of another. The amplitude and phase of particular interferometer pairs will then be affected. Shadowing is discussed further in chapter 9.
- Choose an appropriate 9A spacing. The advantage of the 36 m spacing is that very extended structure is somewhat better visible. The advantage of a 72 m spacing is that one can have more redundant spacings (continuum). The advantage of the 54 m spacing is that $\int_{\Omega} A_N(\Omega) d\Omega$ is well defined within the first grating ring.

Also see the discussion in chapter 8, “WSRT Beams”, of part III.

The following two observing sequences would result in the same u, v coverage.

day 1	0-9	with A	Sequence 1
day 2	0-9	with B	
day 1	1,3,5,7,9	with A,B	Sequence 2
day 2	0,2,4,6,8	with A,B	

Approximate longest baseline	Fixed telescopes used	Movable telescopes used	N_I
5×144	5–9	A	5
10×144	0–9	A	10
19×144	0–9	A,C	20
10×72	5–9	A,B	10
20×72	0–9	A,B	20
38×72	0–9	A,B,C,D	40

Table 3.1: Some possible baseline and telescope combinations

If residual errors do appear in the resulting maps, the causes of the errors are much easier to find if the first sequence is used. We can generally expect the cause of the error to be associated with A on day 1 or B on day 2. Use of the second sequence, however, could mean that a residual error might be associated with A or B on day 1 or A or B on day 2 so four different possibilities have to be investigated. However, one should note that if something is slightly wrong with one of the movable telescopes on only one of the two observing days then only 1/4 of the data is affected if sequence B is used. Since bad data only has 1/4 weight, a residual effect in the maps might lie below the noise and thus might not be visible. In the first sequence, each day gets 1/2 weight and consequently, any error will always be more visible.

Thus the first configuration implies a more visible error that should be relatively easy to track down. The second configuration implies a source of error which, if one is lucky, may not be visible in the map. For the astronomer, the choice is not clear cut. If strong sources are expected in the field, sequence 1 is to be preferred as errors may be visible in any event. If only weak sources are expected then sequence 2 may be a valid choice.

The above discussion is applicable to situations where we may have to find the causes of particular errors visible in maps. We should point out however, that most important varying gain and phase errors are constant over the frequency spectrum. Often we want to produce channel maps of just line radiation. Usually this is done by subtracting off a continuum map made by averaging together frequency channels from the outer parts of the frequency range which are devoid of line radiation. Subtraction of a continuum map which has gain or phase errors usually results in a linemap with the same relative errors, which are much less visible since the line radiation is often much weaker than the continuum radiation.

Such line maps may be acceptable for further analysis without the necessity of making an additional calibration correction.

3.2.1 EXAMPLES

- We want to observe a galaxy in HI. First we have to choose a bandwidth. If the velocity differences in the galaxy are about 300km/s (an average inclination of 45°) we need a bandwidth of 5MHz.

The number of available complex correlation channels will now be 5120.

To make a reasonable rotation curve we will need approximately 128 channels. (The effective resolution using a uniform taper will then be ≈ 10 km/s)

Now 40 complex channels may be divided over N_I , N_P and N_B . If we have a strong source we can choose to observe with high spatial resolution (we might discover something special) in that case we would choose $N_I \times N_P \times N_B = 40 \times 1 \times 1$.

If we do not expect the signal to be strong we choose for a thinned array (0.9 AB, 1500m) and two polarization channels. $N_I \times N_P \times N_B = 20 \times 2 \times 1$. Although the sensitivity does not decrease or increase one can determine the brightness temperature with higher accuracy than in the former case. This is due to the spatial smoothing which occurs when the array is thinned. (Also see page 2-5)

- We want to observe polarization in a Galactic object with internal velocity differences of 60 km/s. Remember that to determine velocity profiles additional continuum channels are needed. We choose a bandwidth of 0.625 MHz so we cover 132 km/s.

With a bandwidth of 0.625 MHz the number of available complex correlator channels is 40960. But because we want to measure polarization we have to take $N_P=4$. This leaves 10240 complex channels. Because generally structures in Galactic clouds do not exceed sizes of order 1 arcminute we can observe the source using the thinned array (without telescopes CD) so N_I becomes 20. This leaves us with 512 complex channels.

We can now take $N_F = 256$ and $N_B = 2$ and so obtain the highest possible sensitivity with enough spectral resolution.

3.3 THE SETUP FOR CONTINUUM OBSERVATIONS

For continuum observations the DCB can be used. As we know from section 1.3.2 the DCB is mostly used for 6 and 21 cm continuum observations.

For 49 and 92 cm the DXB is used for continuum observations. That is because there is not enough IF bandwidth available (2.5 and 5 MHz or 49 and 92 cm respectively)¹.

Below we summarize how to choose the instrumental setup for 6 and 21 cm continuum observations.

Step I

Choose the width and central position of the 8 frequency bands. There are default settings for these but other values can be specified. It is for instance possible to tune bands over the total available frequency range and set the width of the band individually to 5 or 10 MHz. However, due to limitations of the IF the total bandwidth of the observation may not exceed 130 MHz.

The default setting for 6 cm continuum observations is: 8 bands of 10 MHz with a central frequency of $\nu = 4939 + k 10$ MHz with $k = 0, \dots, 7$.

For 21 cm continuum observation the default setting is to organize the 8 bands in the following way:

band no.	1	2	3	4	5	6	7	8
bandwidth	5	10	10	5	10	10	10	5
central freq.	1423.5	1415.0	1405.0	1397.5	1395.0	1385.0	1375.0	1367.5

Step II

Choose the baseline separation 9A. If shadowing is unimportant ($\delta > 40^\circ$) then 9A will generally be a good choice.

When specifying 49 and 92 cm continuum observations one should follow the outline sketched for the specification of line observations in the previous section (section 3.2). Keep in mind however that when you are using the redundant configuration, the default for continuum observations, the limitation on the number of used complex correlator channels becomes.

$$N_F N_B \cdot ((N_I N_P)_{\text{standard}} + (N_I N_P)_{\text{non-standard}}) = 25600/B(\text{MHz})$$

It is possible to change the telescope setting (the redundant baselines used). But the default settings are the same for the continuum observations. *i.e.*: The standard (ST) channels are divided over all the fixed-movable telescope and all polarization combinations. The non standard (NS) channels are divided over 47 XX and 47 YY telescope combinations, all fixed-fixed combinations except 0-5, 0-6, 1-6 and 1-7 are measured.

¹Possibilities for the placement of 8 DCB bands of 5 MHz width in the 92 cm band will be investigated in the fall of 1993

bandwidth	bitmode	nr of freq points	nr of pola- rizations	correlator
≤ 10	1	32	1	DLB
≤ 5	1	32	2	DXB
≤ 5	1	128	1	DXB
≤ 5	2	64	1	DXB
≤ 2.5	1	32	4	DXB
≤ 2.5	1	128	2	DXB
≤ 2.5	1	256	1	DXB
≤ 2.5	2	64	2	DXB
≤ 2.5	2	128	1	DXB
≤ 1.25	1	128	4	DXB (20 sec)
≤ 1.25	1	256	2	DXB (20 sec)
≤ 1.25	2	64	4	DXB
≤ 1.25	2	128	2	DXB
≤ 1.25	2	256	1	DXB
≤ 0.625	2	128	4	DXB (20 sec)
≤ 0.625	2	256	2	DXB (20 sec)

(20 sec) means that the minimum integration time is 20 seconds, else the minimum integration time is 10 seconds.

Table 3.2: Possible settings of DXB/DLB for autocorrelation mode

3.4 THE SETUP FOR OTHER MODES OF OPERATION

3.4.1 AUTOCORRELATION

Measuring with the WSRT in Autocorrelation mode is only possible in a limited sense with the DLB/DXB, and not at all with the DCB. For the DLB/DXB it is possible to operate with correlator configurations in which a part of the correlator channels is allocated to correlations of a receiver with itself.

POSSIBILITIES Table 3.2 lists all possibilities for autocorrelation. In these configurations all of the 14 telescopes are auto correlated.

If not all telescopes are needed, the constraints in the table can be relaxed, however the maximum number of frequency points remains 256.

In all cases the rest of the backend channels is filled with cross correlation channels.

DIFFERENCES WITH RESPECT TO CROSS CORRELATION. Transformation from correlation values into spectra is not differently from cross correlation, however because the auto correlation spectrum is symmetric, the phase will be zero after the transform, so all sine values of autocorrelation spectra will be zero, and the cosine values will contain the spectral line intensity and the receiver bandshape.

The on-line system normalizes the autocorrelation channels different from cross correlation channels because of the larger correlation coefficients involved.

For autocorrelation 1 Westerbork unit is equal to 100 mJy. Especially for auto correlation observations the frequency switch option can be used.

For this option both frequency synthesizers are used. Frequency switching occurs per integration time, during the even integration periods the system observes at the specified frequency, but during the odd integration times, the system observes at a frequency that differs by a specified frequency step size. The switching itself is triggered by the UT clock at the very begin of the first 10 sec period of the integration, and does not damage the data for that period.

REDUCTION OF AUTO CORRELATION OBSERVATIONS. There is no special software for reduction of autocorrelation data in Westerbork or Dwingeloo.

In principle the frequency switched observations can be used for correction of the bandshape. Observations in this mode have been reduced in Leiden.

3.4.2 PULSAR OBSERVATIONS WITH THE DCB.

POSSIBILITIES. The DCB can be used to map fields of known Pulsars.

This correlator distributes its channels over 8 bands, which are normally used to cover different frequency bands, but these bands can also be used to cover different phases of the period of a Pulsar, while the frequency of the bands are set to exactly the same value.

The basic condition is that we know the period of the Pulsar, and that this period is more than about 60 milliseconds, so this system is not suitable for millisecond Pulsars.

In the DCB processor we have control over the data per 10/64 second, or 156.25 millisecond, so it is possible to integrate in band i only those periods of 156.25 milliseconds that are spaced by the apparent period of the Pulsar, and delete the others. The only difference between the bands is a difference in phase of the Pulsar period.

Without knowing the exact arrival time of the pulses, we can be sure that there are some empty bands, and some bands containing the pulsed signals, at least if the Period is not larger than 1.25 second. Because the fixed period of 156.25 milliseconds will never be matched to the Pulsar period, the peak will generally be distributed over at least 2 bands, but for identifying which source is the Pulsar, this is no problem.

The basic configuration as explained above is ideal for Pulsar periods between 0.6 and 1.25 seconds, but by choosing different configurations, using blanking within the 156.25 milliseconds, or combining bands, it is possible to extend the range of observable Pulsars period to a minimum of about 60 milliseconds, and no maximum.

OBSERVATIONS. Usually Pulsar observations are done at 49 and 92 cm, with all DCB bands at the same frequency, and a bandwidth of 5 MHz. For each 10 sec period, the apparent period of the Pulsar is calculated, taking into account the Earth's Doppler motion and the present epoch Pulsar period, and a table is constructed, telling the DCB processor for each band and each of the 64 periods in the 10 sec when to integrate, and when to skip the data. This information (for the next 10 sec) is then sent to the DCB processor.

After reading the data (once per 10 sec), the data must be normalized, using the table information, and can then be treated as a normal DCB observation.

REDUCTION. The data can be calibrated as a normal observation. Maps must be made of each band separately, and the difference between maps must be inspected for any sign of the Pulsar. The difference maps are extremely sensitive for the Pulsar because all global errors, present in all maps are subtracted.

3.5 REFERENCES

Harris, F. (1978): 'On the use of windows for Harmonic analysis with the discrete Fourier Transform' *Proc IEEE*, **66** no.1, pp. 51-83.

POLARIZATION MEASUREMENTS WITH THE WSRT

4.1 DESCRIPTION

A four channel correlation interferometer with linearly polarized feed horns such as Westerbork measures the Fourier transformations of 4 Stokes parameters, I , Q , U and V which completely specify the properties of the incident electromagnetic wave. I is the total intensity of radiation, Q and U specify intensity and position angle of the linearly polarized component of the wave and V gives the amount of circular polarization. For all radiation I is always positive definite and $I^2 \geq Q^2 + U^2 + V^2$ must hold. ($I^2 = Q^2 + U^2 + V^2$ only applies in the case of 100% polarized signal.) Because of the vector nature of linear polarization, it can be represented in either a Cartesian coordinate system (Q and U), or a polar coordinate system (P (or m) and P_A).

Q and U can be either positive or negative and although the orientation of the coordinate system in which they are defined is in principle arbitrary, by convention Q is defined to be positive at position angle 0° on the sky (North). Because a linearly polarized vector has an ambiguity of 180° instead of the normal 360° , measurements of Q and U taken with a single perfectly linearly polarized dipole feed would show the following:

Dipole Position Angle on the sky	Stokes Parameter measured
0°	$+Q$
45°	$+U$
90°	$-Q$
135°	$-U$
180°	$+Q$
225°	$+U$
270°	$-Q$
315°	$-U$

P (or m) and P_A are the quantities usually found specified in the literature. P ($= \sqrt{Q^2 + U^2}$) is the intensity of the linearly polarized component of the radiation. P is always positive and does not have a normal noise distribution because it is determined from squared quantities, m is usually used to represent the fractional polarization so that $P = mI$. (Thus, Percentage Polarization = $100m$.) P_A ($= \frac{1}{2} \arctan(U/Q)$) is the position angle of the linear polarization angle. As had been mentioned above, it has a 180° ambiguity. The direction defined as $P_A = 0^\circ$ is, of course arbitrary, but it is invariably taken to be position angle 0° on the sky *i.e.* the North. The P_A is measured positive through East (90°) and is usually specified between $0^\circ - 180^\circ$.

V , the Stokes parameter specifying the circular polarization of the incident wave, can also be either negative or positive. The magnitude specifies the intensity of the circular polarization and the sign gives the handedness. Again, the sign convention is in principle arbitrary and, in fact, considerable confusion often exist as to what should be used. The convention usually adopted is to represent right hand circularly polarized radiation as defined in radio engineering as $+V$ — *i.e.* a right circularly polarized wave approaching the viewer has its electric vector continually increasing in position angle (rotating counter-clockwise). Except for intense coherent sources of radiation such as pulsars, maser line sources, flare stars, and solar system objects (Jupiter and the Sun), V has been found in all cases to be very small ($\lesssim 0.002I$). Thus, in most types of observation with the WSRT it is possible to assume $V = 0$.

4.2 DEFINITIONS

The telescope feed system on all of the Westerbork telescopes at all frequencies consists of perpendicular linearly polarized probes designated X and Y. In the backend correlation system for Westerbork all 4 possible combinations of these channels can be produced for each interferometer — *i.e.* XX, XY, YX, YY. All feeds can be rotated through at least 45° of position angle on the sky. **However**, due to historical accidents, design constraints, and, occasionally, maintenance errors, the direction of rotation of the feeds, the definition of which is dipole channel X and which dipole channel Y and what the position angles of the dipoles on the sky are for a given observation can vary with receiver, frequency, version of retrofit (a reduction program), etc. For this reason, a method for determining the polarization response of an interferometer for any dipole configuration is given here. Although examples are given for the most common observing configurations, in case of doubt the observer should determine the position angles of the sky actually used for his observation and perform his own solutions. It is important to keep in mind that due to the equatorial mounting of the telescope the position angle on the sky is fixed during an observation.

Important: It should be kept in mind that almost all quantities ($I, Q, U, V, \epsilon, \eta, G$) discussed in this section are complex (vectors) and are usually described by an amplitude and phase. Only two quantities mentioned here (Δ, Θ) are scalars and they are only needed to explain the meaning of the vectors ϵ, η . Also all descriptions in this section are for quantities measured in the telescope (u, v ; Fourier) plane. The real plane of the sky is later obtained by Fourier transforming the corrected quantities.

- $+I$ =(complex; Fourier transform) Total Intensity
- $+Q$ =(complex; Fourier transform) Linear Polarization component = $P \cos(2P_A)$
- $+U$ =(complex; Fourier transform) Linear Polarization component = $P \sin(2P_A)$
- $+V$ =(complex; Fourier transform) Right Circular Polarization (IRE 1942 definition)
- $P = \sqrt{Q^2 + U^2}$ Linearly Polarized Intensity
- $P_A = \frac{1}{2} \arctan(U/Q)$ Linearly Polarized Position Angle
- G =(complex) gain factor
- $j = \sqrt{-1}$ (= phase shift over $\frac{\pi}{2}$ or 90°)
- ϵ =(complex) small instrumental term (= $\Delta^- - i\Theta^+$)
- η =(complex) small instrumental term (= $\Delta^+ - i\Theta^-$)
- Δ^- =(scalar) dipole setting error difference (= $\Delta_{RTWEST} - \Delta_{RTEAST}$)
- Δ^+ =(scalar) dipole setting error sum (= $\Delta_{RTWEST} + \Delta_{RTEAST}$)
- Θ^- =(scalar) dipole ellipticity difference(= $\Theta_{RTWEST} - \Theta_{RTEAST}$)
- Θ^+ =(scalar) dipole ellipticity sum(= $\Theta_{RTWEST} + \Theta_{RTEAST}$)
- χ =nominal position angle of the dipole
- $\chi^+ = \chi_W + \chi_E$
- $\chi^- = \chi_W - \chi_E$
- R =Right hand circular = $I + V$
- L =Left hand circular = $I - V$

After neglecting the second order terms the complex response of a polarization interferometer is given by:

$$R_{WE} = G (I(C^- - \epsilon S^-) + Q(C^+ - \eta S^+) + U(S^+ + \eta C^+) - jV(S^- + \epsilon C^-)) G'G'' \quad (4.1)$$

Position Angle		Gain	Stokes Parameters				Position Angle		Gain	Stokes Parameters			
RT_W	RT_E	G	$I \pm \epsilon$	$Q \pm \eta$	$U \pm \eta$	$V \pm \epsilon$	RT_W	RT_E	G	$I \pm \epsilon$	$Q \pm \eta$	$U \pm \eta$	$V \pm \epsilon$
0°	0°	$\frac{1}{2}$	+1	+1	+ η	- $j\epsilon$	180°	0°	$\frac{1}{2}$	-1	-1	- η	+ $j\epsilon$
0°	45°	$\frac{1}{4}\sqrt{2}$	+1+	+1-	+1+	+ $j-$	180°	45°	$\frac{1}{4}\sqrt{2}$	-1-	-1+	-1-	- $j+$
0°	90°	$\frac{1}{2}$	+ ϵ	+ η	+1	+ j	180°	90°	$\frac{1}{2}$	- ϵ	- η	-1	- j
0°	135°	$\frac{1}{4}\sqrt{2}$	-1+	-1-	+1-	+ $j+$	180°	135°	$\frac{1}{4}\sqrt{2}$	+1-	+1+	-1+	- $j-$
0°	180°	$\frac{1}{2}$	-1	-1	- η	+ $j\epsilon$	180°	180°	$\frac{1}{2}$	+1	+1	+ η	- $j\epsilon$
0°	225°	$\frac{1}{4}\sqrt{2}$	-1-	-1+	-1-	- $j+$	180°	225°	$\frac{1}{4}\sqrt{2}$	+1+	+1-	+1+	+ $j-$
0°	270°	$\frac{1}{2}$	- ϵ	- η	-1	- j	180°	270°	$\frac{1}{2}$	+ ϵ	+ η	+1	+ j
0°	315°	$\frac{1}{4}\sqrt{2}$	+1-	+1+	-1+	- $j-$	180°	315°	$\frac{1}{4}\sqrt{2}$	-1+	-1-	+1-	+ $j+$
45°	0°	$\frac{1}{4}\sqrt{2}$	+1-	+1-	+1+	- $j-$	225°	0°	$\frac{1}{4}\sqrt{2}$	-1+	-1+	-1-	+ $j+$
45°	45°	$\frac{1}{2}$	+1	+ η	+1	- $j\epsilon$	225°	45°	$\frac{1}{2}$	-1	- η	-1	+ $j\epsilon$
45°	90°	$\frac{1}{4}\sqrt{2}$	+1+	-1-	+1-	+ $j-$	225°	90°	$\frac{1}{4}\sqrt{2}$	-1-	+1+	-1+	- $j+$
45°	135°	$\frac{1}{2}$	+ ϵ	-1	- η	+ j	225°	135°	$\frac{1}{2}$	- ϵ	+1	+ η	- j
45°	180°	$\frac{1}{4}\sqrt{2}$	-1+	-1+	-1-	+ $j+$	225°	180°	$\frac{1}{4}\sqrt{2}$	+1-	+1-	+1+	- $j-$
45°	225°	$\frac{1}{2}$	-1	- η	-1	+ $j\epsilon$	225°	225°	$\frac{1}{2}$	+1	+ η	+1	- $j\epsilon$
45°	270°	$\frac{1}{4}\sqrt{2}$	-1-	+1+	-1+	+ $j+$	225°	270°	$\frac{1}{4}\sqrt{2}$	+1+	-1-	+1-	+ $j-$
45°	315°	$\frac{1}{2}$	- ϵ	+1	+ η	- j	225°	315°	$\frac{1}{2}$	+ ϵ	-1	- η	+ j
90°	0°	$\frac{1}{2}$	- ϵ	+ η	+1	- j	270°	0°	$\frac{1}{2}$	+ ϵ	- η	-1	+ j
90°	45°	$\frac{1}{4}\sqrt{2}$	+1-	-1-	+1-	- $j-$	270°	45°	$\frac{1}{4}\sqrt{2}$	-1+	+1+	-1+	+ $j+$
90°	90°	$\frac{1}{2}$	+1	-1	- η	- $j\epsilon$	270°	90°	$\frac{1}{2}$	-1	+1	+ η	+ $j\epsilon$
90°	135°	$\frac{1}{4}\sqrt{2}$	+1+	-1+	-1-	+ $j-$	270°	135°	$\frac{1}{4}\sqrt{2}$	-1-	+1-	+1+	- $j+$
90°	180°	$\frac{1}{2}$	+ ϵ	- η	-1	+ j	270°	180°	$\frac{1}{2}$	- ϵ	+ η	+1	- j
90°	225°	$\frac{1}{4}\sqrt{2}$	-1+	+1+	-1+	+ $j+$	270°	225°	$\frac{1}{4}\sqrt{2}$	+1-	-1-	+1-	- $j-$
90°	270°	$\frac{1}{2}$	-1	+1	+ η	+ $j\epsilon$	270°	270°	$\frac{1}{2}$	+1	-1	- η	- $j\epsilon$
90°	315°	$\frac{1}{4}\sqrt{2}$	-1-	+1-	+1+	- $j+$	270°	315°	$\frac{1}{4}\sqrt{2}$	+1+	-1+	-1-	+ $j-$
135°	0°	$\frac{1}{4}\sqrt{2}$	-1-	-1-	+1-	- $j+$	315°	0°	$\frac{1}{4}\sqrt{2}$	+1+	+1+	-1+	+ $j-$
135°	45°	$\frac{1}{2}$	- ϵ	-1	- η	- j	315°	45°	$\frac{1}{2}$	+ ϵ	+1	+ η	+ j
135°	90°	$\frac{1}{4}\sqrt{2}$	+1-	-1+	-1-	- $j-$	315°	90°	$\frac{1}{4}\sqrt{2}$	-1+	+1-	+1+	+ $j+$
135°	135°	$\frac{1}{2}$	+1	- η	-1	- $j\epsilon$	315°	135°	$\frac{1}{2}$	-1	+ η	+1	+ $j\epsilon$
135°	180°	$\frac{1}{4}\sqrt{2}$	+1+	+1+	-1+	+ $j-$	315°	180°	$\frac{1}{4}\sqrt{2}$	-1-	-1+	+1-	- $j+$
135°	225°	$\frac{1}{2}$	+ ϵ	+1	+ η	+ j	315°	225°	$\frac{1}{2}$	- ϵ	-1	- η	- j
135°	270°	$\frac{1}{4}\sqrt{2}$	-1+	+1-	+1+	+ $j+$	315°	270°	$\frac{1}{4}\sqrt{2}$	+1-	-1+	-1-	- $j-$
135°	315°	$\frac{1}{2}$	-1	+ η	+1	+ $j\epsilon$	315°	315°	$\frac{1}{2}$	+1	- η	-1	- $j\epsilon$

Table 4.1: Relation between Position Angle of the dipoles, the gain and the Stokes Parameters

where $C^- = \cos(\chi^-)$ and $S^+ = \sin(\chi^+)$ and dipole gain factor G' equals 1/2. In practice the nominal position angle of the dipole is an integral multiple of 45° and table 4.1 lists the Stokes coefficients and dipole gain factors for all combinations.

In the on-line observing system an additional gain factor G'' is applied which equals 2 for parallel dipole configurations and equals $2\sqrt{2}$ for crossed modes to give output units of 5mJy independent of dipole setting. Also since september 1979 an additional complex gain factor of -1 is used for the YX channels.

DIPOLE CODES AND POLARIZATION CODES

The position of the X-dipole of an Westerbork antenna is defined by a code number. The reference system is given in figure 4.1. Only signals of interferometers with positive baselines will be considered. The adopted phase convention for an interferometer signal R_{AB} of an element A in the west and an element B in the east is a positive phase increase for a positive hour angle increase of a source South of the baseline.

The polarization code (POLC) of an interferometer is represented by a two digits decimal number, the tens giving the dipole code of the western (fixed), antenna and the units representing the code of the eastern (movable) antenna. For example: POLC = 21 implies: western antenna dipole code: 2 eastern antenna dipole code: 1

Only since fall 1980 does the polarization code on the data tapes completely match the actual settings of the dipoles. Before that time systematic and incidental discrepancies did occur.

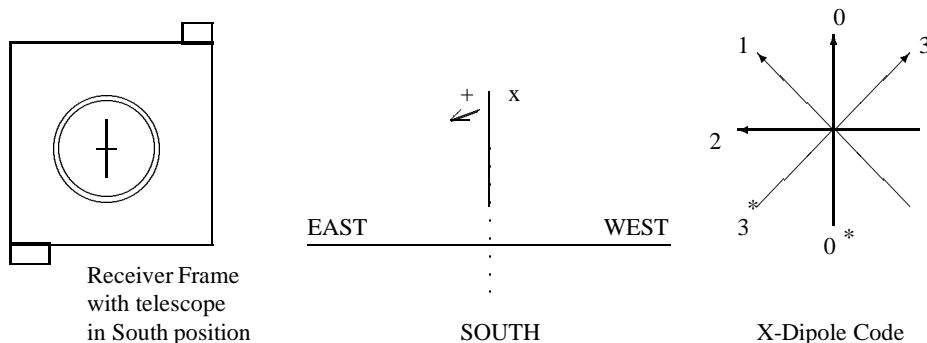


Figure 4.1: Reference system and dipole codes
 Definition of 0° setting of dipole and sense of rotation: One is supposed to look in the Southern direction through the mesh of the telescope into the feed and to the sky

4.3 EXAMPLES

EXAMPLE 1

The most common "crossed dipole" observing configuration for Westerbork until 1982 was to correlate all fixed (West) telescopes with their dipoles at position angles (on the sky) of $X= 90^\circ$, $Y= 180^\circ$ against all movable (East) telescopes with their dipoles at position angles $X= 45^\circ$, $Y= 135^\circ$. The uncalibrated responses of the 4 output channels for each interferometer then become (from table 4.1) (In practice an additional complex gain factor of -1 is used for the XY channels in the on-line observing system and factors G'' which remove effects of dipole orientation.):

POLC	Position Angle		Channel	Response
	RT_W	RT_E		
21	90°	45°	XX_{uncal}	$= (G_{XX})(+I - Q - U - jV)$
	90°	135°	XY_{uncal}	$= (G_{YX})(+I - Q - U + jV)$
	180°	45°	YX_{uncal}	$= (G_{XY})(-I - Q - U - jV)$
	180°	135°	YY_{uncal}	$= (G_{YY})(+I + Q - U - jV)$

Since the (complex) gain factors are unknown, they are determined for each interferometer channel by observing an unpolarized calibrator. ($I = 1; Q, U, V = 0$)

$$\begin{aligned}
 XX' &= G_{XX} \\
 XY' &= G_{XY} \\
 YX' &= -G_{YX} \\
 YY' &= G_{YY}
 \end{aligned}
 \tag{4.2}$$

and the observations of all unknown sources are scaled (calibrated) by these factors. (Note: In principle, a calibrator with known polarization can also be used.)

The calibrated response of the interferometer then becomes:

$$\begin{aligned}
 XX &= \frac{XX_{\text{uncal}}}{XX'} = I - Q + U - jV \\
 XY &= \frac{XY_{\text{uncal}}}{XY'} = I - Q + U - jV \\
 YX &= \frac{YX_{\text{uncal}}}{YX'} = I - Q + U - jV \\
 YY &= \frac{YY_{\text{uncal}}}{YY'} = I - Q + U - jV
 \end{aligned} \tag{4.3}$$

which are the channel values normally available from the calibrated output of Westerbork. The solutions for the 4 Stokes parameters then become

$$\begin{aligned}
 I &= \frac{1}{4}(+XX + XY + YX + YY) \\
 Q &= \frac{1}{4}(-XX - XY + YX + YY) \quad RT_W: X = 90^\circ, Y = 180^\circ \\
 U &= \frac{1}{4}(+XX - XY + YX - YY) \quad RT_E: X = 45^\circ, Y = 135^\circ \\
 V &= \frac{j}{4}(+XX - XY - YX + YY)
 \end{aligned} \tag{4.4}$$

In practice the factor $\frac{1}{4}$ is usually automatically introduced in the mapping stage of the analysis by the beam pattern normalization.

Another common observing configuration has the dipoles of all fixed (West) telescopes at position angles (on the sky) of $X= 0^\circ$, $Y= 90^\circ$ and of all movable (East) telescopes at position angles of $X= 45^\circ$, $Y= 135^\circ$. Similar to the above, the polarization solutions for the calibrated output are

$$\begin{aligned}
 I &= \frac{1}{4}(+XX + XY + YX + YY) \\
 Q &= \frac{1}{4}(+XX + XY - YX - YY) \quad RT_W: X = 0^\circ, Y = 90^\circ \\
 U &= \frac{1}{4}(+XX - XY + YX - YY) \quad RT_E: X = 45^\circ, Y = 135^\circ \\
 V &= \frac{j}{4}(-XX + XY + YX - YY)
 \end{aligned} \tag{4.5}$$

EXAMPLE 2

A more complicated case is obtained when observing with "parallel dipoles" for high accuracy measurements of low level linear polarization or the detection of circular polarization. This has become the standard mode since about 1982. The method which has been most commonly used involves first observing a calibration source with "crossed dipoles" to calibrate the (complex) gain of each interferometer channel, then observing a calibration source with "parallel dipoles" to determine the (complex) instrumental polarization terms, and finally observing the unknown sources with the same "parallel dipole" setting.

For example, using the first "crossed dipole" case described above where the fixed (West) telescopes have their dipoles set at position angles $X= 90^\circ$, $Y= 180^\circ$ and the movable (East) telescopes have their dipoles set at $X= 45^\circ$, $Y= 135^\circ$, the (complex) gain factors obtained by observing an unpolarized calibrator ($I = 1$; $Q, U, V = 0$) are, as found in equation 4.2

Then the dipoles on the movable (East) telescope are rotated to be parallel to those of the fixed telescopes (*i.e.* $X= 90^\circ$, $Y= 180^\circ$).

The uncalibrated responses of the 4 output channels for each interferometer then becomes (cf. table 4.1, with additional on-line G'' dipole configuration factor):

POLC	Position Angle		Channel	Response
	RT_W	RT_E	Response	
22	90°	90°	XX_{uncal}	$= G_{XX}(+I - Q - \eta U - j\epsilon V)$
	90°	180°	XY_{uncal}	$= G_{YX}(+\epsilon I + \eta Q - U + jV)$
	180°	90°	YX_{uncal}	$= G_{XY}(-\epsilon I + \eta Q - U - jV)$
	180°	180°	YY_{uncal}	$= G_{YY}(+I + Q + \eta U - j\epsilon V)$
20	90°	0°	XX_{uncal}	$= G_{XX}(+\epsilon I - \eta Q + U - jV)$
	90°	90°	XY_{uncal}	$= G_{YX}(+I - Q - \eta U + j\epsilon V)$
	180°	0°	YX_{uncal}	$= G_{XY}(-I - Q - \eta U + j\epsilon V)$
	180°	90°	YY_{uncal}	$= G_{YY}(-\epsilon I + \eta Q - U - jV)$

These responses are then scaled (calibrated) by the channel gain determined by the "crossed dipole" observations (equation 4.2) so that the calibrated response of the interferometer is

$$\begin{aligned}
 XX &= \frac{XX_{\text{uncal}}}{XX'} = (I - Q - \eta U - j\epsilon V) \\
 XY &= \frac{XY_{\text{uncal}}}{XY'} = (\epsilon I + \eta Q - U + jV) \\
 YX &= \frac{YX_{\text{uncal}}}{YX'} = (\epsilon I - \eta Q + U + jV) \\
 YY &= \frac{YY_{\text{uncal}}}{YY'} = (I + Q + \eta U - j\epsilon V)
 \end{aligned}
 \tag{4.6}$$

Since Q, U, V, η, ϵ are almost always small quantities, one can generally neglect second order terms in these quantities, and the calibrated output of the telescope is equivalent to

$$\begin{aligned}
 XX &= (I - Q) \\
 XY &= (\epsilon_{XY}I - U + jV) \\
 YX &= (\epsilon_{YX}I + U + jV) \\
 YY &= (I + Q)
 \end{aligned}
 \tag{4.7}$$

However, a solution for all Stokes parameters cannot yet be obtained since the instrumental terms (ϵ) have not yet been determined. To do this, it is necessary to observe another unpolarized calibration source ($I = 1; Q, U, V = 0$) for which the calibrated output will be:

$$\begin{aligned}
 XY'' &= \epsilon_{XY} \\
 YX'' &= \epsilon_{YX}
 \end{aligned}
 \tag{4.8}$$

Substituting these measured quantities into equation 4.7 gives the final calibrated and corrected result

$$\begin{aligned}
 XX &= (I - Q) \\
 XY &= XY''I - (U + jV) \\
 YX &= YX''I + (U + jV) \\
 YY &= (I + Q)
 \end{aligned}
 \tag{4.9}$$

or solutions for the Stoke parameters

$$\begin{aligned}
 I &= +\frac{1}{2}(XX + YY) \\
 Q &= -\frac{1}{2}(XX - YY) \\
 U &= -\frac{1}{2}((XY - YX) - (XY'' - YX'')I) \\
 V &= -\frac{j}{2}((XY - YX) - (XY'' + YX'')I)
 \end{aligned}
 \tag{4.10}$$

Also in this case the factor $\frac{1}{2}$ is automatically introduced in the mapping stage of the analysis by the beam pattern normalization and will not have to be incorporated at some other stage. For older observations without $\sqrt{2}$ compensation in the on-line system, all formulae in the set 4.6 to 4.10 include additional $\sqrt{2}$ factors which have to be taken into account during processing.

4.4 ERRORS

1 In the most common "crossed dipole" observing mode the solutions for the four Stokes parameters are obtained by adding and subtracting 4 interferometer channels with relatively large and almost equal amplitudes. Thus, the accuracy is very dependent in the instrument having high gain stability. Because the interferometers at Westerbork are not all independent for phase and gain changes (e.g. change in radio telescope 0 (RT0) will affect interferometer 0A, 0B, 0C, 0D), solutions for some Stokes parameters will be less gain dependent than others. However roughly speaking the error will be on the order of 1/4 times less than the error of a single interferometer channel. Experience has shown that, if they are not noise limited, the accuracy of polarization measurements is usually $\sim 0.5\%$ of the total intensity ($0.005I$). While this is usually sufficient for linear polarization measurements, it is not, in general, sufficiently accurate to detect circular polarization.

It should be noted that since the amount of circular polarization is almost always negligible in continuum radio sources, even if one of the four channels of an interferometer is bad one can assume $V = 0$ and still obtain a good solution for the Total Intensity and Linear Polarization (Stokes parameters I, Q, U).

2 Observations obtained with 'parallel dipoles', while being more difficult to calibrate, can in principle produce results of much higher accuracy. While two of Stokes parameters (I and Q in the example given in the preceding section) are determined from adding and subtracting interferometer channels containing large signals (see equation 4.10) and are thus as sensitive to gain instabilities as the 'crossed dipoles' solutions, the other two Stokes parameters (U and V in the example) are relatively insensitive to gain changes. It is, in principle, possible for sufficiently strong calibration source to determine the instrumental corrections to a level of $\sim 0.01\%$ ($0.0001I$). Gain changes appear then only as an error proportional to the quantity being measured (U and V in the example) and not as an error proportional to the large Total Intensity (I). Now, however, phase drifts are more important and will tend to mix the real and imaginary parts of the solution (e.g. make a fraction of U appear as V) and can be serious for circular polarization measurements, when the linear polarization is large and there are instrumental phase drifts. Further sources of error are the second order terms ηQ , ηU , ϵV neglected in equation 4.7. Experience has shown that for most continuum radio sources $|V| < 0.005I$, $|Q| < 0.1I$, $|U| < 0.1I$, and that normally for Westerbork $|\eta|, |\epsilon| \lesssim 0.01I$ so that the second order terms are usually very small. (multiplication of one of the quantities $|Q|$, $|U|$, or $|V|$ by $|\eta|$ or $|\epsilon|$ is smaller than $0.001I$). Thus although neglecting second order terms lead to great simplification, one should keep in mind that in areas with strong linear polarization the approximation may fail. In practice, "parallel dipole" measurements have been performed with Westerbork which have achieved accuracies of $\sim 0.02\%$ ($0.0002I$) for Stokes parameter V . (results in e.g. Weiler & Wilson (1977), Weiler & Raimond (1977), and Weiler & de Pater (1980))

Although the example shown in the preceding section only illustrates the method for determining Stokes parameters U and V to high accuracy, by rotating the dipoles of all telescopes through 45° and maintaining them parallel, measurements can be performed which yield Q and V to high accuracy. Thus, by repeating "parallel dipole" measurements at two different position angles separated by 45° all three Stokes parameters (Q, U, V) can be obtained to high accuracy.

4.5 REFERENCES

- Weiler, K.W. (1973): *Astron. & Astrophys.* **403**, p. 403.
Weiler, K.W. and Wilson, A.S.(1977): *Astron. & Astrophys.* **58**, pp. 17-26.
Weiler, K.W. and Raimond E. (1977): *Astron. & Astrophys.* **54**, pp. 965-975.
Weiler, K.W. and de Pater, I (1980): *Astron. & Astrophys.* **91** p. 41.
Morris et al (1964): *Astrophys. J.* **139**, p. 551.

ON THE USE OF REDUNDANT BASELINES

O.M. Kolkman

This chapter contains a short introduction about the use of redundant baselines to self-calibrate your data and obtain high dynamic range, high fidelity, radio maps. The text is based on articles by Noordam & de Bruyn (1982) and Wieringa (1992). Here we will only describe the ideas on which the calibration method is based, for a more thorough discussion, applications and a mathematical treatment the reader is referred to the articles mentioned above. The second part of this chapter will describe the possibilities for redundant baseline observations.

In the NewStar package programs are available for reduction of WSRT data, more information about these packages can be found in part ??.

5.1 A SKETCH OF THE TECHNIQUE

A synthesis observation will generally provide an observer with a 'dirty map' which consists of a convolution of the source brightness distribution with a 'dirty beam'. *i.e.* a pointspread function. In chapter 5 of part II we showed that the shape of the dirty beam is determined by a number of functions like the power pattern of a individual telescope, sampling functions and a taper. Once the dirty beam is known the dirty map can be deconvolved using a deconvolution program like CLEAN (Högbom, 1974) yielding the source brightness distribution. Another way to obtain the brightness distribution is by fitting models of the brightness distribution to the observed visibilities.

In the ideal case all the sidelobe patterns introduced by the convolution of the brightness distribution with the dirty beam can be removed. However, the phase and gain of the (atmosphere-telescope-receiver) system varies during an observation and the actual side lobes will differ from those assumed during the deconvolution. After deconvolution with the dirty beam residual side lobe patterns will therefore cause residuals in the form of sections of elliptical rings and radial spokes emanating from the highest intensity features in the map. Because these sidelobe patterns can contain between 0.1 and 1% of the power in the brightness features they limit the the dynamic rang in a standard WSRT observation to 100-1000 depending on the wavelength and the area of interest in the map.

The redundancy calibration makes use of the fact that:

- The processes that cause the errors in the gain and phase calibrations are almost all telescope dependent e.g. receiver errors, errors due to the delay system and atmospheric errors (each telescope looks through a different part of the atmosphere).
- The visibility function of an interferometer made up of say telescope x and z with a certain baseline length and baseline orientation must be the same as the visibility function of an interferometer made up

Redundant Baselines	length (m)	Redundant interferometers									
1	144	01	12	23	34	45	56	67	78	89	9B
2	288	02	13	24	35	46	57	68	79	8B	
3	432	03	14	25	36	47	58	69	7B		
4	576	04	15	26	37	48	59	6B			
5	720	05	16	27	38	49	5B				
6	864	06	17	28	39	4B					
7	1008	07	18	29	3B						
8	1152	08	19	2B							
9	1296	09	AC	BD	1B						
10	9A+1296	0A	9C	AD							
11	9A+1368	0B	9D								
12	1224	1A	BC								
13	72	AB	CD	9A							

Table 5.1: The redundant baselines of the WSRT, interferometers in boldface are redundant only when 9A=72 m (After Wieringa, 1992)

of say telescope p and q of the same baseline lengths and orientation.

If a large number of baselines of same the length and orientation but consisting of a large number of telescopes is available one can obtain a more accurate estimate of the true visibilities (by taking a sort of weighted mean) for each scan *i.e.* each integration period. By comparing these 'true' visibilities with the observed visibilities one can determine the gain and phase errors for the individual telescopes independently from the actual brightness distribution and apply these to all the interferometers including the non-redundant ones. Only the overall gain and phase slope error are not determined. These residual overall scan parameters can be determined using a model for the field. This process is called alignment. (How the algorithms are implemented is described in the NewStar program description.)

Redundancy can only be used if a sufficient number of identical baseline vectors are available. This is the case for e.g. th 5 km Ryle telescope (Cambridge), the Pentincton array (DRAO), and the WSRT.

For interferometers without redundant baselines increase in dynamic range can be obtained by using the self calibration (self-cal) algorithms. These algorithms are also available for WSRT calibration in the NewStar package but are discussed there (Part ??). For more information about the self-cal see e.g. the review by Pearson and Readhead (1984) or Cornwell and Fomalont in Chapter 9 of Perley *et al.* (1989) and references therein. Wieringa (1992) uses the WSRT to illustrates how both methods can be used to obtain the best possible results with WSRT data.

5.2 REDUNDANCY AND THE WSRT

The configuration of the WSRT permits the recording of data from many redundant baselines. The telescopes are positioned in the East West direction and all the fixed telescopes are 144 m apart. If the movable telescopes are positioned in its standard redundant configuration with 9A=AB=CD=72 m and AC=BD=1296 m a maximum number of 66 redundant baselines is obtained. If 9A \neq 72, only 53 redundant baselines are available. The redundant baselines are shown in table 5.1.

For continuum observations at 6 and 21 cm for which the DCB is used one cannot choose which baselines can be used, the configuration is hardwired in the correlator: all but 4 of the maximum number of 91 baselines are recorded (but only for the XX and YY polarization).

For the DXB many redundant configurations may be specified. There are, however, limitations. Of course the product of the number of interferometers (including the redundant), N_I , the number of polarizations, N_P ,

the bitmode, N_B and the number of frequency channels may not exceed $25600/B$, where B is the bandwidth of the observation in MHz. But due to hardware limitations not every configuration is possible. A number of redundant configurations have been used in the past, if you need a configuration that is different from the standard you are advised to specify one of the existing configurations. The existing configurations can be found in table 5.2 and 5.3. If there is no configuration which fits your scientific needs you may propose yet another configuration, in that case you should contact the telescope astronomer or one of the NFRA astronomers (e.g. Ger de Bruyn or Robert Braun).

Keep in mind that if you want to make the full use of an observation with redundant baselines you need specialized software (NewStar).

5.3 REFERENCES

- Högbom, J.A. (1974): *Astron. & Astrophys. Suppl.* , **15**, p. 417.
Noordam, J.E. and de Bruyn, A.G. (1982): *Nature*, **299**, pp. 597-600.
Perley T.J. and Readhead, A.C.S. (1984): *ARA&A*, **22**, pp. 97.
Wieringa, M.H. (1992): *Experimental Astronomy*, **2**, pp.203-225.

Max Nr of Real Channels	Bit Mode N_B	Nr. Freq Points N_F	Polariz. Channels N_P	Recirculation Type	Config. Nr.	Completeness (Table 5.3)	Comments
BANDWIDTH \leq 10 MHz, Only DLB							
5120	1	8	2	-	128	B2	
5120	1	8	4	-	129	B4	
5120	1	16	1	-	130	V	
5120	1	16	2	-	131	B5	
5120	1	32	1	-	132	B1	
2560	2	8	1	-	133	B2	
2560	2	16	1	-	134	B5	
BANDWIDTH \leq 5 MHz							
7168	1	8	4	1P	140	B2	
9088	1	16	2	1P	141	V	
10240	1	16	4	1P	142	B5	
	1	32	1	1T	150		
9728	1	32	2	1P	143	B1	
3584	2	8	2	1P	144	B2	
	2	16	1	1T	151		
5120	2	16	2	1P	145	B5	
BANDWIDTH \leq 2.5 MHz							
18176	1	16	4	2P	141	V	
	1	32	2	2T	156	V	
19456	1	32	4	2P	143	B1	
11648	1	64	1	2T	153	V	
7168	2	8	4	2P	144	B2	
	2	16	2	1T, 1P	151		Not examined
10240	2	16	4	2P	145	B5	
5824	2	32	1	2T	154	V	
BANDWIDTH \leq 1.25 MHz							
	1	32	4	2T, 1P	152	V	Not examined
23296	1	64	2	2T, 1P	153	V	
23296	1	128	1	2T, 1D	153	V	
11648	2	32	2	2T, 1P	154	V	
11648	2	64	1	2T, 1D	154	V	
BANDWIDTH \leq 0.625 MHz							
45056	1	64	4	2T, 2P	155	B3	'20 sec '
45056	1	128	2	2T, 1P, 1D	155	B3	'20 sec '
45056	1	256	1	2T, 2D	155	B3	'20 sec '
23296	2	32	4	2T, 2P	154	V	
23296	2	64	2	2T, 1P, 1D	154	V	
23296	2	128	1	2T, 2D	154	V	

Table 5.2: Possibilities of redundant configurations with the DLB/DXB (continued on the next page)

Note: configuration numbers may change with time. So be clear on your proposal about what degree of redundancy you would like to get.

Max Nr of Real Channels	Bit Mode N_B	Nr. Freq Points N_F	Polariz. Channels N_P	Recirculation Type	Config. Nr.	Complete- ness (Table 5.3)	Comments
BANDWIDTH \leq 10 MHz, only DLB							
4928	1	32	1	-	170	A1	
BANDWIDTH \leq 5 MHz							
9856	1	32	2	1P	170	A1	
9856	1	64	1	1D	170	A1	
8704	1	128	1	1T	171	A3	
4864	2	64	1	1T	172	A2	
BANDWIDTH \leq 2.5 MHz							
19712	1	32	4	2P	170	A1	
19712	1	64	2	1P, 1D	170	A1	
19712	1	128	1	2D	170	A1	
17404	1	128	2	1T, 1P	171	A3	
17404	1	56	1	1T, 1D	171	A3	
9728	2	64	2	1T, 1P	172	A2	
9728	2	128	1	1T, 1D	172	A2	
BANDWIDTH \leq 1.25 MHz							
39424	1	64	4	2P, 1D	170	A1	'20 sec '
37424	1	128	2	1P, 2D	170	A1	'20 sec '
39424	1	256	1	3D	170	A1	'20 sec '
34816	1	128	4	1T, 2P	171	A3	'20 sec '
34816	1	256	2	1T, 1P, 1D	171	A3	'20 sec '
19456	2	64	4	2P, 1D	172	A2	
19456	2	128	2	1T, 1P, 1D	172	A2	
19456	2	256	1	1T, 2D	172	A2	
BANDWIDTH \leq 0.625 MHz							
38912	2	128	4	1T, 2P, 1D	172	A2	'20 sec '
38912	2	256	2	1T, 1P, 2D	172	A2	'20 sec '

Table 5.2: continued

V	ST	40		
	FF	45		
	MM	6		
	TOTAL	91	COMPLETE	
B1	ST	40		
	FF	30	NOT:	01, 07, 17, 23, 29, 39, 45, 46, 47, 56, 57, 67, 78, 79, 89
	MM	5	NOT:	CD
	TOTAL	75	Missing	16
B2	ST	40		
	FF	30	NOT:	13, 15, 16, 17, 19, 35, 36, 37, 39, 56, 57, 59, 67, 69, 79
	MM	6		
	TOTAL	76	Missing	15
B3	ST	40		
	FF	34	NOT:	01, 07, 08, 12, 17, 18, 19, 28, 29, 78, 79
	MM	6		
	TOTAL	80	Missing	11
B4	ST	40		
	FF	30	NOT:	13, 15, 16, 17, 19, 35, 36, 37, 39, 56, 57, 59, 67, 69, 79
	MM	0		ALL Missing !!
	TOTAL	70	Missing	21
B5	ST	40		
	FF	24	NOT:	01, 05, 08, 15, 18, 23, 24, 26, 27, 29, 34, 36, 37, 39, 46, 47, 49, 58, 67, 69, 79
	MM	5	NOT:	CD
	TOTAL	69	Missing	22
B6	ST	40		
	FF	25	NOT:	03, 02, 01, 13, 12, 49, 48, 47, 46, 45, 59, 58, 57, 56, 69, 68, 67, 79, 78, 89
	MM	5	NOT:	CD
	TOTAL	65	Missing	26
A1	ST	17	NOT:	0C, 0D, 1C, 1D, 2A, 2D, 3A, 3B, 3C, 4A, 4B, 4C, 4D, 5A, 5C, 5D, 6A, 6B, 6C, 6D, 7A, 7C, 7D
	FF	33	NOT:	05, 06, 07, 17, 25, 26, 27, 37, 38, 45, 56, 89
	MM	6		
	AUTO	14		
	TOTAL	56	Missing	35 (exclusive autocorrelation)
			Solution -IF-	correction possible
A2	ST	8	ONLY:	7A, 7B, 8A, 8B, 9A, 9B, 9C, 9D
	FF	15	ONLY:	01, 02, 03, 04, 12, 13, 14, 23, 24, 25, 26, 45, 78, 79, 89
	MM	1	ONLY:	BC
	AUTO	14		
	TOTAL	24	Missing	67 (exclusive autocorrelation)
			Solution -IF-	correction not possible
A3	ST	7	ONLY:	7A, 7B, 7C, 8B, 8C, 9C, 9D
	FF	12	ONLY:	02, 03, 04, 05, 12, 14, 15, 25, 26, 36, 79, 89
	MM	1	ONLY:	AD
	AUTO	14		
	TOTAL	20	Missing	71 (exclusive autocorrelation)
			Solution -IF-	correction not possible

Table 5.3: Completeness descriptions of the DLB/DXB setup.

ST: number of standard (fixed-movable) telescope combinations, FF: number of fixed-fixed telescope combinations, MM: number of movable-movable telescope combinations

MOSAICING

This chapter is based on an original article by Robert Braun and Ger de Bruyn in NFRA newsletter no.3

6.1 INTRODUCTION

Although there has been a long history of multiple pointing observations directed at objects too large to fit comfortably into a single interferometer primary beam, it has only been within the last few years that the theoretical basis of this technique has become better understood. This article provides the interested user with some theoretical background, a description of the what mosaicing has been implemented at the WSRT and the authors' conclusions concerning the quality of the images that can be expected.

6.2 THEORETICAL BACKGROUND

The radio interferometry technique was developed some thirty years ago to allow higher resolution observations than could be obtained with the filled apertures of the time. The same incentive motivates us today to form synthesized apertures even more extended than an earth diameter for some applications. The instantaneous field-of-view (FOV) of a filled aperture is identical to the power response pattern (the 'primary beam'). Imaging an extended area requires fully sampling it (*i.e.* at intervals less than about one HWHM) with the primary beam. The Fourier transform of the resulting image will contain information at spatial frequencies extending out, with decreasing sensitivity, to the aperture diameter.

The instantaneous FOV of a correlation interferometer is determined by the product of the voltage response patterns of each pair of elements. Traditionally, interferometric observations have been limited to this single FOV. In isolated cases, observers have resorted to a small number of widely spaced interferometer pointings, which were individually reduced and then linearly combined with weights appropriate for the primary beam attenuation afterwards. This scheme is far from optimal because the resulting sensitivity is non-uniform and the additional constraints on the sky brightness given by the overlapping pointings are not utilized during the reduction process. However, in analogy with the filled aperture case, an extended area could be fully sampled in cross-correlations (with a fixed phase and delay tracking center) at HWHM intervals of the primary beam of the interferometer elements. A Fourier transform with respect to this *sampling grid*, would yield visibility samples over a range of projected baselines with decreasing sensitivity out to a dish diameter around each originally discrete visibility sample. This concept is explained clearly by Cornwell in chapter 15 of Perley *et al.* (1989).

An especially important portion of the spatial frequency plane is that near the origin. By extracting visibilities with reasonable sensitivity down to 1/2 dish diameter from the cross-correlations and supplementing these with auto-correlation data from the same elements between 0 and 1/2 dish diameter, it becomes possible to successfully image regions of arbitrary size with a single instrument.

In practice, it is unnecessary to explicitly extract the the additional visibility samples via an intermediate Fourier transform or to keep the delay and phase tracking center fixed during the cause of such an observation. Sampling the desired region at HWHM intervals of the primary beam is already sufficient to guarantee the information content to obtain both the desired uniform sensitivity and the supplemental visibility sampling (assuming the data are subsequently used in parallel to constrain the sky brightness). A practical method of extracting the supplemental sampling is the joint deconvolution of the multi pointing database with the Maximum Entropy Method (MEM)- based algorithm such as that developed by T.J.Cornwell (see page 277 of Perley *et al.* (1989) and references therein) and available within the AIPS reduction package. Since the supplemental sampling is especially important for the reconstruction of the most extended structures, hybrid reduction schemes employing joint deconvolution at low and individual reduction and combination at high resolution have been found to be very effective with only a modest computational impact.

6.3 MOSAIC IMPLEMENTATIONS

An ideal mosaic implementation calls for rapid cycling through the positions which define the image area, preferably sampling each before earth rotation has significantly altered the projected baselines, so as to retain the most complete coverage possible. Practical limitations on the telescope move and backend setup time make this an elusive goal.

A further, practical desire is for a user-friendly interface for the specification of mosaic mode observations as well as a stream-lined data acquisition, calibration and reduction path.

Some effort has been made to address the issue of high observing efficiency in the mosaic implementation at the WSRT. Initial measurements of move and setup overhead, carried out during late 1989, indicated that 40 seconds were typically lost for a requested move. Investigations into the drive mechanism and braking algorithm resident in the microprocessors at each telescope led to a better understanding of the systems' limitations. The telescopes are accelerated (and decelerated) to (and from) slew speed with a ramped voltage to the drive motors. The individual slew speeds and ramp slopes were therefore adjusted to be nominally equal for all telescopes, after which actual, individual values of the slew speed and braking distance were measured and tabulated. On the basis of this information, the drive parameters appropriate for a given displacement could be calculated and sent to the telescope microprocessors. (A more complete description of this procedure can be found in NFRA ITR-193.) This procedure has made it possible to routinely carry out moves between about 10 and 120 arcminutes with only a 10 second overhead. By carefully timing the issuing of move and backend setup commands in the on-line software, the total overhead involved in repositioning is kept to this value. At the same time an efficient user interface has been developed for the definition of a mosaic observation.

The parameters which define a complete observation are: a single reference position, begin and end times., integration time and dwell time per position (an integer unit of 10 seconds, the basic WSRT time unit), a mosaic pattern will be cycled through continually for the duration of the observation. It may be simply an ordered list of required offsets with respects to the reference position or may be produced interactively with a cursor on the terminal screen. A maximum of 120 different positions may be specified in a single mosaic pattern. With the adopted minimum dwell time of 20 seconds per position, one could obtain 18 scans at each of the 120 positions within a single 12 hour observation.

At a wavelength of 92 cm this would correspond to sampling a region of about 15 degrees on a side with uniform sensitivity. The entire multi-pointing observation is subsequently stored and archives as a self-contained database. Off-line software to allow efficient parallel processing of WSRT mosaic databases is still is available in the NewStar package.

6.4 SPATIAL FREQUENCY COVERAGE OPTIMIZATION

Although a 10 second move overhead allows reasonable observing efficiency, it is still places a limit on the degree of sampling which can be obtained over extended regions. Complete sampling in he spatial frequency plane (uv plane) entails obtaining visibilities at $D/2$ intervals in both coordinates. The regular east-west configuration of the WSRT, gives a radial sampling interval of normally 72 m (declination and position angle dependent). By observing at six different basic separations (of telescopes 0 to 9 with A to D) a radial sampling

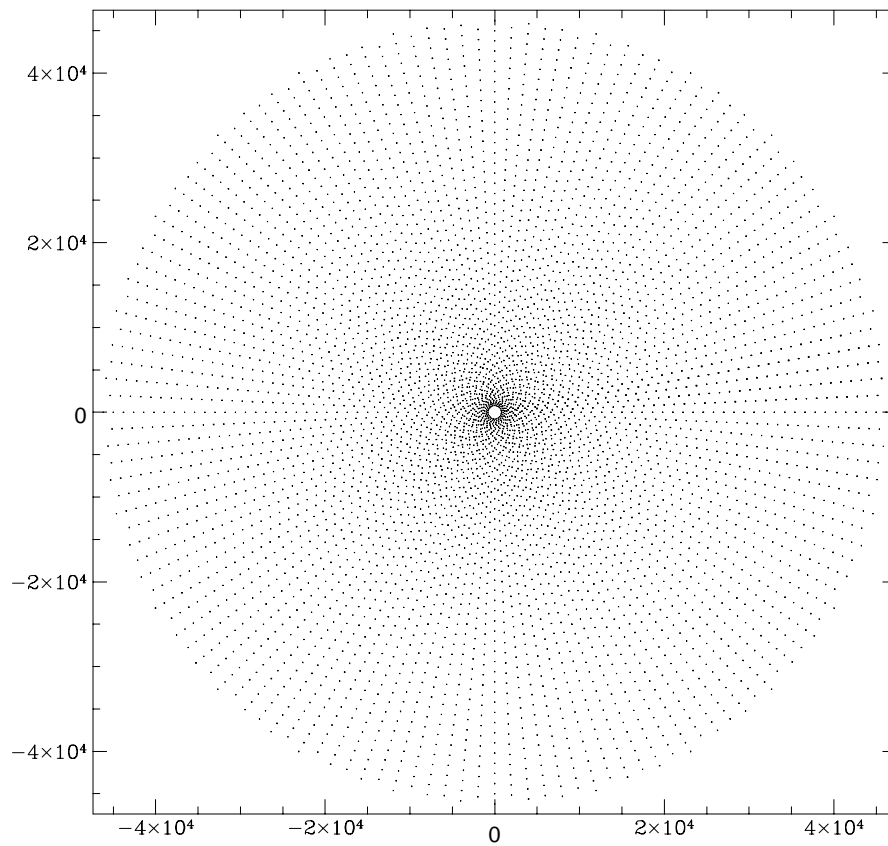


Figure 6.1: U,V coverage for a mosaic observation with 72 spokes resulting from a combination of 12 spokes from 6 array configurations (12 meter increment). The scale is for a wavelength of 6 cm and for clarity the tracks are shown for a source at $\delta = 90^\circ$

of $D/2 = 12\text{ant}$). By observing at six different basic separations (of telescopes 0 to 9 with A to D) a radial sampling of $D/2 = 12\text{ m}$ can be obtained. The azimuthal sampling obtained along the elliptical tracks with a given time sampling interval is inversely dependent on the track radius. A sampling density of 72 m in azimuth is obtained at a radius of 410 m radius in this example. Depending on the relative power in compact and extended sources in the field, it may be desirable to trade off radial against azimuthal sampling density by modifying the number of spokes versus the number of tracks. Subsequent 12 hour observations can be used to improve the sampling in either of these dimensions and so to move the matched sampling radius in or out.

6.5 INFORMATION FOR USERS INTERESTED IN THE USE OF MOSAICING OBSERVATIONS

Mosaicing can be done at all standard WSRT wavelengths (6, 21, 49 and 92 cm). Certain parameters, like the grid separation at the chosen wavelength, will be fixed because it is dedicated by the wish to obtain uniform sensitivity across the surveyed region. The move time will also probably be fixed at 10 seconds for all wavelengths. The telescope astronomer and the WSRT program committee will help in selecting the appropriate pattern and u,v coverage best suited for the astrophysical problem proposed, on the basis of information provided by the proposer. The minimum technical information a proposal for WSRT mosaicing should contain is the following:

- the center of the mosaic pattern
- the angular dimension and the shape of the area that one wants to map
- the largest structure expected to be visible within the area
- the number of line channels that one wants to output
- an estimate of the total amount of time (extrapolating from the nominal sensitivity of the WSRT; given in e.g. chapter 2)
- the sensitivity that one would like to reach

We realize that the handling of WSRT mosaicing data is an enormous task that may present a formidable threshold for users. To lower this threshold the NFRA has developed a software package to take care of the sorting, (self-) calibration and further reduction of the mosaic data. This package is described in part ??.

6.6 REFERENCES

Perley, R.A., Schwab, F. and Bridle, A.H. (Editors) (1989): “*Synthesis Imaging in Radio Astronomy*”. Astronomical Society of the Pacific.. ISBN:0-937707-23-6. (see also review in part II Chapter 9.1, Book 2).

For more information also see:

Ekers, R.D. and Rots, A.H. (1979): “Short spacing synthesis from a primary beam scanned interferometer” in Proc. IAU Coll. 49 “*Image Formation from Coherence Functions in Astronomy*”, Ed. C. van Schooneveld. D. Reidel (Dordrecht, Holland), pp. 61-66

WSRT PART III

USER DOCUMENTATION CHAPTER 7

THE WSRT CORRELATORS

7.1 DIGITAL CORRELATORS - A SYNOPSIS OF THEORY

Ed. O.M. Kolkman, with a contribution by J.M. v.d. Hulst

The realization that the power spectrum of a signal is the Fourier transform of its autocorrelation function signified a revolution in spectral line observations. The first autocorrelator receiver was designed by Weinreb (1963) and used to try to detect the Deuterium line at 327 MHz.

The basic principle of a digital correlating receiver is the measurement of the correlation function of an incoming signal by sampling and digitizing an incoming signal and using computer hardware (memory, shift registers, digital delays) to form the auto or cross correlation function of the incoming signal. Once this is done the power spectrum of the signal is obtained by Fourier transforming the correlation function. For details one is referred to e.g. chapter 6 and 8 in the textbook by Thompson *et al.* (1986), chapter 4 in the book by Perley *et al.* (1989) or the thesis of Bos (1985).

The sampling and analog to digital (A/D) conversion of the signal is done in a simple way and hence causes loss of sensitivity compared to an analog system and loss of amplitude information. This is very easy to understand intuitively: the simplest digitization is the so-called one-bit system where all samples of the incoming signal above the mean input voltage are registered as 1, while all samples below the mean input power are registered as 0. A series of 1's and 0's then represents the fluctuations in the incoming signal (and hence the spectral information is kept), but all information about the amplitude of the incoming signal is lost. This means that a separate recording of the amplitude of the input signal is still required. How this is done will be described below. A more subtle way of digitizing the input signal is to use more than one level for discriminating the fluctuations of the incoming signal. This leads to the so-called two-bit digitization using two or three levels set at the $\pm V$ from the mean input voltage and at the mean input voltage. These schemes are illustrated in figure 7.2

The sampling of the incoming signal has to be performed at a frequency which must at least be twice the bandwidth B one wants to analyze. This requirement is set by the Nyquist sampling criterion, which requires sampling at 2B for a bandwidth limited signal in a band B. The WSRT line backend is designed with samplers of 20 MHz, so that the maximum possible bandwidth is 10 MHz. This means that if one chooses to observe smaller bandwidths, one does not need to sample at the full clock speed. This extra power can be used to sample more delays to get a longer correlation function (or higher spectral resolution) or to sample more IF or telescope combinations. This capability to add correlation products is achieved by recirculating the sampled signals through the correlator using different time delays and/or telescope/IF combinations. The original WSRT correlator did not have this capability and is referred to as the DLB (Digital Line Backend). The addition of a recirculation buffer upgraded the correlator to what is called the DXB, the Digital eXtended line Backend)

Though the sampling and digitization of the incoming signals preserves the time fluctuations (within a

bandwidth of half the sampling rate) the amplitude information is lost completely. The output of the correlator after proper digitization and quantization correction and Fourier transformation to the frequency domain is a normalized spectrum, which can be viewed as a correlation coefficient measuring the correlated fraction of the system temperature of an interferometer. In order to denormalize this correlation coefficient one has to determine the system temperature of the interferometer, which is the geometric mean of the system temperatures of the individual elements. The system temperatures are measured using a noise source injection into the signal path during a fraction f of a basic integration period and measuring the total power with P_{on} and without P_{off} the noise source switched on. Once the equivalent noise temperature T_n of the noise source is known one can determine the system temperature from:

$$T_{sys} = \frac{T_n P_{off}}{P_{on} - P_{off}} \quad (7.1)$$

Then renormalization of the spectrum measured on baseline $i - j$ is obtained by multiplying the normalized spectrum by $\sqrt{T_{sys}(i) \cdot T_{sys}(j)}$, the system temperature for that interferometer.

This amplitude correction is applied on-line and the total power data is recorded on tape. Though not implemented in the current software, one could in principle use the total power data to undo the on-line amplitude correction.

7.2 THE DLB/DXB

The DLB/DXB is the digital correlator which is used for spectral line observations. The DLB can form 2560 one bit correlation products. This backend is used when the bandwidth of the observation is exactly 10 MHz. If the bandwidth of the observation is less than 10 MHz the DXB is used. The DXB is the digital correlator (DLB), equipped with a recirculation buffer, which is used for spectral line observations and for continuum observations at 327 and 610 MHz.

In the documentation we refer to the DLB/DXB backend simply as DXB.

For a more general description see section 1.3.1. The autocorrelation mode is discussed in section 3.4.1. Redundancy and the DLB/DXB is discussed in chapter 5.

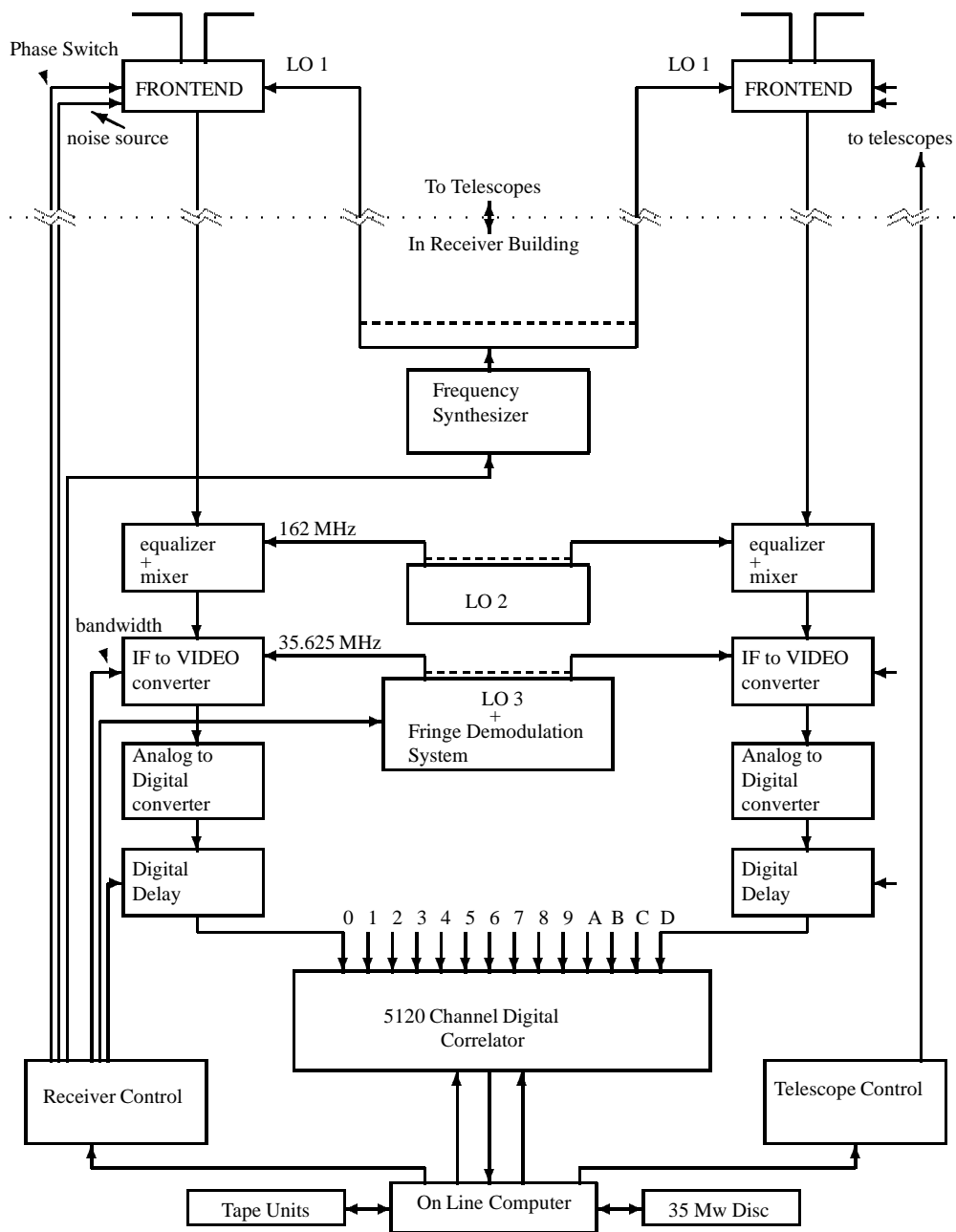


Figure 7.1: A block diagram of the telescope receiver system. Nota that this is the configuration with the DLB/DXB backend. The configuration for the DCB differs in some details from this figure. (copied from Bos(1985))

7.2.1 THE WSRT RECEIVER SYSTEM

The 14 telescopes of the WSRT can in principle provide 91 interferometer combinations, each interferometer having four combinations of the two independent receivers. For simplicity we only describe the system for a single interferometer. A simplified block diagram of a single interferometer is given in Figure 7.1. This diagram refers to the DXB and is briefly described here. The systems for the DCB differs in some details in the system described here. The main differences are that the DCB system has a different correlator and that the correlator setting is hard wired *i.e.* cannot be changed according to the wishes of the observer. If you have specific questions about the DXB or DCB which are not answered here please contact the NFRA telescope group.

The operating frequency of the frontends is determined by a central frequency synthesizer controlled by the on-line computer. The available frequencies and bandwidths are given in table 1.2. The IF signals coming from the telescopes into the central control building with a frequency of around 132 MHz are converted to 25 - 35 MHz and pass through an equalizer to rectify the shape of the passband which is skewed by frequency dependent losses in the cables between the telescopes and the control building. They then are converted to a video band with a selectable width varying from 0 - 10 MHz down to 0 - 78 kHz in factors of two. During this process the on-line computer adjusts the frequencies of the phase rotators in each of the 28 local oscillator lines in such a way that the fringes for the center of the observed field are demodulated to remove the fast component of the fringe phase variation with time. This way the spatial sampling rate is reduced and the low frequency of the residual fringe makes longer integration times of 10 seconds or more possible.

After the video conversion the incoming signal is digitised by a 2-bit analog-to-digital (A/D) converter. Subsequently the digitised signal passes through the delay system which compensates for the differences in pathlength between the two telescopes of the interferometer. The 5120 channel digital correlator provides complex correlation functions integrated over 10 seconds. Recirculation of the data for bandwidths less than 10 MHz will increase the number of complex channels by B/10 where B is the bandwidth in MHz. The on-line computer reads the output buffer of the correlator, sorts and integrates the data, performs the Fourier transform to the frequency domain, applies various corrections (amplitude correction, van Vleck correction, taper etc.) and stores the results on disk for further off-line processing.

A short description of each of the components is given below. Much of this summary was taken from A. Bos his Ph.D. Thesis (1985) on instrumental effects in spectral line synthesis observations.

7.2.2 THE FRONTENDS

Table 1.2 (section 1.3.1) summarizes the most important parameters and their implications for the total system performance. (Details can be found in for example Casse *et al.* 1981). It may be noted that each frontend has a programmable noise source used for calibration of the gain and system temperature. A 180-degree phase switch in the local oscillator chain can suppress crosstalk and certain types of offsets in the analog-to-digital converters.

7.2.3 THE IF TO VIDEO CONVERSION

One of the properties of a digital correlator is that its spectral resolution can be varied by simply changing the clock rate (which is usually equal to the sampling rate of the analog input signal). This requires that the bandwidth of the incoming analog signal is changed accordingly in order to obey the Nyquist sampling criterium and avoid aliasing. The main function of the IF system therefore is to move the input band down to video and to limit the video bandwidth. The shape of the video band and its amplitude and phase stability are rather crucial for the quality of the data: the sharper the edges the better the rejection of signal causing aliasing; the higher the phase and amplitude stability, the greater the spectral dynamic range of the output data. For the design of the IF system the basic concept of single sideband rather than double sideband mixing has been used because of its inherently low spurious level and low cost. The 25 - 35 MHz signal is converted to video using a 35.625 MHz local oscillator signal driving the single sideband mixer. The video output of the mixer is then applied to a set of eight lowpass filters used for the selection of the appropriate bandwidth. A total power detector measures the power in the output video band for amplitude calibration purposes (see section 'On-Line corrections' (1.1 in part IV)). The total power is recorded using a voltage to frequency

- Amplitude stability: < 0.1% over 12 hours.
- Phase stability: 0.5 degree over 12 hours.
- Gain differences for all interferometers: $\pm 5\%$.
- Maximum differential phase for all interferometers: ± 20 degrees.
- unwanted sideband suppression: > 30 dB.
- spurious level: > 75 dB below normal signal level.
- total power detector accuracy: 1% for a 3 dB range.
- total power detector stability: $10^{-4}/^{\circ}C$.

B c.	B 20dB	Fr 3 dB	Fr 3-20 dB	Tot. 3dB
0	10.	-	7	7
1	5.	-	7	7
2	2.5	-	7	7
3	1.25	0.24	7	7.25
4	0.625	0.5	7	7.5
5	0.3125	1	7	8
6	0.15625	2	7	9
7	0.078625	4	6	10

B.c bandwidth code

B 20dB Bandwidth at -20 dB point (MHz)

Fr 3 dB Fraction (%) of bandwidth below -3 dB at low freq. edge

Fr 3-20 dB Fraction (%) of bandwidth between -20 dB and -3 dB at high freq. edge

Tot. 3dB Total fraction (%) of the bandwidth below -3 dB

Table 7.1: IF performance and bandwidth parameters

converter connected to a frequency counter in the AD digital correlator. Reading the counter can be gated in phase with the noise injection in the frontends.

The performance of the IF units and the character of the 8 passbands is given in table 7.1

The fringe demodulation (removing the fast moving fringe phase) is antenna based rather than interferometer based to simplify the hardware and control. Fringe demodulation is performed by phase rotating the 35.625 local oscillator signal which is used in the IF video conversion system. Details of the fringe demodulation system can be found in A. Bos' Ph.D Thesis (1985).

The phase tracking accuracy obtained is better than 0.1 degrees with a zero point setting accuracy of better than 0.1 degrees. The amplitude decorrelation resulting from errors in the phase tracking is less than 1% per interferometer.

7.2.4 THE A/D CONVERSION

The digitization of the analog signal causes a loss of sensitivity depending of the number of bits used for the digitization. The worst case is a loss of $2/\pi$ in the minimum case of 1-bit digitization. As the maximum improvement is obtained by going from 1-bit to 2-bit digitization a 2-bit quantization was adopted. The three bit-modes possible are illustrated in Figure 7.2. The reference voltage V_0 is kept constant by means of a feedback gain loop. This is necessary because variations in reference level, even if properly corrected, introduce variations in signal to noise ratio. The V_+ and V_- reference levels are kept at +1 r.m.s. and -1 r.m.s of the input signal respectively, also by a feedback loop. The stability of the reference level is better than 1% worst case.

The sampling of the A/D converters is 20 MHz (twice the maximum video bandwidth to obey the Nyquist sampling theorem). For bandwidths smaller than 10 MHz the A/D converter output is resampled in the correlator at the bandwidth dependent rate of 2B MHz.

7.2.5 THE DIGITAL DELAY

Pathlength (delay) compensation is necessary to remove the fast component of the pathlength difference variation with time (hour angle) between the two telescopes of an interferometer. Ideally one would like to do this at the signal frequency. It is, however, more practical to insert the delay corresponding to the pathlength difference at the IF frequency band. The maximum delay required for a 3 km baseline is 10 μ sec and the maximum tracking rate is 5000 dh/dt = 0.37 nsec/sec. The delay is approximated in discrete steps and discontinuities are avoided by adding a constant offset to the stepping rate. The delay is adjusted every ten seconds when the on-line computer loads a delay offset and a delay rate for each of the 28 delay units. The delay consists of a bulk delay covering 25.6 μ sec in steps of 50 nsec and a fine delay covering 50 nsec in 16

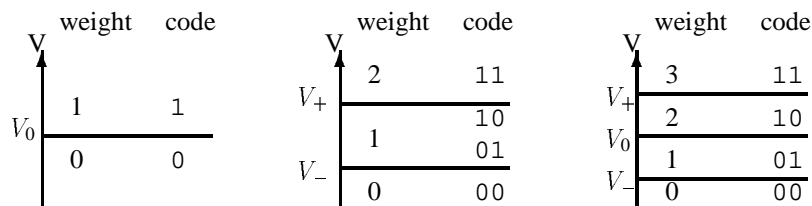


Figure 7.2: The conversion codes for the three bit modes of the analog digital converters. The input signal voltage V is divided into maximally four regions by the reference levels V_0 , V_+ and V_- . Each of these regions is given a weight used during correlation.

steps of 3.125 nsec using a tapped delay line. The fine delay is introduced in the 20 MHz clock signals for the A/D converters.

The delay tracking accuracy is ± 0.3 nsec r.m.s. with a zero point setting accuracy of 0.0122 ns. The delay stability is better than 0.1 nsec over a 12 hour period. Amplitude decorrelation is less than 0.5% for properly set delays and delay tracking.

7.2.6 CORRELATOR MODES

The DXB/DLB correlator is rather flexible and supports a large number of configurations consisting of different combinations of input baselines and polarizations, number of frequency channels and number of bits used for digitization.

Configurations settings of the DLB/DXB can be changed manually. A number of special purpose configurations have been build and tested successfully. See e.g. tables 5.2, 5.3 and 7.2.

Special configurations can be designed for special purposes. Consult the NFRA telescope group for more information.

7.3 THE DCB

The DCB (Digital Continuum Backend) is a wide band correlator consisting of 8 independent correlators with their own IF systems and A/D converters and samplers. Each independent correlator can measure 256 complex correlation products in a 5 or 10 MHz band. In this way one can observe over a wide bandwidth by tuning the IFs to 8 consecutive frequencies separated by 10 MHz thus covering a maximum bandwidth of 80 MHz. The advantage of observing 8 independent 10 MHz bands rather than one single 80 MHz wide band is that bandwidth smearing at the edges of the field is limited. This bandwidth smearing arises because the fringe stopping and delay tracking are done for the center frequency and hence cause radial smearing (chromatic aberration) of sources at large distances from the fringe stopping center. This smearing scales linearly with the distance from the field center and the bandwidth of the observation.

For a more general discussion see section 1.3.2, the special pulsar observation mode is discussed in section 3.4.2

7.4 REFERENCES

Bos, A. (1985): 'On instrumental effects in spectral line observations' Ph.D. Thesis, University of Leiden

Casse, J.L., Woestenburg, E.E.M. and Visser, J.J. (1981): *I.E.E.E. Trans. Micr. Theory and Techn.*, **30**, 2, pp. 201-209

Conf Nr	S Code	Back-end	N_B	N_F	N_P	Comp. descr. (see table 5.3)	Comments
128	47	DLB	1	8	XX,YY	B2	Bandwidth = 10MHz.
129	48	DLB	1	8	all	B4	Bandwidth = 10MHz.
130	46	DLB	1	16	XX	V	Bandwidth = 10MHz.
131	61	DLB	1	16	XX,YY	B5	Bandwidth = 10MHz.
132	45	DLB	1	32	XX	B1	Bandwidth = 10MHz.
133	51	DLB	2	8	XX	B2	Bandwidth = 10MHz.
134	39	DLB	2	16	XX	B6	Bandwidth = 10MHz.
140	53	DXB	1	8	XX,XY	B2	Recirculation in polarization.
141	50	DXB	1	16	XY	V	Recirculation in polarization.
142	60	DXB	1	16	XX,XY	B5	Recirculation 1 time over polarization.
143	56	DXB	1	32	XY	B1	Recirculation in polarization.
144	38	DXB	2	8	XY	B2	Recirculation in polarization.
145	37	DXB	2	16	XY	B6	Recirculation in polarization.
150	33	DXB	1	32	XY		Recirculation 1 time over telescopes.
151	29	DXB	2	16	XY		Recirculation 1 time over telescopes.
152	27	DXB	1	32	XX,XY	V	Recirculation at least 2 times over telescopes. $B \leq 2.5$.
153	58	DXB	1	64	XY	V	Recirculation at least 2 times over telescopes. $B \leq 2.5$.
154	59	DXB	2	62	XY	V	Recirculation at least 2 times over telescopes. $B \leq 2.5$.
155	55	DXB	1	64	XY	B3	Special version of 153 suitable for recirculation 4 times.
156	28	DXB	1	62	XX,XY	V	Recirculation at least 2 times over telescopes. $B \leq 2.5$.
170	49	DXB	1	62	XY	A1	Auto Cross correlation. Special noise source sequence.
171	54	DXB	1	128	XY	A3	Auto correlation.
172	52	DXB	2	64	XY	A2	Auto correlation.

Table 7.2: General overview of the special DLB/DXB configuration

- Perley, R.A., Schwab, F. and Bridle, A.H. (Editors) (1989): "*Synthesis Imaging in Radio Astronomy*". Astronomical Society of the Pacific.. ISBN:0-937707-23-6. (see also review in part II Chapter 9.1, Book 2).
- Thompson, A.R., Moran, J.M. and Swenson Jr., G.W. (1986): "*Interferometry and Synthesis in Radio Astronomy*". John Wiley & Sons, New York.. ISBN 0-471-80614-5. (see also review in part II Chapter 9.1, book 3).
- Weinreb, S. (1963): 'A digital Spectral Analysis Techniwue and Its Aplication to Radio Atronomy, *Technical report no. 412*, Res. Lab. for Electronics, Massachusetts Institute of Technology, Cambridge, Mass.

WSRT BEAMS

8.1 WSRT PRIMARY BEAM PROPERTIES

contributed by J.D.Bregman June 7, 1993

8.1.1 INTRODUCTION

With a synthesis array like the WSRT the sky brightness distribution can be reconstructed from the signals collected by the array elements. The strength of a received signal depends on the direction of the collected radiation relative to the boresight direction of a radio telescope. Consequently the intensity of a mapped source depends on its position relative to this telescope pointing center. Here we must realize that the effective pointing center is some average over all telescopes used.

Also we must realize that in a synthesis array not only the collecting elements have to be directed toward the field of interest, but also the fringe and the delay tracking of the correlating receiver system. A point source with a position offset from the fringe stopping center gives a signal with a residual fringe at the correlator output. This causes signal attenuation depending on the integration time. The differential delay causes a signal attenuation depending on the bandwidth of the correlator channel. In the synthesis imaging process these two effects show up as an attenuated peak response of a radially and tangentially smeared point source at increasing distance from the fringe center. These two effects have to be properly dealt with in the imaging process and should not be absorbed in the antenna response pattern.

8.1.2 SOME THEORY

The polarized power of the complex electric field column vector (E_x, E_y) is given by the coherence matrix \mathbf{S} , which is given as a time average by

$$\mathbf{S} = \langle \mathbf{E} \cdot \mathbf{E}^{T*} \rangle \quad (8.1)$$

where T indicates transposition and $*$ indicates complex conjugation. The four Stokes parameters of polarized radiation flux are related to the four elements of the coherence matrix \mathbf{S} in the following way

$$\begin{pmatrix} S_{xx} & S_{xy} \\ S_{yx} & S_{yy} \end{pmatrix} = \begin{pmatrix} (I + Q) & (U + jV) \\ (U - jV) & (I - Q) \end{pmatrix} \quad (8.2)$$

The x direction points towards the North celestial pole, and y towards the East.

A practical antenna can be described by a response matrix \mathbf{F} giving the output voltage column vector (V_x, V_y)

$$\mathbf{V} = \mathbf{F} \cdot \mathbf{E} \quad (8.3)$$

as response on a given input electric field column vector (E_x, E_y) . The power response of a two element full polarization correlation receiver is given by

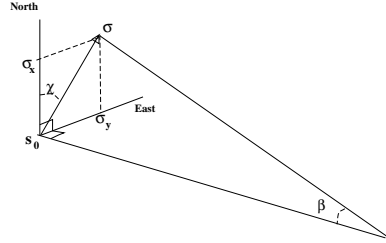
$$\mathbf{P} = \langle \mathbf{V} \cdot \mathbf{V}^{T*} \rangle \quad (8.4)$$

Inserting 8.3 into 8.4 and using 8.1 gives

$$\mathbf{P} = \mathbf{F} \cdot \mathbf{S} \cdot \mathbf{F}^{T*} \quad (8.5)$$

For two ideal receiving elements each with two orthogonal dipoles X and Y the response matrix is a unity one, which readily evaluates 8.5 to identify the four power response elements with the four elements of the coherence matrix.

The four elements $\mathbf{F}_{ij}(\sigma)$ of the voltage response matrix have each their own radiation pattern as function of the position vector (σ_x, σ_y) . The direction vector to a source, described within the telescope beam with position angle χ (cf. chapter 4), from North through East, and boresight angle β , can be projected on a plane tangent to the celestial sphere at the pointing center position. The projected coordinates σ_x, σ_y in the map plane are then given by



$$\begin{pmatrix} \sigma_x \\ \sigma_y \end{pmatrix} = \begin{pmatrix} \beta \cos(\chi) \\ \beta \sin(\chi) \end{pmatrix} \quad (8.6)$$

When the antenna is rotated over angle ρ , the response matrix \mathbf{F} has to be multiplied by rotation matrix $\mathbf{R}(\rho)$

$$\mathbf{R}(\rho) = \begin{pmatrix} \cos(\rho) & \sin(\rho) \\ -\sin(\rho) & \cos(\rho) \end{pmatrix} \quad (8.7)$$

In the equatorial mounted WSRT telescopes only some receiver dipoles can be rotated. Then we have to realize that the radiation pattern changes because of the changed relative orientation of the quadripod, which interferes with the radiation pattern of the receiver feed system.

The complete polarization interferometer response $\mathbf{P}(\sigma)$ for a single source \mathbf{S} at position σ from the fringe pointing center is now given by

$$\mathbf{P}(\sigma) = \mathbf{F}_1(\sigma + d\sigma_1) \cdot \mathbf{R}(\rho_1) \cdot \mathbf{S}(\sigma) \cdot \mathbf{R}^T(\rho_2) \cdot \mathbf{F}_2^{T*}(\sigma + d\sigma_2) \quad (8.8)$$

where $d\sigma$ is the pointing deviation of the two telescopes (with their own response matrices) indicated by the subscripts $_1$ and $_2$. Alternatively we can interpret the rotations by ρ_1 and ρ_2 as negative Faraday rotation angles, which may be different for the two parts of the wavefront arriving at the two different telescopes. For wide fields as is the case for 92 cm observations, the Faraday rotation angle ρ is even a function of the position at the sky, so $\rho = \rho(\sigma)$. So far this non-isoplanicity is neglected in the current processing systems.

For a field with a complete source brightness distribution coherence matrix $\mathbf{S}(\sigma)$, we find the complex visibility power matrix $\mathbf{P}(\mathbf{D}_\lambda)$ for the baseline vector \mathbf{D}_λ between the two telescopes by integration over all source elements weighted by the complex baseline phase factor $e^{2j\pi\mathbf{D}_\lambda \cdot \sigma}$. This integral is in essence a Fourier transformation (\mathcal{FT}), so

$$\mathbf{P}(\mathbf{D}_\lambda) = \mathbf{F}_{d1} \cdot \mathcal{FT}(\mathbf{P}(\sigma)) \cdot \mathbf{F}_{d2}^{T*} \quad (8.9)$$

The dipole crosstalk of the two telescopes is here described by the matrices \mathbf{F}_{d1} and \mathbf{F}_{d2} . To complete the formal description of the correlator power response it should be mentioned that all telescope based complex gain effects can be described with multiplicative matrices, that may be time dependent. Careful attention has to be paid whether such matrices have to be inserted before or after the Fourier transformation in 8.9, *i.e.* whether they are field dependent or not.

During a synthesis observation, \mathbf{D}_λ changes due to the earth rotation. Also the Faraday rotation angles changes as function of time and needs to be corrected. Inverse Fourier transformation of all complex visibility powers

gives the observed brightness distribution $\mathbf{P}(\sigma)$ of the field, which includes all the effects described by 8.8. We must realize that getting back $\mathbf{S}(\sigma)$ from 8.8 then requires multiplication of $\mathbf{P}(\sigma)$ with the inverse matrices in the proper order. Current reduction packages do this in some approximate way. This results into some power pattern averaged over all pointing deviated telescope voltage responses.

For the simple case of a single antenna element or a perfect interferometer with $d\sigma_1 = d\sigma_2 = \rho_1 = \rho_2 = 0$, and an unpolarized source, for which \mathbf{S} is a unity matrix, we find

$$\mathbf{P}(\sigma) = \mathbf{F}(\sigma) \cdot \mathbf{F}^{T*}(\sigma) \quad (8.10)$$

Evaluation of the matrix elements and substitution into 8.2 gives

$$\begin{pmatrix} I \\ Q \\ U \\ jV \end{pmatrix} = \begin{pmatrix} [(F_{xx}F_{xx}^* + F_{xy}F_{xy}^*) + (F_{yx}F_{yx}^* + F_{yy}F_{yy}^*)] / 2 \\ [(F_{xx}F_{xx}^* + F_{xy}F_{xy}^*) - (F_{yx}F_{yx}^* + F_{yy}F_{yy}^*)] / 2 \\ [(F_{xx}F_{yx}^* + F_{xy}F_{yy}^*) + (F_{yx}F_{xx}^* + F_{yy}F_{xy}^*)] / 2 \\ [(F_{xx}F_{yx}^* + F_{xy}F_{yy}^*) - (F_{yx}F_{xx}^* + F_{yy}F_{xy}^*)] / 2 \end{pmatrix} \quad (8.11)$$

This formula clearly demonstrate that symmetry properties of the telescope voltage beam matrix elements of \mathbf{F} cannot be traced easily to symmetry properties of the interferometer power beam expressed in Stokes parameters. This is especially true when the rotational symmetry is broken by different pointing deviations of the two elements of an interferometer. (We have to realize that I , Q , U , and V are only real because the voltage responses of the two elements are identical, which causes imaginary terms to cancel in the sums of the complex products.)

8.1.3 BEAM PROPERTIES

To illustrate the transformation of the symmetry properties of the matrix elements of \mathbf{F} to the symmetry properties of the Stokes parameters we take an example with simplified expressions for F_{xx} and F_{xy} which still reflect basic properties of antennas, such as that the dominant components are in phase quadrature

$$\begin{aligned} F_{xx} &= H(\beta_1) + (A + jB)K(\beta_2) \cos(2\chi) \\ F_{xy} &= (C + jD)K(\beta_2) \sin(2\chi) \end{aligned} \quad (8.12)$$

Here is $H(\beta_1)$ the normalized voltage main beam response and $K(\beta_2)$ the normalized voltage crosstalk term, both of which are radial functions of normalized angles, β_1 and β_2 , which make the functions independent of telescope scale. The rotational dependence is described by a single $\cos(2\chi)$ term.

For a properly aligned telescope with the feed on the rotational symmetry axis we can derive F_{yx} and F_{yy} by replacing the position angle relative to the dipole by a value relative to the telescope. Then

$$\begin{aligned} F_{yx}(\chi) &= F_{xy}^*(\chi - 90) \\ F_{yy}(\chi) &= F_{xx}^*(\chi - 90) \end{aligned} \quad (8.13)$$

where the conjugation gives the phase flip between xy and yx interference, Evaluation according to 8.11 then gives

$$\begin{pmatrix} I \\ Q \\ U \\ V \end{pmatrix} = \begin{pmatrix} HH & + & KK \cos^2(2\chi)(AA + BB) + KK \sin^2(2\chi)(CC + DD) \\ 2HK A \cos(2\chi) & & \\ & - & KK \sin(4\chi)AC \\ & & KK \sin(4\chi)(AC - BC - AD - BD)/2 \end{pmatrix} \quad (8.14)$$

We now see functions with KK and HK terms. This illustrates that the relation between telescope and interferometer beam parameters is not a straight forward one. It reflects the general property that U has a different magnitude than Q and that V is small. The imaginary terms B and D that dominate the voltage pattern, turn out to give only second order effects in the interferometric polarization. The weak terms A and C become after multiplication with the zero order term H , the dominant contribution in the power beam pattern.

Expressed in relative polarization at a particular position within the beam we get

$$\begin{aligned} |Q/I| &= (K/H)A \\ |U/I| &= (K/H)^2 AC \\ |V/I| &= (K/H)^2 AD \end{aligned} \quad (8.15)$$

Especially when the dipoles of one telescope are rotated with respect to the other element in the interferometer, the patterns of Q and U become more complicated. In formula 8.8 we have then to take into account that the rotations ρ_1 and ρ_2 have to be absorbed into the position angle of \mathbf{F}_1 and \mathbf{F}_2 as well.

Off-axis position of the feed, as is the case for the VLA, causes a different symmetry in the pattern of Y-dipole w.r.t. the X-dipole *i.e.* additional beam polarization components in formula 8.14.

8.1.4 POINTING EFFECTS

When there is a pointing offset, of magnitude p and position angle ζ between the two telescopes of an interferometer, we get an A term

$$\cos(\chi - \zeta) \cdot K_p(\beta) \quad (8.16)$$

This gives the following contributions

$$\begin{aligned} I &= HH + HK_p [\cos(\chi - \zeta) - \sin(\chi - \zeta)] + \frac{1}{2} K_p K_p \\ Q &= HK_p [\cos(\chi - \zeta) + \sin(\chi - \zeta)] + \frac{1}{2} K_p K_p \cos(2\chi - 2\zeta) \end{aligned} \quad (8.17)$$

For a Gaussian beam profile $H(\beta)$ we get for a pointing offset p of one telescope relative to the average

$$K_p = 5.54 H(\beta) \cdot \beta \cdot p / \beta_f^2 \quad (8.18)$$

This gives, for $H > K$ a relative polarization

$$Q/I = 5.54 [\cos(\chi - \zeta) + \sin(\chi - \zeta)] \beta p / \beta_f^2 \quad (8.19)$$

When there are more telescopes with random pointing deviations we get in a synthesis map a relative Q component that depends on the source structure. In an extended object, where only short baselines contribute, only the pointing deviations of the contributing telescopes are involved. So we must be very careful with polarization contributions that show a single position angle dependence. This means that they are probably caused by pointing effects, which contribute differently as function of source structure and with observing period. The latter is because of changing wind-loading effects.

For an average pointing deviation of 0.007 degrees at best we can calculate the polarization contribution at half-power beamwidth for a point source at 6cm wavelength. When we assume that only interferometers from fixed and movable telescope combinations are involved, and that the pointing variations of the dominating four movable antennas have random position error, the contribution in Q/I is about 6%.

8.1.5 BEAM DETERMINATION

There are two ways to determine the interferometric beam pattern. A direct one observes an unpolarized point source at different positions from the beam center. An indirect one calculates the power pattern from the observed voltage pattern of a telescope element. The latter has the advantage of higher sensitivity and is less depending on contamination with other sources in the field. Also we can then exclude the effects of pointing deviations, which are different for fields at different positions and even when observed in different epochs. This is particularly true for 6 cm observations where sources are weaker and pointing deviations cause stronger effects.

Over the years several attempts have been made to establish the beam properties at the various observing wavelength.

ITR 117 (Weiler *et al.*, 1973) gives polarization data that are based on values derived from synthesis maps, where an unpolarized has been placed at different positions within the telescope beam. The observations have

ν_0	$\beta_f \nu_0$	$\beta_m \nu_0$	$\beta_0 \nu_0$	A	B	C	D	Ref	Remarks	
327	857	850	-		0.09			1	+	scan in H-plane
327	831	859	1063			0.015	0.07	1	×	scan in cross plane
608	821	1064	1064		0.032			1	+	
608	821	851	1064				0.022	1	×	
608	821	1500				0.040		1	×	
4995	884	899	1249	0.003	0.074	0.007	0.044	2	*	scans in E-,H-, C-plane

Ref:

1. Bregman (1983)
2. Bregman *et al.* (1982)

Table 8.1: Telescope Voltage response Pattern parameters

been done in the so called crossed dipole mode, where the dipoles of the eastern telescope of the interferometer are 45 degrees rotated with respect to the western telescope. This was the standard observing mode in the seventies. Polarization calibration is straight forward, but interferometer based. Also the polarization is larger then when observed in the so called parallel mode, which became the standard observing mode in the eighties. Polarization calibration is complicated, but all interferometers, including the redundant ones can be self calibrated on telescope basis. QMC (1978), Henneken and Robijn (1989) and de Blok and Woudt (1992) use the same technique, however the definition of position angle is unclear.

References Bregman (1983) and Bregman *et al.*(1982) use the voltage beam technique, where one element of an interferometer tracks an unpolarized point source, while the other telescope scans the object to place it at various positions within the beam. Although we expect Bessel functions for $H(\beta)$ and $K(\beta)$, the following approximations hold very well up to the first null

$$\begin{aligned} H(\beta_1) &= \cos^3(0.943 \cdot \beta_1) \text{ where } \beta_1 = \beta/\beta_f \\ K(\beta_2) &= \sin^2(1.571 \cdot \beta_2) \text{ where } \beta_2 = \beta/\beta_m \end{aligned} \quad (8.20)$$

where β_f is the full width at half maximum of the power beam and β_m the distance from the center to the point at which the voltage polarization has its maximum.

In figure 8.1 a summary is given of all the functions involved so far.

The main terms are summarized in table 8.1, where ν_0 is the observing frequency in MHz and β_0 the distance in degrees of the beam center to the first null of the voltage pattern. The beam parameters have been multiplied with the observing frequency to get scale independent antenna parameters for inter comparison.

Since the 21 cm feed is a scaled version of the 6 cm one, the same beam characteristics are expected.

It is very difficult to determine the A term in the voltage pattern, since it is only a small deviation from the dominating H term.

The quadripod gives a pattern with also a four quadrant symmetry which interferes with the dipole pattern of the feed. These effects are smaller than 10% at 6 cm, but are in the 10 - 30% range at 92 cm.

8.1.6 MAIN BEAM TOTAL POWER AND POLARIZATION PATTERNS

So far good approximations are available in the following form, where I_0 is the intensity of the object when it is observed at the pointing center of the telescope

$$\begin{aligned} I/I_0 &= H(\beta_a)^2 \\ Q/I_0 &= qK(\beta_b) \cos(2\chi) \\ U/I_0 &= uK(\beta_b) \sin(2\chi) \\ V/I_0 &= vK(\beta_b) \sin(2\chi) \end{aligned} \quad (8.21)$$

Where β_a and β_b are now scaled from the observed frequency ν_0 in MHz to a frequency ν according to

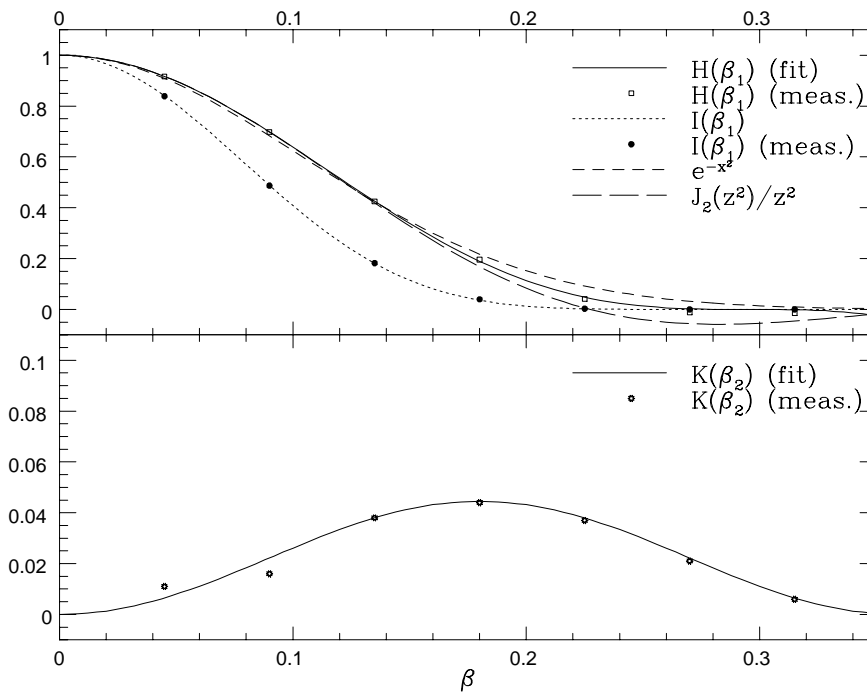


Figure 8.1: The functions $H(\beta_1)$ and $K(\beta_2)$ (see text) are plotted together with other functions with which the parameterization of the behavior of the primary beam was tried. The boresight angle is in degrees and the scale is for 6 cm

ν_0	$\beta_f \nu_0$	$\beta_m \nu_0$	q	u	v	Ref		Remarks
327	858	546	-0.021	+0.049	+0.020	1	++	valid from Jan 1989
608	835	603	+0.006	+0.008	-0.003	?	+×	March 1983, 0.06 degree pointing offset in telescope B
1415	831	609		-0.015		2	++	parallel dipoles
1415	831	680	+0.0050		+0.0018			
1415	891	563	+0.013	+0.026	< 0.002	3	+×	crossed dipoles
4995	899	899	-0.006	+0.040	< 0.002	4	+×	

Ref:

1. Henneken and Robijn (1989)
2. Blok and Woudt (1992)
3. Weiler *et al.* (1973)
4. QMC (1978)

Table 8.2: Interferometric Power Beam parameters

$$\begin{aligned}\beta_a &= \beta \nu / (\beta_f \nu_0) \\ \beta_b &= \beta \nu / (\beta_m \nu_0)\end{aligned}\tag{8.22}$$

The main beam is fitted by the \cos^6 function up to the first null within the accuracy of the measurements. The quality of the fit to the actual polarization patterns is worse and allows deviation up to 10% or 0.001, whichever is larger.

The values of β_m are considerably smaller than the ones found for the telescope voltage patterns. If we fit with functions $H(\beta_a)K(\beta_b)$ we get the proper values for β_m and find q and u values consistent with those of A , B , C and D . However the quality of the fits is worse.

In the references more detailed formula have been tried to fit the observed data. Terms with $\sin(\chi)$ and $\cos(\chi)$ components, caused by possible pointing deviations, give less than 10 % contribution. These are of the same order as the accuracy of the observations and their associated reduction procedures. Especially the effects of pointing deviations of the telescopes are important, as is demonstrated by the 608 MHz observation.

For 49 cm and 92 cm observing wavelength the polarization patterns are less regular than the 6 cm and the 21 cm ones, because of interference of radiation reflected from the quadripod structure with radiation received by the illumination pattern of the feed.

For a given feed system, which illuminates the 25 m dish from the prime focus, the radiation pattern is almost independent of frequency within band, so the main beam scales with frequency, although not exactly because of partial compensation. Details are not available yet. We expect to use for frequency scaling functions of the following type

$$\beta_a = \beta (1 + c(\nu - \nu_0)/\nu_0) / \beta_f\tag{8.23}$$

where c deviates slightly from unity.

8.1.7 SIDELobe PATTERNS

At 92 cm and 49 cm the sidelobe patterns have been observed in the voltage mode by scanning the source Tau A with one telescope of a short baseline interferometer. The scan range extends to 130 degrees on a non linear scale and is presented in figure 8.2. This range covers the so called spill-over region, where the feed looks over the rim of the telescope. There is no such thing as a spill-over lobe! From graph's of F_{xx} , F_{xy} , F_{yx} and F_{yy} on a logarithmic dB scale in power, the envelope has been drawn in figure 8.2, which gives the highest signal that can be expected in a side lobe. This is particular useful to estimate solar interference and order of magnitude effects caused by Cas, Cyg and Tau, when they are above the horizon.

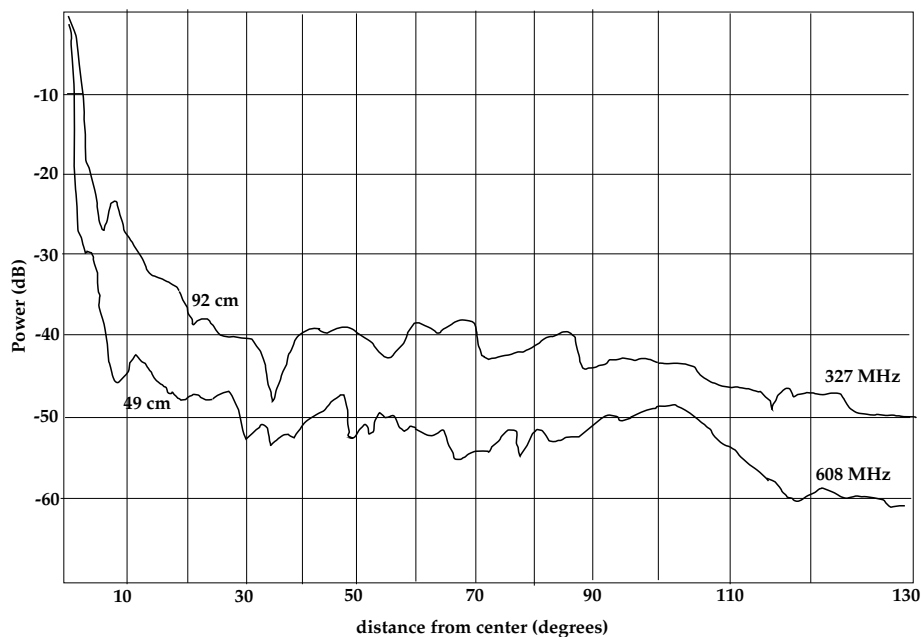


Figure 8.2: Far sidelobe patterns at 49 and 92 cm.

8.1.8 SUGGESTIONS FOR FURTHER WORK

Investigate as a function of frequency for a given feed system the dipole crosstalk terms and the beam polarization.

This will become especially important for the wide band 92 cm system which covers the range 305 - 385 MHz. A method where voltage and power pattern observations are combined should be preferred, with sufficient sampling in polarization angle to see (4χ) terms, and sufficient extend in β up to the first null.

8.1.9 REFERENCES

- Weiler, K.W., v. Someren Gréve, H.W. and Piersma (1973): '21 cm primary beam properties of the WSRT' *NFRA internal tech. report, 117* (available at NFRA).
- Q.M.C. (1978): 'Quality Monitoring Committee report on 6 cm beam properties'.
- Bregman, J.D. *et al.* (1982): '6 cm bundel van een 25 m SRT spiegel', *NFRA NOTE, Draft* (available at NFRA).
- Bregman, J.D. (1983): 'WSRT antenna pattern reference data', *NFRA NOTE, 417* (available at NFRA).
- Henneken and Robijn, (1989): 'WSRT polarization at 327 MHz' students radio practicum report.
- de Blok and Woudt, (1992): 'WSRT polarization at 21 cm' students radio practicum report.

8.2 WSRT BASELINES

Ed. O.M.Kolkman, this text was copied and updated from the old manual

Standard separations between fixed telescope 9 and movable telescope A are $36 + k \cdot 12\text{m}$ with $k = 0, 1, 2, \dots, 8$ or $36 + n \cdot 18\text{m}$ with $n = 1, 2, 3, 4$. The position of telescope B is normally 72 meters to the east of A. Telescope C and D are normally placed 1296 meters to the east of A and B respectively. The baseline combinations that result from correlating the signals of the fixed telescope with those of the movable telescopes are given in table 8.3. It is clear that any of the normal configurations with $9A = 36, 54, 72$ or 90m always result in an array in which the baseline increment is 72 meters although the starting baseline will be different. By combining observations from configurations with $9A = 36\text{m}$ and 72m or $9A = 54\text{m}$ and 90m we obtain an array with an increment of 36m although the starting baseline may be different. However the grating rings will be twice as far away from a source as they were with the 72m increment array. Finally, by combining observations with $9A = 35, 54, 72$ and 90m we obtain an array with a baseline increment of 18 meter and a shortest spacing of 36 meter. The grating rings are then 4 times as far away from the source as they were with 72 meter increment array. For occasional projects which require rings to have very large radii (8 times those of the rings in the 75 meter increment array) additional observations with $9A$ spacings of 45,63,81 or 99 meter can be combined with the observations with $9A$ at 36,54,72,and 90 meter to give a baseline increment of 9 meter and a shortest baseline of 36 meter.

While all the above combinations result in arrays which have baseline increments which are multiples of 36 meters, we can never have any baselines shorter than 36 meter and the starting baseline need not to be equal to the baseline increment. Thus the WSRT never has a $u-v$ plane sampling increment which is entirely constant in the range from $(u, v) = -\infty$ to $(u, v) = +\infty$. There will always be a gap of some size around $(u, v) = 0$ since, at a minimum, we can never measure a simple at $(u, v) = 0$. The presence of this gap causes an amplitude ripple or zero level offset to be present in the synthesized antenna pattern. The effect of this ripple or offset on the total area of the synthesized beam within some given distance from its center (which we need to know to accurately convert flux density per beam to brightness temperature) are described in more detail in chapter 5 in Part II.

The exact choice of baseline combinations and increments depends on several parameters: sensitivity, angular size of the source, declination of the source.

The baseline increment used should be small enough that the smallest of the grating rings in the synthesized antenna pattern has a radius larger than the diameter of the source of interest in the field. This will prevent the source from ‘interfering’ with itself.

If sensitivity is required such that a field has to be observed $n \times 12h$ and the source is smaller than the the grating ring radius then, in principle, all observations could be done with the same baselines. However by doing the additional observations on different baselines so that the baseline increment is smaller, and thus the grating ring radius is larger, grating ring confusion is always reduced. Thus this latter observing procedure is always to be preferred, especially at 49 and 21 cm wavelengths where, in addition to the source of interest, many background sources are detected.

At declinations below 40° , shadowing (see chapter 9) will affect short baseline data at large positive or negative hour angles. Thus baseline combinations should be selected so as to minimize this difficulty as possible.

If a source is above declination 40° , and is small enough an strong enough that a single $12h$ observation will suffice, then the array configuration with a shortest spacing of 54 meter and a baseline increment of 72 meter is often used for that observation. This configuration is often used since out to the first grating ring of the resulting synthesized antenna paten there is essentially no zerolevel offset and no amplitude ripple. Thus the area of the synthesized beam is constant out to the first grating ring.

8.3 SYNTHESIZED BEAM CROSS-CUTS AND INTEGRALS

Ed. O.M. Kolkman

This section was produced by combining, editing and updating material from two articles from the 1980 version of this documentation. The original articles were written by J.M. van der Hulst and R.J. Allen and by J.J.H Woldringh and K.W. Weiler

9 meter increments AB = CD = 72 meter

9A	9B	8A	8B	7A	7B	6A	6B	5A	5B	4A	4B	3A	3B	2A	2B	1A	1B	0A	0B	9C	9D	8C	8D	7C	7D	6C	6D	5C	5D	4C	4D	3C	3D	2C	2D	1C	1D	0C	0D
36	108	180	252	324	396	468	540	612	684	756	828	900	972	1044	1116	1188	1260	1332	1404	1476	1548	1620	1692	1764	1836	1908	1980	2052	2124	2196	2268	2340	2412	2484	2556	2628	2700		
45	117	189	261	333	405	477	549	621	693	765	837	909	981	1053	1125	1197	1269	1341	1413	1485	1557	1629	1701	1773	1845	1917	1989	2061	2133	2205	2277	2349	2421	2493	2565	2637	2709		
54	126	198	270	342	414	486	558	630	702	774	846	918	990	1062	1134	1206	1278	1350	1422	1494	1566	1638	1710	1782	1854	1926	1998	2070	2142	2214	2286	2358	2430	2502	2574	2646	2718		
63	135	207	279	351	423	495	567	639	711	783	855	927	999	1071	1143	1215	1287	1359	1431	1503	1575	1647	1719	1791	1863	1935	2007	2079	2151	2223	2295	2367	2439	2511	2583	2655	2727		
72	144	216	288	360	432	504	576	648	720	792	864	936	1008	1080	1152	1224	1296	1368	1440	1512	1584	1656	1728	1800	1872	1944	2016	2088	2160	2232	2304	2376	2448	2520	2592	2664	2736		
81	153	225	297	369	441	513	585	657	729	801	873	945	1017	1089	1161	1233	1305	1377	1449	1521	1593	1665	1737	1809	1881	1953	2025	2097	2169	2241	2313	2385	2457	2529	2601	2673	2745		
90	162	234	306	378	450	522	594	666	738	810	882	954	1026	1098	1170	1242	1314	1386	1458	1530	1602	1674	1746	1818	1890	1962	2034	2106	2178	2250	2322	2394	2466	2538	2610	2682	2754		
99	171	243	315	387	459	531	603	675	747	819	891	963	1035	1107	1179	1251	1323	1395	1467	1539	1611	1683	1755	1827	1899	1971	2043	2115	2187	2259	2331	2403	2475	2547	2619	2691	2763		
108	180	252	324	396	468	540	612	684	756	828	900	972	1044	1116	1188	1260	1332	1404	1476	1548	1620	1692	1764	1836	1908	1980	2052	2124	2196	2268	2340	2412	2484	2556	2628	2700	2772		

12 meter increments AB = CD = 72 meter

9A	9B	8A	8B	7A	7B	6A	6B	5A	5B	4A	4B	3A	3B	2A	2B	1A	1B	0A	0B	9C	9D	8C	8D	7C	7D	6C	6D	5C	5D	4C	4D	3C	3D	2C	2D	1C	1D	0C	0D
36	108	180	252	324	396	468	540	612	684	756	828	900	972	1044	1116	1188	1260	1332	1404	1476	1548	1620	1692	1764	1836	1908	1980	2052	2124	2196	2268	2340	2412	2484	2556	2628	2700		
48	120	192	264	336	408	480	552	624	696	768	840	912	984	1056	1128	1200	1272	1344	1416	1488	1560	1632	1704	1776	1848	1920	1992	2064	2136	2208	2280	2352	2424	2496	2568	2640	2712		
60	132	204	276	348	420	492	564	636	708	780	852	924	996	1068	1140	1212	1284	1356	1428	1500	1572	1644	1716	1788	1860	1932	2004	2076	2148	2220	2292	2364	2436	2508	2580	2652	2724		
72	144	216	288	360	432	504	576	648	720	792	864	936	1008	1080	1152	1224	1296	1368	1440	1512	1584	1656	1728	1800	1872	1944	2016	2088	2160	2232	2304	2376	2448	2520	2592	2664	2736		
84	156	228	300	372	444	516	588	660	732	804	876	948	1020	1092	1164	1236	1308	1380	1452	1524	1596	1668	1740	1812	1884	1956	2028	2100	2172	2244	2316	2388	2460	2532	2604	2676	2748		
96	168	240	312	384	456	528	600	672	744	816	888	960	1032	1104	1176	1248	1320	1392	1464	1536	1608	1680	1752	1824	1896	1968	2040	2112	2184	2256	2328	2400	2472	2544	2616	2688	2760		
108	180	252	324	396	468	540	612	684	756	828	900	972	1044	1116	1188	1260	1332	1404	1476	1548	1620	1692	1764	1836	1908	1980	2052	2124	2196	2268	2340	2412	2484	2556	2628	2700	2772		
120	192	264	336	408	480	552	624	696	768	840	912	984	1056	1128	1200	1272	1344	1416	1488	1560	1632	1704	1776	1848	1920	1992	2064	2136	2208	2280	2352	2424	2496	2568	2640	2712	2784		
132	204	276	348	420	492	564	636	708	780	852	924	996	1068	1140	1212	1284	1356	1428	1500	1572	1644	1716	1788	1860	1932	2004	2076	2148	2220	2292	2364	2436	2508	2580	2652	2724	2796		

The spacings of the interferometers are set when spacing between the telescopes 9 and A is set (assuming the standard setup AB=CD=72 meter and spacings 9C=0A and 9D=0B i.e. position of C= position of A+1296 m. and position of D= position of B =1296 m.). The table is useful for determining the position of grating rings.

Table 8.3: WSRT spacings.

example	number of spacings	shortest spacing (m)	spacing increment (m)	maximum spacing (m)	Ω_A (")	comments
1	20	36	72	1404	570.03	1 × 12h, 0..9,A,B
2	20	54	72	1422		1 × 12h, 0..9,A,B
3	20	72	72	1420		1 × 12h, 0..9,A,B
4	20	90	72	1458		1 × 12h, 0..9,A,B
5	40	36	36	1422		synthesis, 2 × 12h, 0..9,A,B
6	40	54	36	1458		synthesis, 2 × 12h, 0..9,A,B
7	80	36	18	1448		synthesis, 4 × 12h, 0..9,A,B
8	38 [†]	36	72	2700		1 × 12h, 0..9,A,B,C,D
9	152 [†]	36	18	2754		synthesis, 4 × 12h, 0..9,A,B,C,D
10	230 [†]	36	12	2784		$\lambda = 92\text{cm}$, synthesis, 8 × 12h, 0..9,A,B,C,D

[†] The number of non-redundant spacings is tabulated, see table 8.3.

Table 8.4: Configuration of the example calculations. Examples 1 through 7 are illustrative for the effect of synthesis on the beamshape.

8.3.1 CALCULATION OF SYNTHESIZED BEAMS

In this section we present cross-cuts through and integrals of theoretical two dimensional beams at a declination of 90°. Except for one example all calculations have been done at $\lambda = 21\text{cm}$. The calculations have been made using a Gaussian grading.

In practice one uses a Gaussian grading to reduce the near sidelobes with a minimum broadening of the synthesized beam. Ideally we would like to see the level between the main lobe and the first grating ring to be at a zero level. This is however not always the case as one can see from the calculated integrals. The integrals would be constant with increasing radius in case of an on average zero baselevel. The deviations in the baselevel are largely due to the shortest spacings. These are u, v points near the origin and correspond to the slow Fourier components.

The integrals are important when determining the precise conversion between flux density per beam to brightness temperature. The deviation from zero level is the limiting when determining fluxes at large radii *i.e.* the shortest spacing limits the largest structure that can be seen with an interferometer.

The calculations also graphically illustrate the effect of synthesis on the grating rings. In a second set of calculations the configuration is fixed but telescopes are deleted to show the effect of missing spacings.

In table 8.4 we summarize the configurations for which we did the calculations. The theoretical synthesized beam for a uniformly and completely filled aperture with Gaussian grading is $\Omega_A = 0.588362 \left(\frac{D_{\lambda, \text{max}}}{\lambda} \right)^{-2}$. Ω_A is tabulated in column 6 of the table.

THE ALGORITHM USED

We used the following algorithms to calculate the beam intensity and the integral over the beam:

$$I_b(k\Delta R) = \frac{\pi}{4} (\Delta R)^2 \sum_{j=1} k 2\pi \cdot A_N(j\Delta R) \cdot j\Delta R \cdot \Delta R \quad (8.24)$$

$$A_N(k\Delta R) = \frac{\sum_{n=1}^{N_D} 2\pi \cdot G(D(n)) \cdot D(n) \cdot J_0(2\pi \cdot k\Delta R \cdot D(n))}{\sum_{n=1}^{N_D} 2\pi \cdot G(D(n)) \cdot D(n)} \quad (8.25)$$

where:

$I_b(k\Delta R)$: integral of synthesized beam over circular area with radius $k\Delta R$.

$A_N(k\Delta R)$: normalized synthesized beam intensity at radius $k\Delta R$.

ΔR : spacing of points in (l, m) plane at which I_b and A_N are evaluated (we used 3 arcsec).

$D(n)$: spacing number n $D(n) = (n - 1) \cdot D_{\lambda, inc} + D_{\lambda, min}$.

$D_{\lambda, min}$: shortest spacing.

$D_{\lambda, inc}$: spacing increment.

N_D : number of spacings.

$G(x)$: grating $G(x) = e^{-ln4 \cdot \frac{x^2}{D_{\lambda, max}^2}}$ is used. $D_{\lambda, max}$ is the longest spacing.

J_0 : zero order Bessel function: response of one interferometer. (In polar coordinates the zeroth order Hankel transform is often used to do the two dimensional Fourier transform. The Hankel transform of a delta function $1/2\delta(q - a)$ —which is a ring in the u, v plane— is a zeroth order Bessel function $\pi a J_0(2\pi a)$. Also see e.g. Bracewell (1986) page 244-250.)

Note:

- The $\frac{\pi}{4}(\Delta R)^2$ in equation 8.24 is the contribution to the sum for $j = 0$.
- When calculating the beams with missing telescopes all spacings with the "defect" telescope were not included in the sum in equation 8.25 We used table 8.3 to see which spacings missed. e.g. In the case of a dropout of telescope 5 the following spacings are not available anymore: 612, 684, 1908 and 1980 meter.

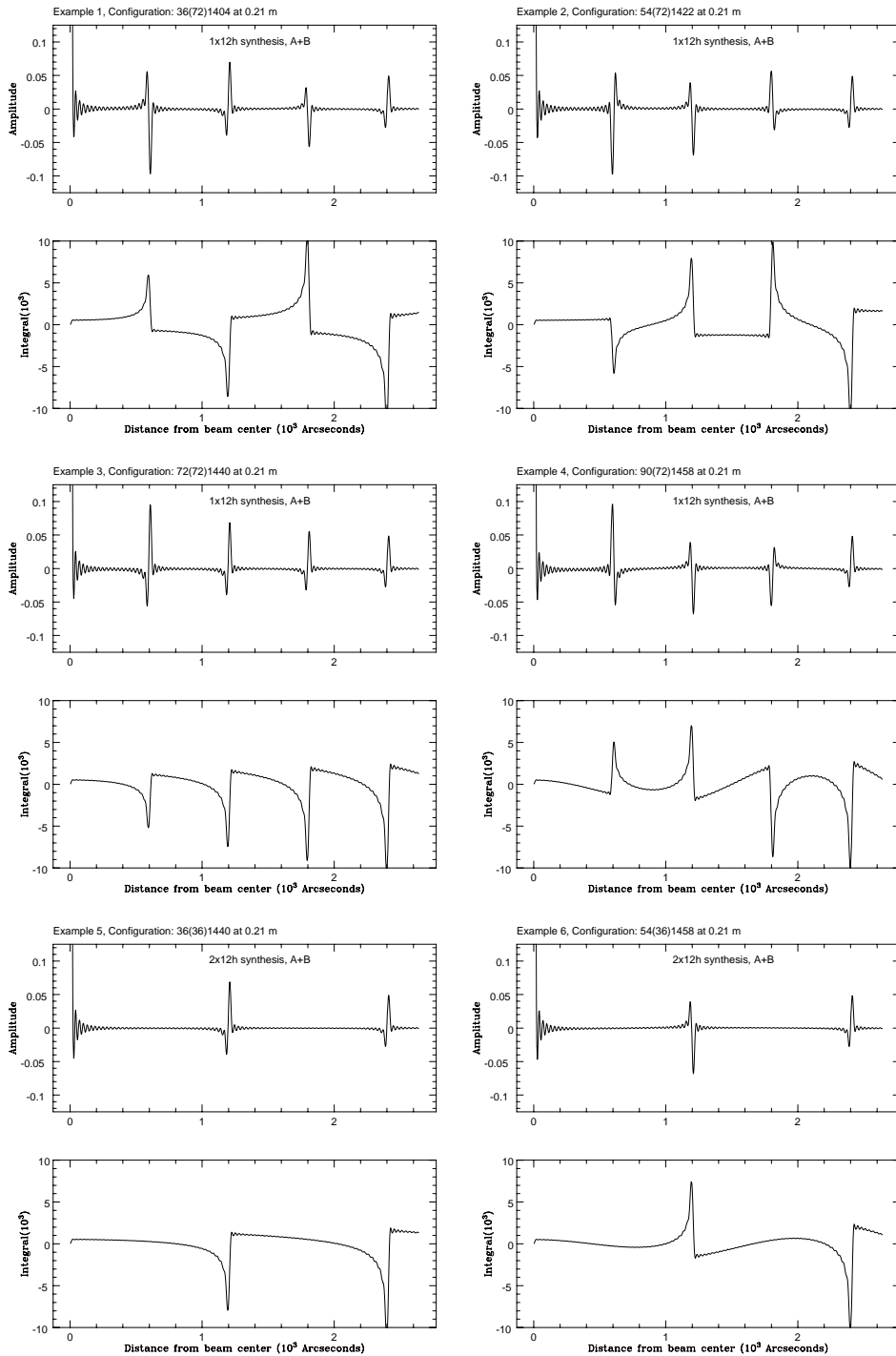


Figure 8.3: Examples of calculation of synthesized beam (top) and integral over the synthesized beam(bottom). Configurations are denoted by $D_{\lambda,min}(D_{\lambda,inc})D_{\lambda,max}$. Calculation no 10 was done at 92 cm. The others at 21 cm. (Note all x-axis are on the same scale)

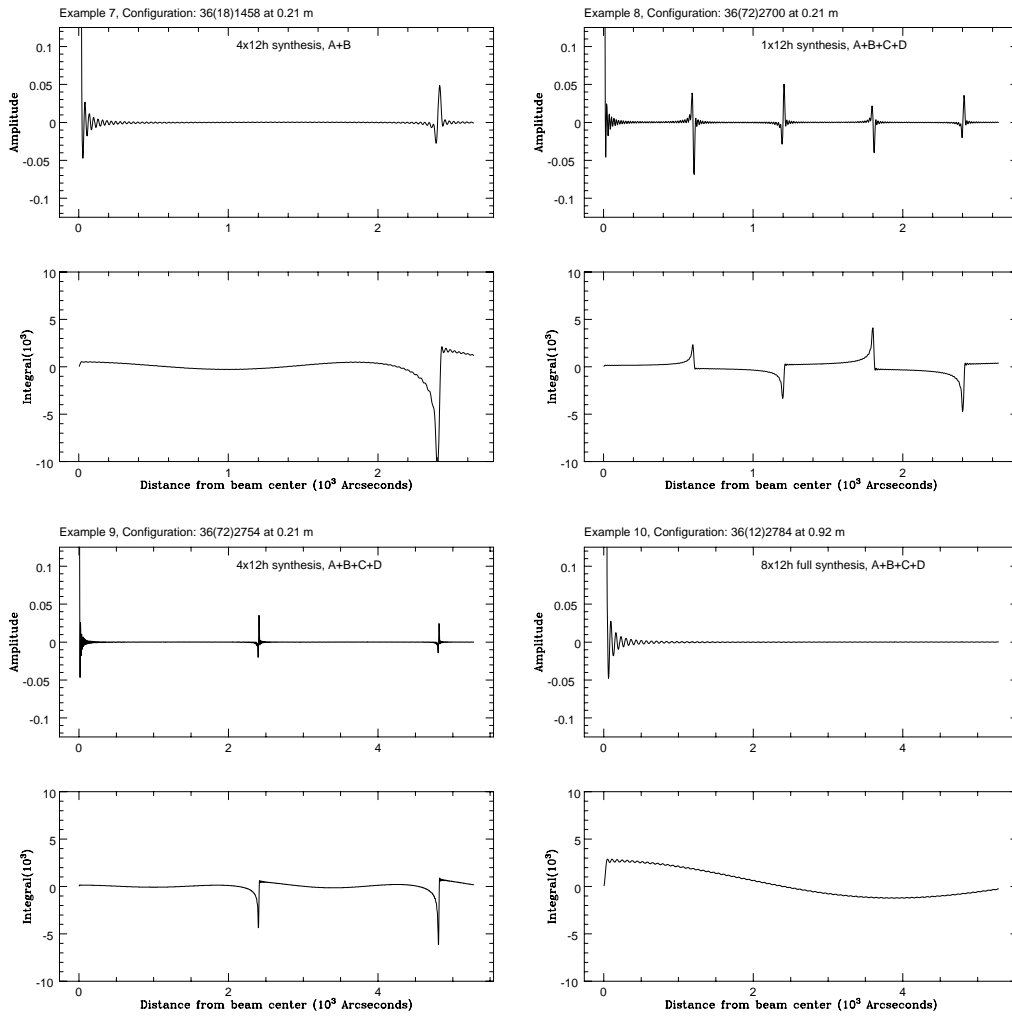


Figure 8.3:continuing

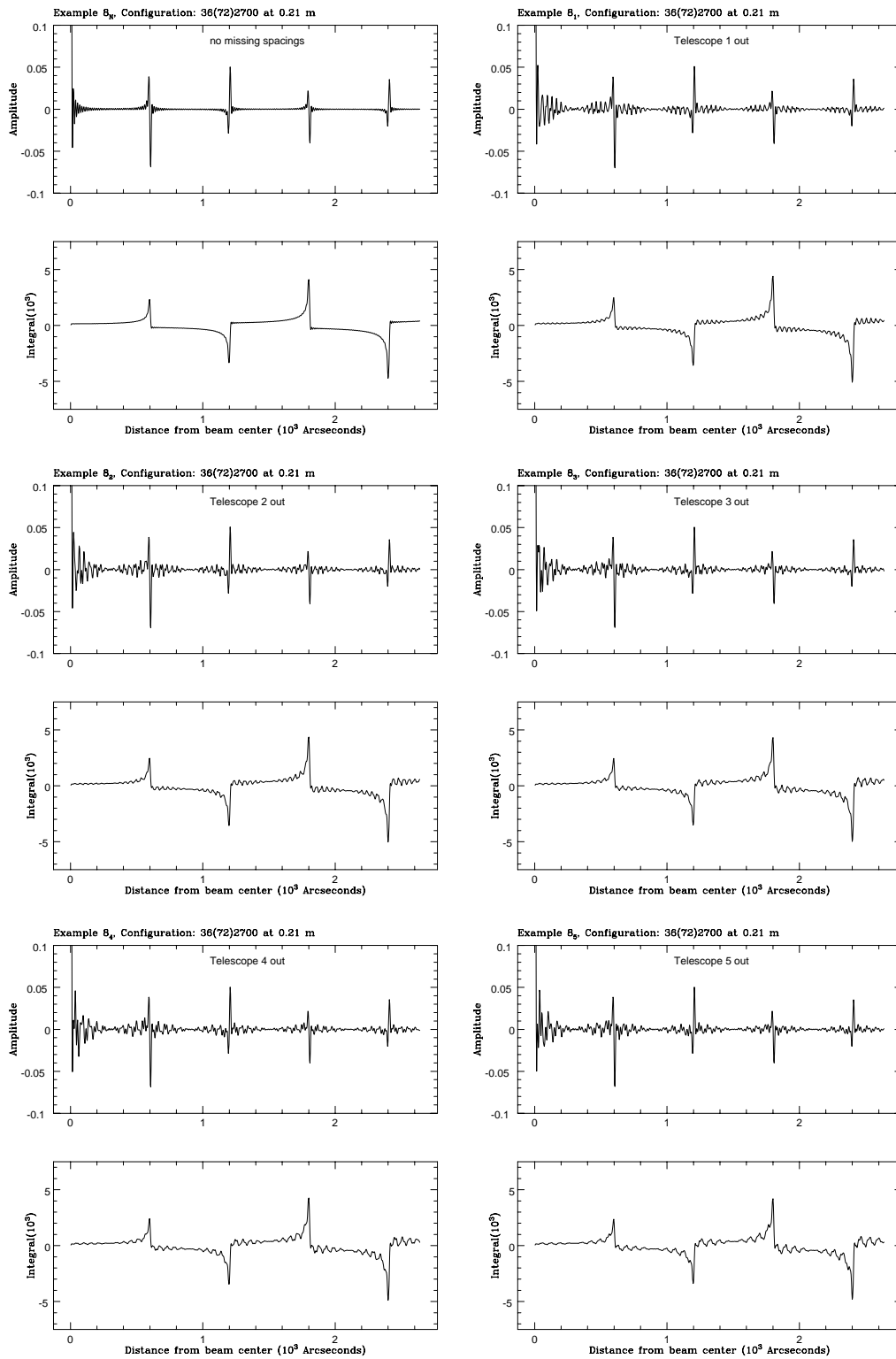


Figure 8.4: Configuration 8 (*i.e.* 36(72)2700) with telescopes switched off. top panels show normalized power, bottom panels show integrated beams

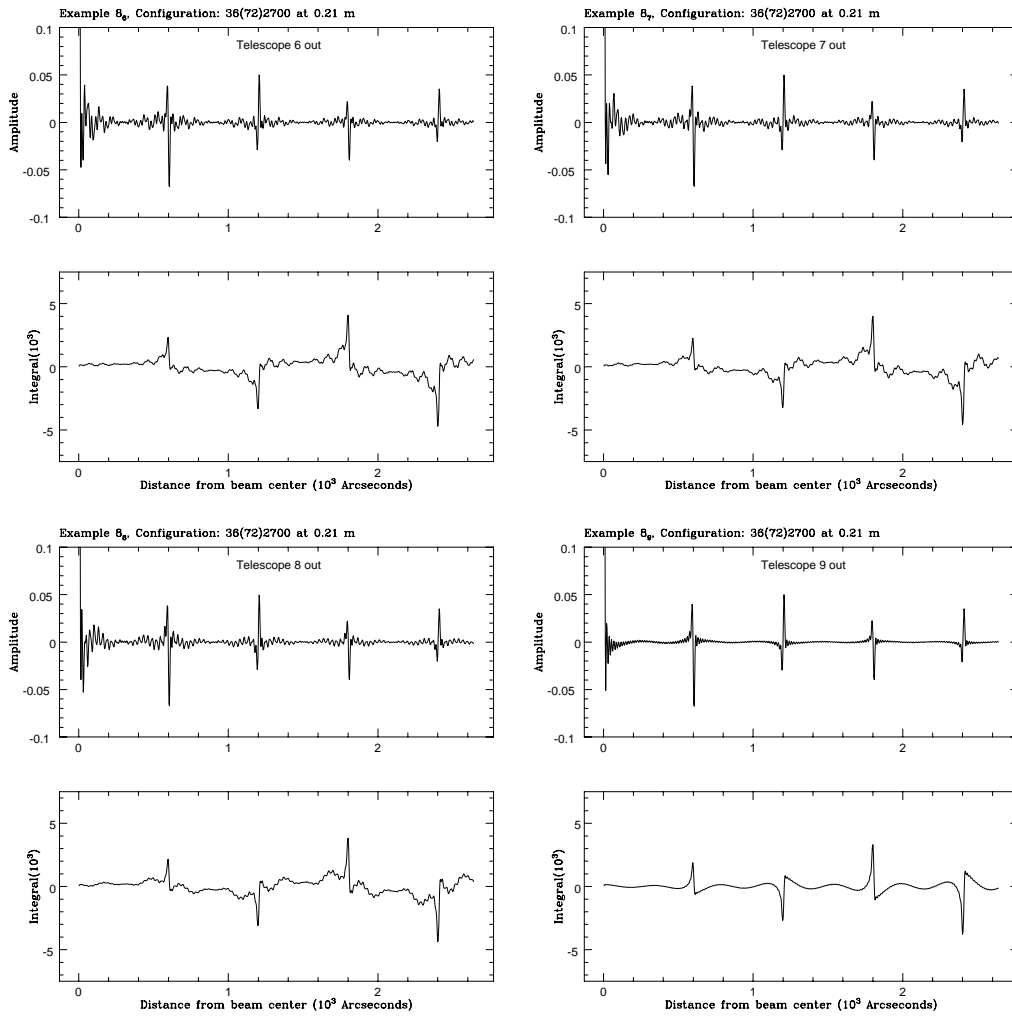


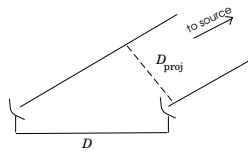
Figure 8.4:continuing

SHADOWING

9.1 INTRODUCTION

At low declination and high hour angle one telescope in an East-West array can look into the back of another telescope in the array. This effect is known as shadowing. Below we will present a simplified explanation of the effect and we give the observing limits for which shadowing can become a problem.

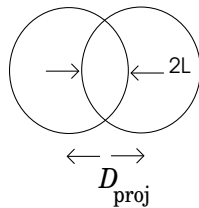
9.2 GEOMETRICAL SHADOWING CALCULATION



For an East-West interferometer with baseline D , the projected baseline length, D_{proj} , is given by:

$$D_{\text{proj}} = D \sqrt{1 - \cos^2 \delta \sin^2 h}$$

where δ is the declination and h is the hour angle.



A Westerbork antenna will be shadowed whenever $D_{\text{proj}} < 25$ meters.

$$2L_s = 25 - D_{\text{proj}}$$

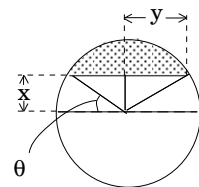
thus, L_s , which is defined as linear shadowing, is given by:

$$L_s = \frac{25 - D_{\text{proj}}}{2} = 12.5 - \frac{D}{2} \sqrt{1 - \cos^2 \delta \sin^2 h}$$

See figure 9.1 and figure 9.2.

The shaded area = segment of a circle. The segment has the area

$$\text{area} = \frac{\pi r^2}{2} - 2 \left(\frac{1}{2} x y \right) - \pi r^2 \frac{2\theta}{360} = \frac{\pi r^2}{2} - x \sqrt{r^2 - x^2} - r^2 \text{asin} \left(\frac{x}{r} \right)$$



where 2π was set equal to 360 and $\theta = \text{asin} \left(\frac{x}{r} \right)$.

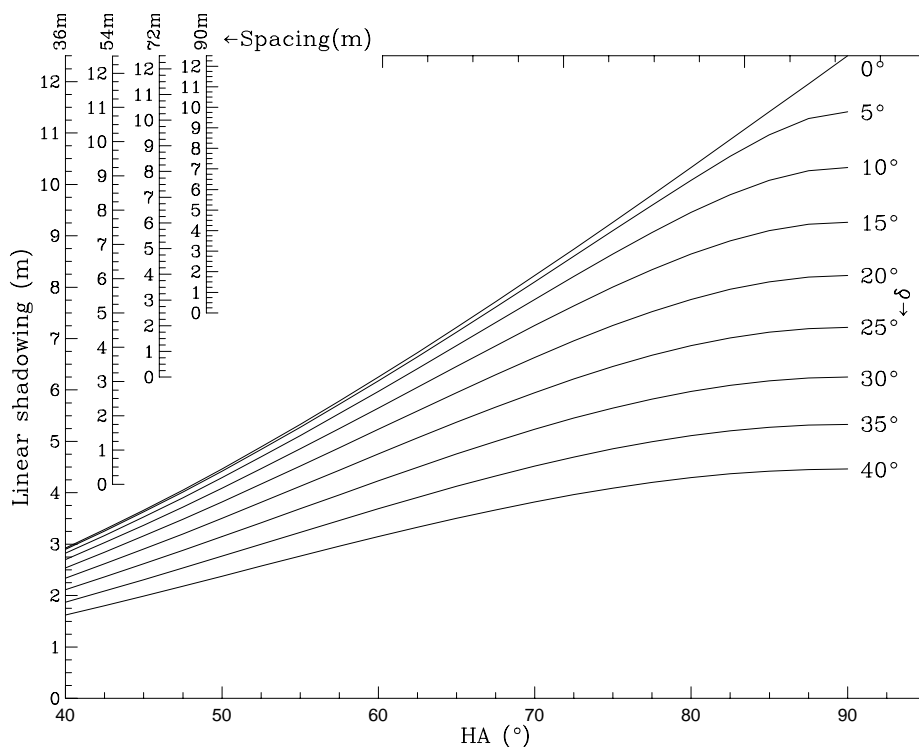


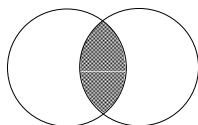
Figure 9.1: Linear shadowing L_s as a function of hour angle and declination for different antenna spacings (left vertical axes)

The shaded area to the left has an equal area to that of two segments:

$$\text{area} = \pi r^2 - 2x\sqrt{r^2 - x^2} - 2r^2 \text{asin}\left(\frac{x}{r}\right)$$

However $x = \frac{25}{2} - L_s = r - L_s$

Then substituting, the total shadowed area of one antenna is



$$\begin{aligned} & \pi r^2 - 2(r - L_s)\sqrt{r^2 - (r - L_s)^2} - 2r^2 \text{asin}\left(\frac{r - L_s}{r}\right) \\ &= \pi r^2 - 2(r - L_s)\sqrt{2rL_s - L_s^2} - 2r^2 \text{asin}\left(\frac{r - L_s}{r}\right) \\ &= 490.87 - 3(r - L_s)\sqrt{25L_s - L_s^2} - 312.50 \text{asin}\left(\frac{r - L_s}{r}\right) \end{aligned}$$

If we replace L_s by the values that are given in the shadowing tables 9.1, we obtain the values for the shadowed area that are listed there.

Whenever shadowing occurs part of an antenna's aperture is blocked; thus there will be a drop in the aperture efficiency of the antenna and thus a decrease in the correlated signal for the interferometer of which the shadowed antenna is an element.

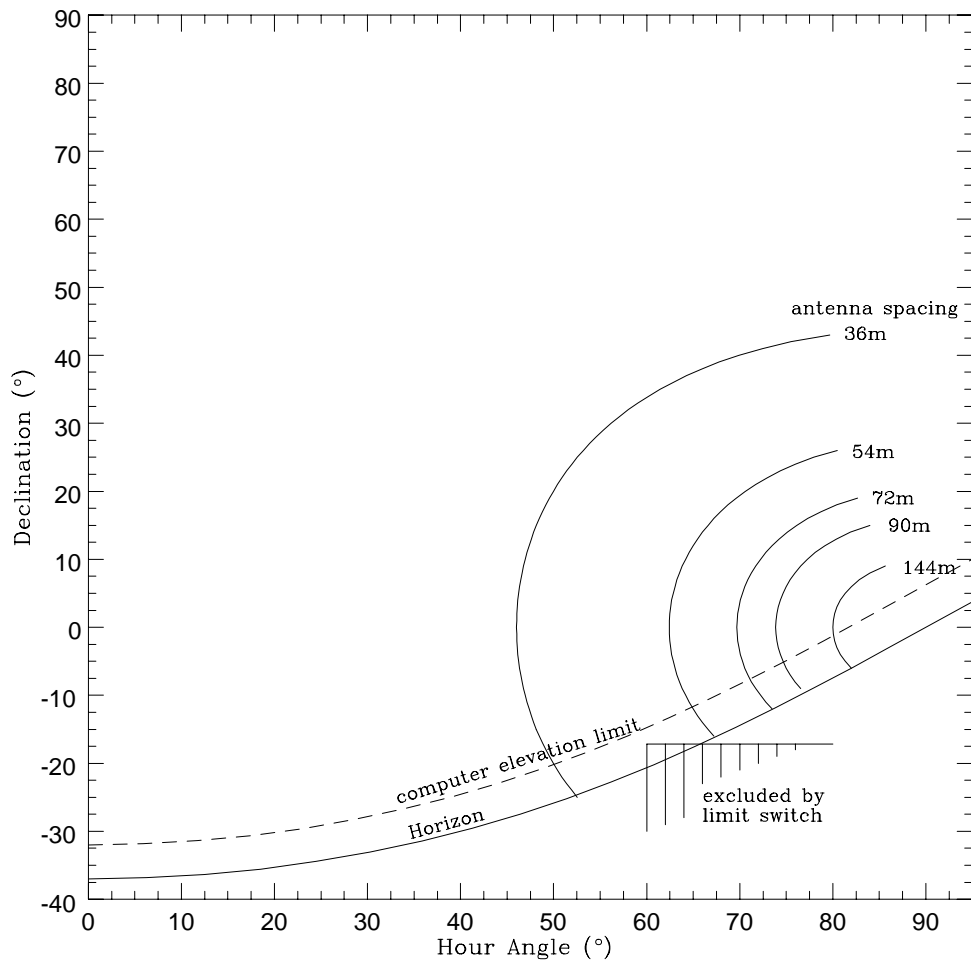


Figure 9.2: Shadowing limits for the WSRT. For a given spacing the line indicates linear spacing, $L_s = 0$.

9.3 ANTENNA SHADOWING AND OBSERVING LIMITS

When considering observations at low declination shadowing can occur and one should keep in mind the following.

1. In the East ($h < 0$)

- Depending on the position of telescope A, the first telescope to be shadowed will generally be 9 looking into the back of A. This will affect all interferometers 9A, 9B, 9C and 9D. (and 90, 91, ... if non-standard baselines are used)
- The next telescope will be A looking into the back of B and C looking into the back of D. Their separation will generally be 72 m. This will affect all interferometers with A (0A, 1A, ..., 9A) and C (0C, 1C, ..., 9C).
- The last telescopes to be shadowed will be all of the fixed telescopes looking into the backs of each other. Their separation is fixed at 144 m. All interferometers except perhaps those with 9 will be affected.

2. In the West ($h > 0$)

- Depending on the position of telescope A, the first telescope to be shadowed will generally be A looking into the back of 9. This will affect all interferometers 9A, 9B, 9C and 9D.
- The next telescope will be B looking into the back of A and D looking into the back of C. Their separation will generally be 72 m. This will affect all interferometers with A (0B, 1B, ..., 9B) and D (0D, 1D, ..., 9D).
- The last telescope to be shadowed will be all of the fixed telescopes looking into the backs of each other. Their separation is fixed at 144 m. All interferometers except perhaps those with 0 will be affected.

9.4 REMARKS

We presented a simplified model of shadowing. In practice shadowing is of course a more complicated effect. We want to note two important complications.

First, because of the illumination taper (signals coming from different parts of the telescope dish have different weight) the shaded area is not directly proportional to the loss of signal.

Second, phase effects have to be taken into account as well (see Hamaker(1978)). The phase effects are dependant on the position of the source in the field. This effect cannot be corrected for because correction programs can only make phase corrections for the field center.

It is best to delete shadowed data.

9.5 REFERENCES

Hamaker J. (1978): ...

Separation 36 m			
h	Linear sh. (m)	Area sh. (m^2)	% sh.
$\delta = 0$	Shadowing begins at $h = 46^\circ.0 \sin h = 0.7195$		
50°	0.93	11.82	2.41
55°	2.18	41.65	8.48
60°	3.50	83.54	17.02
65°	4.89	135.51	27.61
70°	6.34	196.00	39.93
75°	7.84	263.45	53.67
80°	9.37	336.22	68.50
85°	10.93	412.64	84.06
90°	Complete Shadowing		
$\delta = 10$	Shadowing begins at $h = 46^\circ.9 \sin h = 0.7306$		
50°	0.68	7.49	1.53
55°	1.86	33.13	6.75
60°	3.10	70.06	14.27
65°	4.38	115.68	23.56
70°	5.68	167.59	34.14
75°	6.95	222.71	45.37
80°	8.11	276.12	56.25
85°	9.01	318.83	64.95
90°	9.37	336.23	68.50
$\delta = 20$	Shadowing begins at $h = 50^\circ.0 \sin h = 0.7657$		
55°	1.01	13.36	2.72
60°	2.04	37.87	7.71
65°	3.07	68.89	14.03
70°	4.05	103.30	21.04
75°	4.95	137.62	28.04
80°	5.68	167.59	34.14
85°	6.17	188.46	38.39
90°	6.34	196.00	39.93
$\delta = 30$	Shadowing begins at $h = 56^\circ.2 \sin h = 0.8309$		
60°	0.59	6.06	1.23
65°	1.35	20.49	4.17
70°	2.04	37.87	7.71
75°	2.64	55.25	11.26
80°	3.10	70.06	14.27
85°	3.40	80.03	16.30
90°	3.40	83.54	17.02
$\delta = 40$	Shadowing begins at $h = 69^\circ.6 \sin h = 0.9393$		
75°	0.39	3.26	0.66
80°	0.68	7.49	1.53
85°	0.87	10.66	2.17
90°	0.93	11.82	2.41
$\delta = 50$	No Shadowing		
Separation 144 m			
$\delta = 0$	Shadowing begins at $h = 80^\circ.0 \sin h = 0.9848$		
h	Linear sh. (m)	Area sh. (m^2)	% sh.
85°	6.22	190.84	38.88
90°	Complete Shadowing		
$\delta = 10$	No Shadowing		

Separation 54 m			
h	Linear sh. (m)	Area sh. (m^2)	% sh.
$\delta = 0$	Shadowing begins at $h = 62^\circ.4 \sin h = 0.8864$		
65°	1.09	14.96	3.05
70°	3.27	75.52	15.38
75°	5.51	160.63	32.72
80°	7.81	262.07	53.39
85°	10.15	373.91	76.17
90°	Complete Shadowing		
$\delta = 10$	Shadowing begins at $h = 64^\circ.2 \sin h = 0.9001$		
65°	0.32	2.45	0.50
70°	2.27	44.29	9.02
75°	4.17	107.78	21.96
80°	5.92	177.76	36.21
85°	7.27	237.22	48.32
90°	7.81	262.07	53.39
$\delta = 20$	Shadowing begins at $h = 70^\circ.6 \sin h = 0.9433$		
75°	1.17	16.61	3.38
80°	2.27	44.29	9.02
85°	3.00	66.87	13.62
90°	3.27	75.52	15.38
$\delta = 30$	No Shadowing		
Separation 78 m			
$\delta = 0$	Shadowing begins at $h = 69^\circ.7 \sin h = 0.9378$		
h	Linear sh. (m)	Area sh. (m^2)	% sh.
70°	0.19	14.08	0.22
75°	3.18	72.74	14.82
80°	6.25	191.88	39.09
85°	9.36	335.66	68.38
90°	Complete Shadowing		
$\delta = 10$	Shadowing begins at $h = 72^\circ.2 \sin h = 0.9523$		
75°	1.40	21.64	4.41
80°	3.73	91.49	18.64
85°	5.53	161.25	32.85
90°	6.25	191.88	39.09
$\delta = 20$	Shadowing begins at $h = 83^\circ.3 \sin h = 0.9523$		
90°	0.19	1.08	0.22
$\delta = 30$	No Shadowing		
Separation 90 m			
$\delta = 0$	Shadowing begins at $h = 73^\circ.9 \sin h = 0.9608$		
h	Linear sh. (m)	Area sh. (m^2)	% sh.
75°	0.85	10.40	2.12
80°	4.68	127.36	25.95
85°	8.58	298.04	60.72
90°	Complete Shadowing		
$\delta = 10$	Shadowing begins at $h = 77^\circ.3 \sin h = 0.9755$		
80°	1.53	24.83	5.06
85°	3.78	93.54	19.06
90°	4.69	127.36	25.95
$\delta = 20$	No Shadowing		

Table 9.1: WSRT shadowing tables

BASELINES, DELAYS AND FRINGES

A selection from chapter 9 from the old manual. Figures have all be (re)drawn by O.M. Kolkman.

10.1 DELAY PATH LENGTHS

Imagine that, as shown in the figure 10.1, we have two telescopes joined together to form an interferometer. The geometrical delay, τ_g , is the extra path length that radiation must travel to get to the West telescope.

$$\tau_g = D \cos \Theta$$

It may be shown that for any interferometer $\cos \Theta$ can be written as

$$\cos \Theta = \sin \delta \sin \delta_p + \cos \delta \cos \delta_p \cos(h - h_p) \quad (10.1)$$

where δ is the declination of the source, h is the hour angle of the source, δ_p is the declination of the baseline pole, and h_p is the hour angle of the baseline pole. For an East–West interferometer, such as the WSRT, $\delta_p = 0$ and $h_p = \frac{3\pi}{2}$ when the declination pole is defined to lie in the easterly direction. In this case

$$\cos \Theta = -\cos \delta \sin h \quad (10.2)$$

$$\tau_g = -D \cos \delta \sin h \quad (10.3)$$

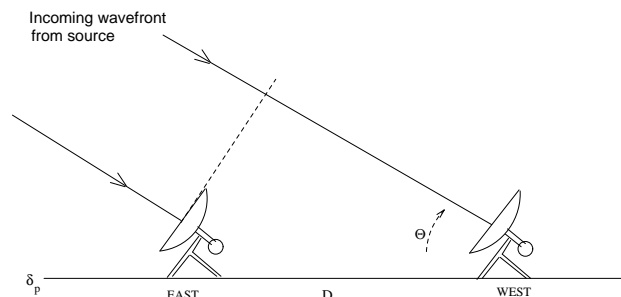


Figure 10.1: An East-West interferometer receiving a signal from a source at infinite distance.

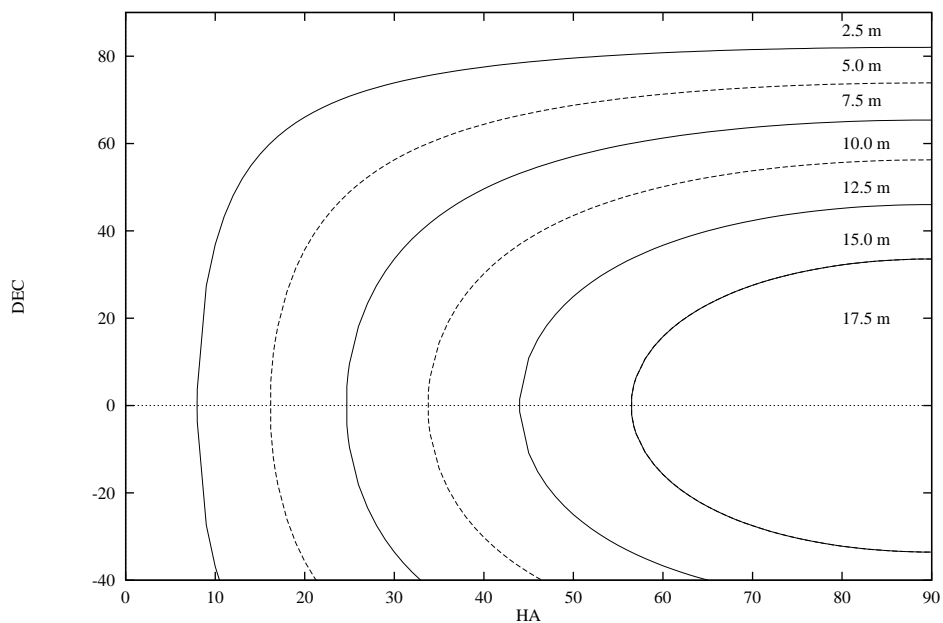


Figure 10.2: Lines of constant delay, τ_g , in meters at 18m spacing. ($\tau_g = D \cos \delta \sin h$)

For a negative hour angle, $\sin h$ is negative so τ_g is positive and an extra path length is needed to reach the western telescope. For positive hour angles, $\sin h$ is positive and the delay as defined here, is negative which just means that the longer path length is to the eastern telescope.

The graph of figure 10.2 gives

$$|\tau_g| = D \cos \delta \sin h \tag{10.4}$$

where D is 18 meters. To find $|\tau_g|$ for any telescope pair, multiply the values determined from the graph by the factor $\frac{D}{18}$ where D is the actual baseline length in meters.

10.2 FRINGE FREQUENCY

The expression for the delay (section 10.1) was

$$\tau_g = -D \cos \delta \sin h$$

The rate of change of the delay as a function of time, t , is thus

$$\frac{d\tau_g}{dt} = -D \cos \delta \cos h \frac{dh}{dt} \tag{10.5}$$

$$\frac{dh}{dt} = \text{The rotation of the Earth}$$

$$= \frac{2\pi}{3600 \times 24} = 7.272 \times 10^{-5} \text{radians/sidereal second}$$

$$\text{thus } \frac{d\tau_g}{dt} = -7.272 \times 10^{-5} D \cos \delta \cos h \tag{10.6}$$

Equation 10.6 is the change of the delay in meters per second if D , the distance between the interferometer elements, is expressed in meters. If we express the baseline in units of wavelength $D_\lambda = \frac{D}{\lambda}$ then

$$\frac{d\tau'}{dt} = -7.272 \times 10^{-5} D_\lambda \cos \delta \cos h$$

is the fringe frequency, or number of wavelengths per second by which the delay changes. $\frac{d\tau'}{dt}$ is also called the natural fringe rate.

The response of an interferometer to a point source may be written as

$$r(\mathbf{D}_\lambda, \mathbf{s}) \propto \cos 2\pi\nu\tau_g = \cos(2\pi\mathbf{D}_\lambda \cdot \mathbf{s}) \quad (10.7)$$

(cf. equation 2.3 in II) where \mathbf{s} is a unit vector pointing to the source. (For an E-W interferometer $\mathbf{D}_\lambda \cdot \mathbf{s} = D_\lambda \cos \delta \sin h$)

To avoid bandwidth decorrelation we normally insert an extra delay, τ_0 , in the path length between the telescope closer to the source and the correlators (see e.g. section 2.3). This extra delay is equal to the extra distance (or delay) which radiation from the field center must travel to reach the telescope farther from the source.

For purposes of this discussion we assume that τ_0 is continuously changed as the hour angle, h , of the field center changes (i.e. we include the fringe stopping process). Then

$$r \propto \cos(2\pi\nu(\tau_g - \tau_0)) \quad (10.8)$$

$$= \cos(D_\lambda(\cos \delta \sin h - \cos \delta_0 \sin h_0)) \quad (10.9)$$

Here δ_0, h_0 are the declination and hour angle of the field center and δ and h are the declination and hour angle of a radiation source.

Then the rate of change of the relative delay, $\tau_g - \tau_0$, is

$$\frac{d}{dt}(\tau_g - \tau_0) = -7.272 \times 10^{-5} D_\lambda (\cos \delta \cos h - \cos \delta_0 \cos h_0) \quad (10.10)$$

This expression gives the relative number of wavelength changes per second that we will see if we are observing a field center at δ_0, h_0 but we have a source at δ, h (or equivalently, the number of fringes/second that we will count). We can use this expression, for instance, to check if the interference fringes sometimes seen on short baselines are due to the Sun or some other strong source at known δ, h by inserting the δ, h of the suspected interfering source and the δ_0, h_0 of the field center in the formula and then checking if the calculated interference fringe rate agrees with that observed.

If the interference source (e.g. radar) is located on earth then the interference will appear at the natural fringe rate, $|-7.272 \times 10^{-5} D_\lambda \cos \delta_0 \cos h_0|$, of the fringe stopping center.

The graph in figure 10.3 gives values for $\cos \delta \cos h$.

10.3 POSITION ANGLE OF THE PROJECTED BASELINE ON THE SKY

An East-West interferometer baseline vector, \mathbf{D}_λ , of length D_λ may be projected on two components, one oriented along the u axis (towards the easterly direction) and one along the v axis (toward north).

In Brouw's (see e.g. part II, chapter 6) coordinate system, with declination of the baseline pole toward hour angle $\frac{3\pi}{2}$, we find that

$$u = D_\lambda \cos h \quad (10.11)$$

$$v = D_\lambda \quad (10.12)$$

The total length of the projected baseline, D_{proj} , equals

$$\begin{aligned} D_{\text{proj}} &= \sqrt{u^2 + v^2} \\ &= D_\lambda \sqrt{\cos^2 h + \sin^2 h \sin^2 \delta} \end{aligned} \quad (10.13)$$

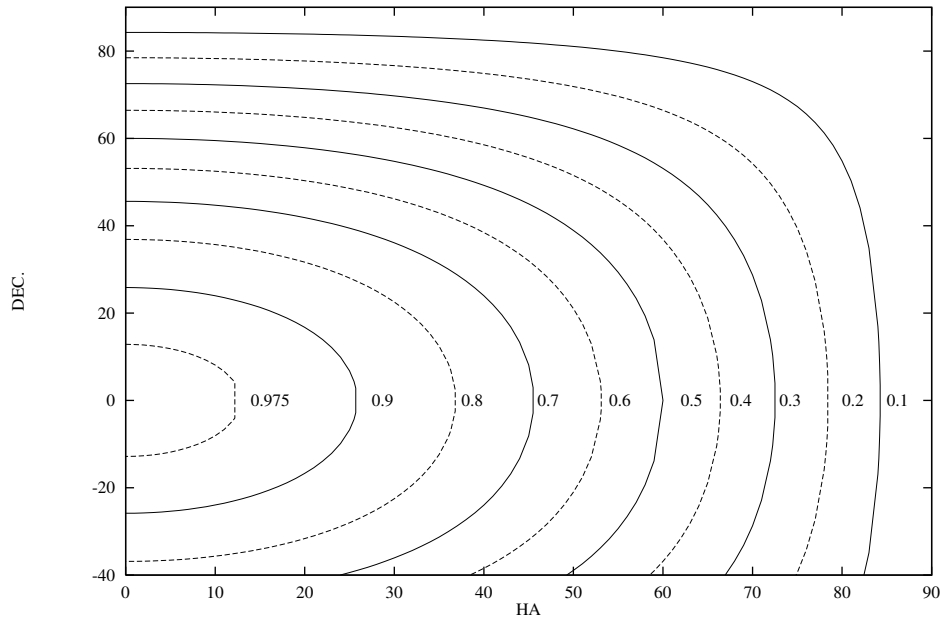


Figure 10.3: Lines of constant $\cos \delta \cos h$. Multiplication by $7.272 \times 10^{-5} D_\lambda$ gives the natural fringe rate.

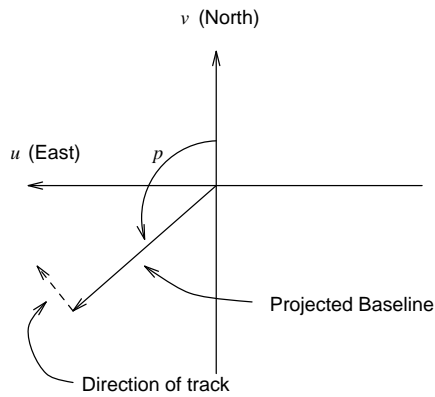


Figure 10.4: Baseline projected on the sky globe

δ (°)	h	0^h	0^h	1^h	1^h	2^h	2^h	3^h	3^h	4^h	4^h	5^h	5^h	6^h
		00'	30'	00'	30'	00'	30'	00'	30'	00'	30'	00'	30'	00'
90		90	83	75	68	60	53	45	38	30	23	15	8	0
85		90	83	75	68	60	53	45	38	30	23	15	8	0
80		90	83	75	68	60	53	45	38	30	23	15	8	0
75		90	83	75	68	61	53	46	38	31	23	16	8	0
70		90	83	76	69	62	54	47	39	32	24	16	8	0
65		90	83	76	69	62	55	48	40	32	25	16	8	0
60		90	83	77	70	63	56	49	42	34	26	17	9	0
55		90	84	78	71	65	58	51	43	35	27	18	9	0
50		90	84	78	72	66	60	53	45	37	28	19	10	0
45		90	85	79	74	68	62	55	47	39	30	21	11	0
40		90	85	80	75	70	64	57	50	42	33	23	12	0
35		90	86	81	77	72	66	60	53	45	36	25	13	0
30		90	86	82	78	74	69	63	57	49	40	28	15	0
25		90	87	84	80	76	72	67	61	54	44	32	17	0
20		90	87	85	82	79	75	71	66	59	50	38	21	0
15		90	88	86	84	82	79	75	71	66	58	46	27	0
10		90	89	87	86	84	82	80	77	73	67	57	37	0
5		90	89	89	88	87	86	85	84	81	78	72	56	0
0		0	0	0	0	0	0	0	0	0	0	0	0	0

Table 10.1: Position angle of the fringe normal for an E-W baseline. ($\cot p = \sin \delta \tan h$)

If we imagine we are looking at the array from within the earth, then the array appears projected on the sky. (e.g. figure 10.4) The position angle, p , of the array (North through East) is given by

$$\begin{aligned} \cot p &= \frac{\cos p}{\sin p} = \frac{\frac{v}{\sqrt{u^2+v^2}}}{\frac{u}{\sqrt{u^2+v^2}}} = \frac{v}{u} \\ &= \frac{\sin \delta \sin h}{\cos h} = \sin \delta \tan h \end{aligned} \quad (10.14)$$

Table 10.1 and figure 10.5 gives value of p for the projected baseline, or fringe normal, for positive hour angles. For negative hour angles, take the value given in the table for the positive hour angle, make them negative and then add them to 180°.

These angles give the position angle along which the interferometer array is projected on the sky. The value by which we must scale the true baseline length D to get the projected baseline is

$$\begin{aligned} \text{scale factor} &= \sqrt{\cos^2 h + \sin^2 h \sin^2 \delta} \\ &= \sqrt{\cos^2 h + \sin^2 h (1 - \cos^2 \delta)} \\ &= \sqrt{1 - \sin^2 h \cos^2 \delta} \end{aligned} \quad (10.15)$$

The resolution is directly proportional to the projected baseline so we then get the formula and graphs of figure 10.6 and figure 10.7.

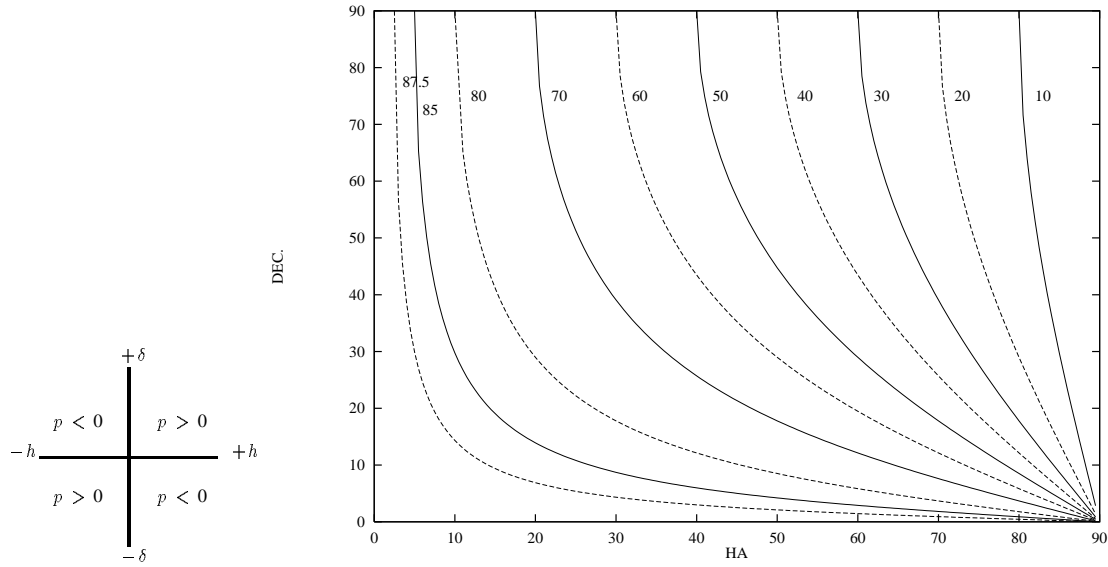


Figure 10.5: Position angle of the fringe normal for an E-W baseline

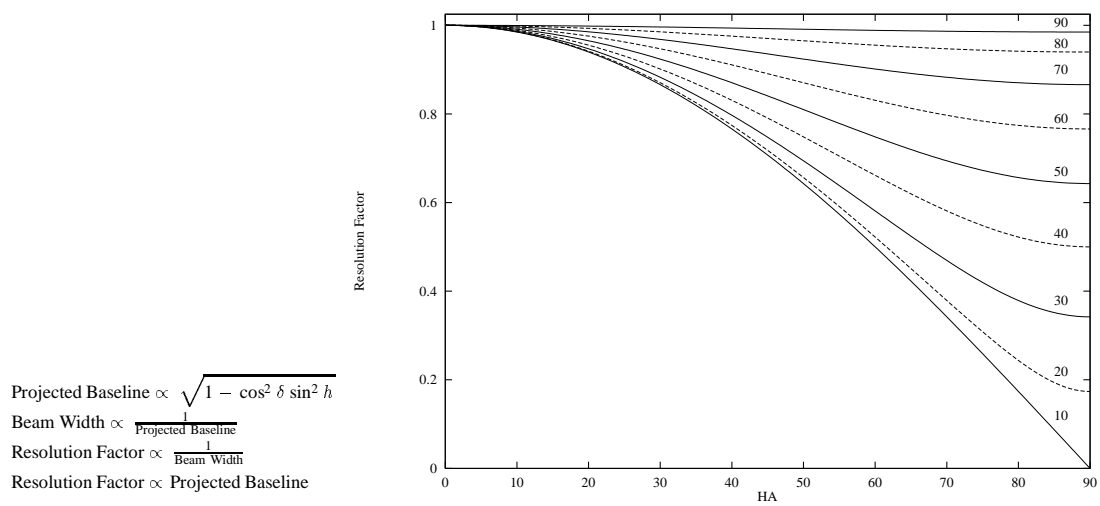


Figure 10.6: Resolution factor for an East-West baseline. Lines of constant declination, δ ($^\circ$), are shown.

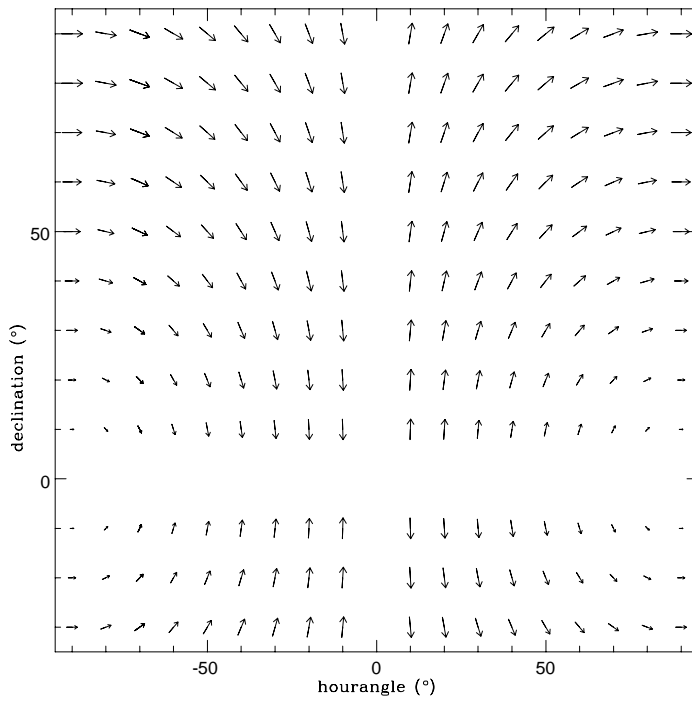


Figure 10.7: Resolution factor (\propto the length of the vector) and position angle of the fringe normal (direction of the vector) in a $h - \delta$ diagram.